SCUOLA
NORMALE
SUPERIORE

Classe di Scienze

Corso di perfezionamento in
Neuroscienze

XXXIII ciclo

A cartography of learning-induced synaptic potentiation using the genetically encoded SynActive toolbox

Settore Scientifico Disciplinare BIO/09

Candidato
dr. Andrea FARAONE

Relatore	Supervisione interna
Prof. Antonino CATTANEO	Prof. Marco MAINARDI

Anno accademico 2023/2024

Abstract ……………………………………………………………………….... Page 2

1. Introduction ……………………………………………………………….... Page 4

1.1 Fear and memory: insights from the fear conditioning paradigm ………………….... Page 4

1.2 Two key nodes for the fear memory circuitry ………………………………………Page 8

1.3 Looking for the physical substrates of memory ……………………………………...Page 14

1.4 Activity-dependent synaptic plasticity ……………………………………………….Page 23

1.5 Structural substrates of activity-dependent synaptic plasticity ………………………Page 28

1.6 The postsynaptic density: a moving mosaic…………………………………………Page 32

1.7 Synaptic tagging and capture ………………………………………………………Page 38

1.8 Arc ……………………………………………………………………………………Page 41

1.9 Analyzing plasticity at the single-synapse resolution ……………………………... Page 44

2. Aims of the project ………………………………………………………… Page 49

3. Materials and methods ……………………………………………………… Page 51

3.1 Animals and surgical procedures …………………………………………………Page 51

3.2 Contextual fear conditioning and doxycycline injections ……………………………Page 53

3.3 Histological fixation ………………………………………………………………...Page 55

3.4 Immunofluorescence and confocal imaging ………………………………………Page 56

3.5 Image post-processing……………………………………………………………....Page 58

3.6 Slice quantifications …………………………………………………………………..Page 60

3.7 Statistical analyses …………………………………………………………………..Page 62

4. Results ……………………………………………………………………… Page 63

4.1 SA-Map: labeling and imaging of dendritic spines
and translation-dependent structural potentiation ……………………………………Page 63

4.2 SA-Map: labeling spines showing structural potentiation……………………………Page 67

4.3 SA-Map: detection of synaptic potentiation triggered in the CA1 and dentate gyrus by exposure to contextual fear conditioning …..…………..……..Page 70

4.4 SA-Map: calculation of nearest neighbor distance …………………….…………Page 72

4.5 SA-Map: mapping of dendritic spine density along the dendritic arbor……………………...………….……..………..……Page 75

4.6 SA-Map: correlation of synaptic structural potentiation labeling with the expression of CFC-related behavior …………..…………………Page 77

4.7 SA-Mol: validation of the in vivo expression pattern of constructs for the analysis of the PSD-95 interactome at potentiated synapses ………………..Page 78

5. Discussion …………………….……………………………………..Page 82

6. Bibliography ……………………….…………….…...………………...Page 86

Acknowledgments………………………….………......………………..Page 109

Abstract

During learning tasks, specific neuronal populations are recruited and are thought to be responsible for the physical storage of memories (Josselyn and Tonegawa, 2020). However, each neuron has thousands of synaptic contacts with its peers, and these synapses can adapt to the strength of incoming stimuli individually and bidirectionally, playing a fundamental role in the plasticity underlying the formation of long-term memories (Rogerson et al., 2014). Despite this, knowledge of how individual synaptic contacts are involved in this process is still limited.

To address this gap, our lab developed a method called SynActive (SA) to label and manipulate potentiated dendritic spines, the postsynaptic elements of excitatory synapses where most of plasticity occurs. This dual targeting strategy exploits Untranslated Regions (UTRs) of the Arc mRNA and a short postsynaptic Density (PSD)-binding synthetic peptide to allow activity-dependent expression of any reporter protein at dendritic spines undergoing translation-dependent potentiation, improving expression and retention of these proteins at the postsynaptic density (Gobbo et al., 2017). In the first proof of principle application of the SynActive experimental strategy, the expression of the SA reporter in the mouse brain was achieved by a transgenic approach, via *in utero* electroporation of embryos.

In order to facilitate the use of the Synactive strategy, the first objective of my thesis was to develop a set of adeno-associated viral vectors (AAVs) directing the expression of SA-based genetically encoded reporters. Using *in vivo* delivery of SA-based reporters via AAV vectors, we aimed (i) to create a map of potentiated synapses in the hippocampus induced by associative learning, and (ii) to analyze the proteomic signature of learning-induced synaptic potentiation.

To achieve the first goal, we used an SA-based vector encoding a shortened version of PSD95, the most abundant scaffolding protein of the excitatory postsynaptic density (Cheng et al., 2006), fused with a fluorescent protein, to selectively detect the subset of potentiated spines among all dendritic spines. Taking advantage of a Tet-ON inducible system (Sun et al., 2007), we temporally confined the expression of the SA-construct to the formation of a contextual fear

memory (encoding). Then, by imaging the SA-positive dendritic spines, we produced a database of the distribution and geometry of potentiated spines along different branches of the dendritic tree. We found notable differences in their distribution between discrete regions of the hippocampus and sections of the same neuron.

Next, we constructed a SA-based proteomic bait, by tagging the full-length PSD-95 protein fusing it to a FLAG epitope (Einhauer and Jungbauer, 2001) to define the proteomic signature of dendritic spine potentiation. Exposure to contextual fear conditioning triggered the expression of FLAGged PSD-95 at the level of potentiated spines, thus demonstrating the validity of this tool for future analysis of the PSD-95 interactome and analyzing changes in the proteic content specific to potentiated synapses.

These findings offer insights into the distribution, geometry, and molecular composition of potentiated dendritic spines, which are thought to play a crucial role for learning and memory.

1. Introduction

1.1 Fear and memory: insights from the fear conditioning paradigm

«Life is all memory, except for the one present moment that goes by you so quick you hardly catch it going». These are the words of Tennessee Williams in "The Milk Train Doesn't Stop Here Anymore" (1962), and these are the unavoidable dynamics of how we perceive reality and experience our world. Whether you like it or not.

The rules of physics and biology dramatically reduce our possibilities to really grab a moment, that is already in the past even before being processed as such. But, at the same time, moments are the constitutive pieces of our life: our mind clings to them uninterruptedly, every single minute of the day. A rapid and free access to them is both sufficient and necessary for a human being aware of his own story and, consequently, with a purpose, a future direction.

This is an explicit (or declarative) level of memory: a set of learned information that we can consciously manipulate and "declare" to ourselves and others. Explicit memory can be intimately connected with a specific experience, or – at the opposite – totally independent of a given event, like the factual knowledge about the world: Elden Tulving (1972) first traced this clear distinction, separating an episodic memory from a semantic memory. An "intentional" retrieval of information is the common element, and it can be tested with a very simple and highly controlled behavioral paradigm in animal models. For instance, in the Object Recognition Test (ORT), a rodent is first presented with two similar objects: the animal will spend an equal amount of time exploring both objects. In a second session, one of the two objects is replaced by a new one: now, due to its innate preference for novelty, the animal will spend most of its time exploring the new object (see Eichenbaum et al., 2007 for a review). It "chooses" its future actions, relying on the acquired configuration of the past environment.

But actions often become routine. Throughout our life, a vast array of skills is learned and maintained: we are scientists, or musicians, or cooks, or football players, or all four; even more simply, we all know how to run to catch a bus, or how to pour a glass of water. In these cases, thanks to experience, our body seems to know exactly how to answer to the circumstances, and it directly transforms information into action. There might be several declarative components, but the fluid execution of movements is due to an implicit (or procedural) level of memory that is totally untied from awareness. That is responsible for what neuroscience calls priming, a facilitated processing of a stimulus following prior exposure to the same stimulus (Brewer et al., 2007), and conditioning, a rapid and unconscious association between two stimuli, or between a stimulus and a response.

The critical role of conditioning in studying memory is in providing controlled and replicable experimental designs that allow to investigate the neural mechanisms and underlying processes of different and discrete phases of memory. By investigating fear conditioning, in particular, researchers can understand how the brain processes and stores emotionally salient information: fear is a powerful and evolutionarily conserved emotion that plays a crucial role in survival and adaptive behavior, which makes it an excellent choice for approaching learning mechanisms. In this regard, fear-related behaviors are easy to detect in laboratory rodents, resulting in clear and quantifiable parameters for the study of learning and memory.

One of the most widely used protocols adopted by researchers, cued fear conditioning (CFC), is an adaptation of classical Pavlovian conditioning that involves the association of an auditory cue (conditioning stimulus, CS) or tone with an aversive event (unconditioned stimulus, US). When the animal is exposed to the CS alone, it may demonstrate a freezing response if it recalls the memory of an association between CS and US. Freezing, defined as the complete absence of movements except for respiration, is a species-specific response to fear when escape is not possible, and its duration is a strong indicator of the strength of the memory: the survival advantage is that a moving animal is more likely to be detected by a predator than a still one (Rudy, 2014).

Similarly, Contextual Fear Conditioning (CFC) involves placing a mouse in a novel environment (CS), where the US is experienced. In this case, the memory recall test is performed by placing the animal again in the conditioning context (Figure 1).

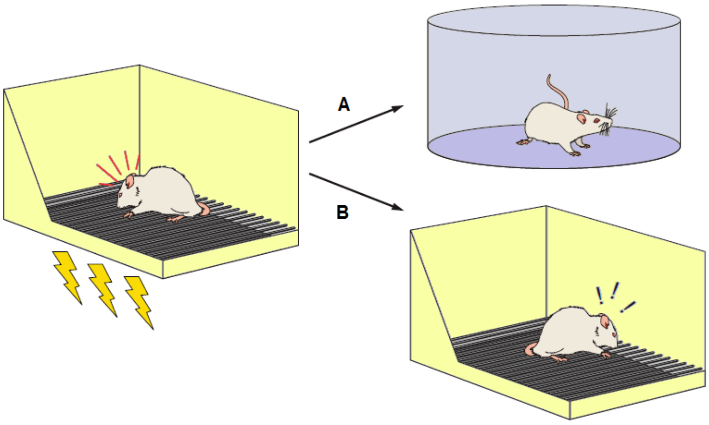

Figure 1. Classical contextual fear conditioning. The mouse undergoes a footshock (US) in a first environment (CS) and, subsequently, is moved to a second environment: in A there is no association or conditioned response, as the perceptual characteristics between the first and second environment are too different; conversely, in B the re-presentation of CS will be sufficient to elicit a freezing response even in the absence of the US. (Modified from Izquierdo et al., 2016)

For CFC, it is also possible to vary the timing between CS and US: the two stimuli can be temporally overlapping (delay fear conditioning) or be spaced by a time interval (trace fear conditioning) (Curzon et al., 2009).

Fear conditioning is a complex and dynamic process that incorporates distinct phases: during the acquisition phase, the animal learns to associate the CS with the US, resulting in the formation of a fear memory. After acquisition, fear memories undergo a consolidation process, in which they become stable over time (see Britton et al., 2015). This phase involves molecular and cellular processes that transform memory from a labile state to a stable form (Schafe et al., 2000; see section 1.6). Reactivation of a previously consolidated fear memory can make it labile again and subject to reconsolidation, a process that strengthens the memory and promotes its persistence (Nader et al., 2000). Extinction concerns the gradual reduction of a conditioned fear response by repeated exposure to the CS, but without the aversive US: this process does not erase the original fear memory but instead forms a new memory that inhibits the expression of fear (Quirk and Mueller, 2008). Over time, fear memories can weaken and eventually be forgotten: mechanisms underlying forgetting are still not fully understood but may involve active processes or interference with the original memory trace (White, 2001). Despite successful extinction, fear memories can also spontaneously recover over time. Spontaneous relapse refers to the reappearance of the fear response without any further conditioning or explicit cues (Bouton, 2002). Finally, reinstatement occurs when the extinguished fear response is reinstated by a reminder of the original fear-inducing event (Bouton and Bolles, 1979).

So, thanks to this great variety of fear discrete phases and conditioning tecnhiques, neuroscientists enjoy a certain degree of freedom in focusing on one or more cognitive, neural and molecular mechanisms underlying learning and memory.

1.2 Two key nodes for the fear memory circuitry

Although neuroscience is now far from the anti-location paradigm of mid-twentieth century psychology (according to which it is not only impossible to find a particular brain region underlying the memory function, but this ability is not even independent from other functions such as perception, language, and movement), it is still not possible to speak of a “memory center”. Karl Lashley (1950) first tried to identify univocal areas of the cerebral cortex that might be responsible for learning: after the rats had learned a maze, he surgically removed some specific areas of the brain. Then, rats were tested again to see if their learning had been affected by that removal; however, results suggested that learning was distributed throughout the brain, and no single area could be considered as unique responsible for learning.

Despite these first unsuccessful attempts to strictly restrict the target, we know about the existence of many specific circuits in mammalian brains that have a prominent role. A small C-shaped structure, in particular, is the key node of a whole brain network that is necessary for learning and memory: the hippocampus, whose anatomy is exceptionally clear and easy to study. The entorhinal cortex (EC), main interface region between the hippocampus and neocortex, projects to the first section of the cornu Ammonis region (CA1) through two different pathways: direct or temporo-ammonic (EC → CA1) and indirect, or trisynaptic, which involves several subregions. In this pathway, afferent fibers from the EC first reach the dentate gyrus (DG) via the perforant path. Then, DG neurons connect to the CA3 region through mossy fibers, which are so-called because of their resemblance to moss. Next, the information is relayed to the CA2 region, which serves as an intermediary between CA3 and CA1; it has been shown to receive direct input from the EC and to send output to CA1 through the Schaffer collaterals (Chevaleyre and Siegelbaum, 2010). After passing through CA2, information is finally transported to CA1 neurons via Schaffer collateral fibers (DG → CA3 → CA2 → CA1. See Figure 2). The subiculum completes the loop by sending information back to the EC: this is supposed to facilitate the comparison of incoming sensory information with stored memories (Lisman and Grace, 2005).

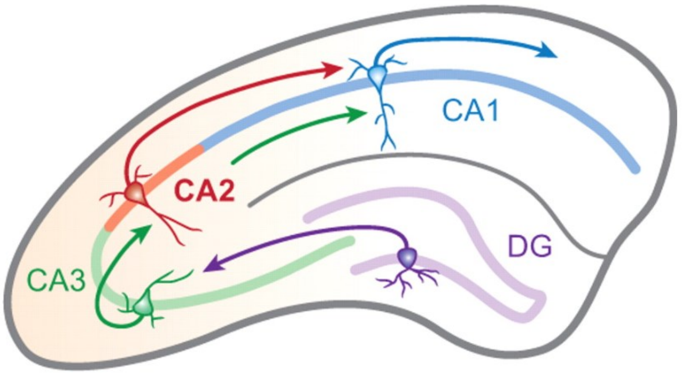

Figure 2. Simplified diagram of hippocampal information flow. DG granule cells form synapses on pyramidal cells in CA3 via the mossy fibers; CA3 neurons form synapses on pyramidal cells in both CA2 and CA1 via the Schaffer collaterals; CA2 projects mainly to the stratum oriens (red arrow) of CA1, but also to the stratum radiatum (green arrow). (Modified from Caruana et al., 2012)

Inhibitory interneurons are known to play a fundamental role in the hippocampus as well, by regulating the activity of excitatory neurons. One example is the basket cell, which inhibits the firing of pyramidal neurons and helps regulate the synchronization of neural activity; another example is the oriens-lacunosum moleculare (O-LM) interneuron, which inhibits the activity of other interneurons as well as pyramidal neurons, and they are involved in regulating the plasticity of synaptic connections in the hippocampus (for a review, see Pelkey et al., 2017).

Hippocampal neurons have a vital function in the organization of memory in a hierarchical manner, playing a key role in processing and consolidating different sensory inputs into a coherent memory representation (Lavenex and Amaral, 2000). The level of integration of sensory input informations progressively increases as visual, auditory, somatosensory information flows from different regions of the neocortex to the perirhinal and parahippocampal cortices to the entorhinal cortex and to the hippocampus; here information is processed in an abstract and integrated manner, leading to a compressed representation of memories that is not tied to any specific sensory modality (Petrantonakis and Poirazi, 2014). According with the indexing theory of hippocampal memory (Teyler and DiScenna, 1986), features of a particular episode establish a memory trace by activating patterns of neocortical activity, which then project to the hippocampus and activating here a set of cells and synapses (as we will see later). So, “learning” would consist of a hippocampal representation of co-occurring input patterns of activity in the neocortex, while “memory” would consist of an index that hippocampus projects back to neocortical input patterns, when a subset of the initial neocortical pattern activates the hippocampal representation.

Even if just a portion of the experience that originally established the memory trace activates the hippocampus, the indexing activity can activate the entire pattern of neocortical activity generated by the episode, thus recapitulating the entire experience: this is a process known as pattern completion. The CA3 region of the hippocampus is thought to be particularly involved in performing pattern completion of conjunctive representations of an entire event from a partial cue (Guzman et al., 2016). On the other hand, similar inputs are likely to converge onto different hippocampal neurons, and this is fundamental to create different indices and to keep representations of similar experiences segregated: this is a second process called pattern separation. The dentate gyrus is believed to contribute significantly to play a major role in performing pattern separation (Santoro, 2013): it receives convergent input from various cortical regions and generates highly differentiated representations, allowing for the discrimination and separation of similar input patterns. These operations are compromised by manipulations that impair DG pattern separation (McHugh et al., 2007). Also CA1 supports pattern separation, establishing connections between distinct CA3 representations and corresponding input patterns in the entorhinal cortex (Norman, 2010). CA1 plays a critical role in mnemonic discrimination by functioning as a "match-mismatch" detector, highlighting disparities between the retrieved original item and the lure (Duncan et al., 2012): in this sense, CA1 cells show greater autonomy from a pattern-specific mechanism, enabling a higher level of arbitrary associations (Leutgeb and Leutgeb, 2007) and encoding spatio-temporal information of the context (Barrientos and Tiznado, 2016). Both these two processes are necessary to form a representation of the context in which events are experienced, that critically depends on the hippocampus: hippocampal damage profoundly impairs CFC, regardless of any particular procedural manipulation used (Broadbent and Clark, 2013).

However, these functions integrate within a much more complex fear circuit, ultimately leading to the engagement of the amygdala component and the subsequent manifestation of the behavioral response (Figure 3; for a complete review, see Tovote et al., 2015).

The amygdala can be thought as the command center for initiating fear-related behaviors, playing a central role in forming associations between neutral stimuli and aversive events (LeDoux, 2000). The amygdala's internal circuitry consists of densely interconnected nuclei that facilitate the processing of fear-related information. First of all, the basolateral nuclei of the amygdala (BLA) receive inputs from various brain sources, including the hippocampus, sensory areas, and the prefrontal cortex and serves as a critical hub, integrating and processing sensory information related to the current environmental state (Janak and Tye, 2015). Principal neurons receive inputs from the hippocampus and sensory areas and send outputs to other amygdala nuclei, as well as to cortical and subcortical regions; interneurons, on the other hand, modulate the activity of principal neurons and play a crucial role in shaping the flow of information within the amygdala (LeDoux, 2007). The output pathways from the BLA involve projections to the lateral hypothalamus and the periaqueductal gray: connections with the first trigger autonomic arousal responses, such as increased heart rate and sweating, which are important components of the fear response; connections with the second leads to freezing behavior (Phelps and LeDoux, 2005). Finally, reciprocal connections with the prefrontal cortex allow a top-down regulation of fear responses: here the integration of emotional and cognitive processes allow the amygdala to modulate behavior and perception based on the context and individual experiences (LeDoux, 2007).

Concerning the amygdala microcircuitry, central nucleus (CeA) receives inputs from the BLA and other amygdala nuclei, as well as from cortical and subcortical regions, and it coordinates autonomic, endocrine, and behavioral responses to fear; the medial nucleus (MeA), receives inputs from the olfactory system and is particularly involved in the processing of olfactory-related fear responses, detecting and integrating chemosensory information associated with threatening stimuli. Finally, the lateral nucleus (LA) serves as a primary sensory entry point for auditory information: it receives direct inputs from the auditory thalamus and

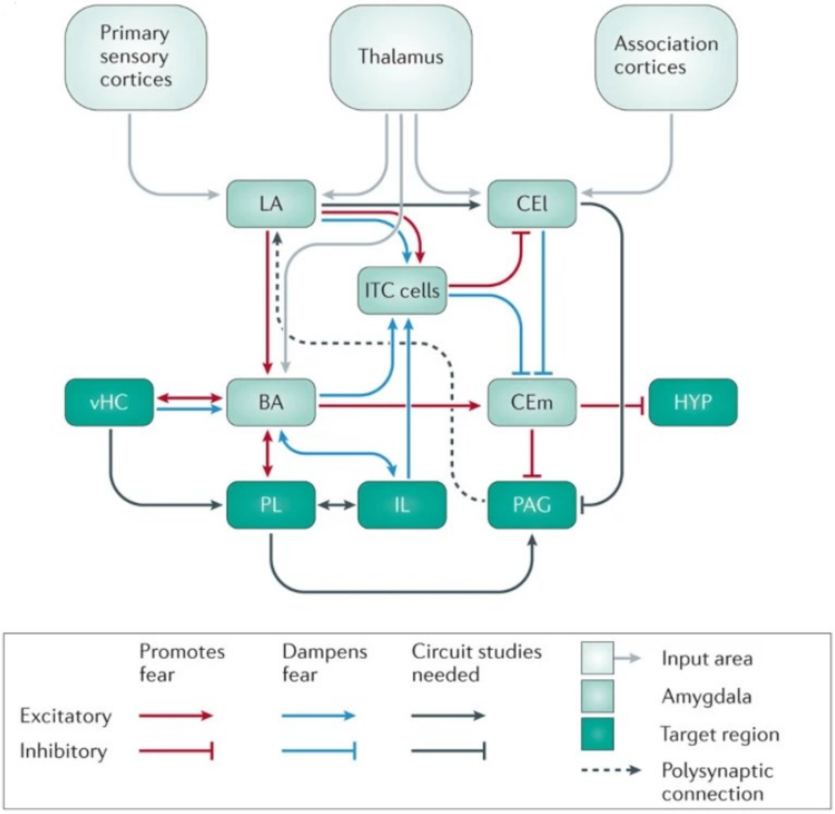
Primary sensory cortices
Thalamus
Association cortices
LA
CEl
ITC cells
vHC
BA
CEm
HYP
PL
IL
PAG
Promotes fear
Dampens fear
Circuit studies needed
Excitatory
Inhibitory
Input area
Amygdala
Target region
Polysynaptic connection

Figure 3. Schematic representation of the excitatory and inhibitory pathways that make up the fear circuitry. Numerous nuclei within the amygdala, including lateral amygdala (LA) and lateral central amygdala (CEl), are employed in receiving sensory signals from various corticothalamic hubs, serving as crucial sites for fear-related plasticity. This plasticity is influenced by interconnected communication pathways made by the basal amygdala (BA) with the ventral hippocampus (vHC) and the prelimbic cortex (PL). In turn, central amygdala nuclei (such as those in the medial central amygdala, Cem) transmit signals to hypothalamic and brainstem centers, regulating fear-driven behaviors. Information originating from the infralimbic cortex (IL) directed towards the basal amygdala (BA) and intercalated cells (ITC) plays a pivotal role in suppressing fear signals emerging from the lateral central amygdala (CEl) nuclei heading towards the hypothalamus (HYP) and the periaqueductal grey (PAG). (From Tovote et al., 2015)

projects to the BLA, contributing to the auditory processing of fear-related stimuli (for a review see LeDoux, 2007, or Janak and Tye, 2015).

So, by virtue of their neural correlation, the amygdala can strongly modulate the activity of the hippocampus. In CFC, inactivation of the BLA attenuates the consolidation of hippocampus-dependent context memory (Huff and Rudy, 2004), while the activation of the BLA, whether through behavioral stress or direct electrical stimulation, exerts a biphasic influence on hippocampal plasticity: an immediate excitatory impact and, subsequently, a persistent inhibitory effect

(Akirav and Richter-Levin, 1999). Studies have also shown that hippocampal theta oscillations, the “on-line” state of the hippocampus (Buzsáki, 2002), are associated with amygdala activity during fear conditioning (Seidenbecher et al., 2003), suggesting the involvement of synchronized neural activity between these regions.

Collectively, these studies underscore the tight interaction between these two key nodes of a complex and hierarchical system, due to their relationship with other structures of the central nervous system and to their intrinsic organization. In conclusion, the amygdalohippocampal network represents a powerful correlate of conditioned fear and, if the amygdala detects potential threats, the hippocampus provides a functional map to the relevant cortical sites that host the content of experiences and organize a behavioral outcome.

1.3 Looking for the physical substrates of memory

There are two strict requirements to determine if a neuron (or a set of neurons) is a candidate to sustain the formation or the retrieval of a mnestic trace: its inactivation must impair memory (requirement of necessity) and its activation must be sufficient to activate memory (requirement of sufficiency). For some, even necessity and sufficiency may be not “necessarily sufficient” (Denny et al., 2017) and at least three criteria should be met: increase of activity should be observed only in a population of cells activated by the specific learning; the increase should be dependent on plasticity associated with the learning episode; third, reactivation of these cells should result in behavioral recall (Tonegawa et al., 2015).

On the road to come to these conclusions, Josselyn and colleagues (2007) first provided evidence for a neuronal selection during memory formation, finding that the probability that LA neurons (see section 1.2) were recruited into a conditioned-fear memory trace was strongly influenced by their available levels of cAMP-responsive element-binding (CREB), an intracellular protein that plays a key role in RNA transcription that supports LTP (Nguyen and Woo, 2003): although many of these neurons received sensory inputs related to the fear conditioning experience, neurons infected with CREB (fused to a green fluorescent protein, GFP) had a three times greater chance of being activated by the task than their noninfected neighbors (Figure 4a); in CREB-deficient animals, the chance was even 10 times greater (Han et al., 2007; Figure 4b).

To identify those neurons activated by fear conditioning and, at the same time, infected by the CREB-vector, researchers took advantage of the transcriptional time course of the activity-dependent gene Arc (activity-regulated cytoskeleton-associated protein; see section 1.8): under basal conditions, neurons contain very low levels of ARC, but neuronal activation produces a transient burst in this RNA synthesis, that is rapidly delivered to the neuron and its dendrites (Guzowski, 1999). Arc belongs to a specific class of genes, the immediate early genes (IEGs), whose transcription is rapidly and transiently induced in response to neuronal activity (Bahrami and Drabløs, 2016); unlike many other genes, IEG expression

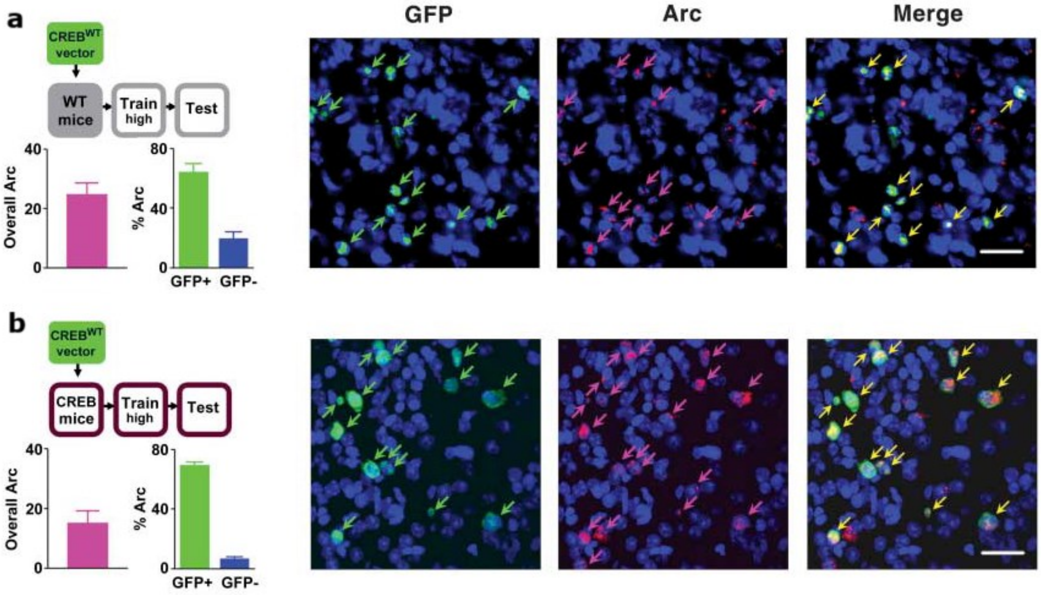

Figure 4. Neurons that most express CREB are those that are most recruited to the fear memory trace. a) On the left, proportion of Arc+ LA neurons (i.e., involved in the memory trace) in WT mice infused with CREB-vector. In the middle, the probability of detecting Arc+ nuclei was higher by a factor of ~3 in neurons with CREB- vector than in non-infected neighbors. On the right, confocal images of LA nuclei (in blue): GFP+ labeling (green arrows), ARC+ labeling (pink arrows), GFP+/Arc+ double labeling (yellow arrows). **b**) In CREB-deficient mice, probability of detecting Arc+ nuclei was even higher by a factor of ~10. (Modified from Han et al., 2007)

is directly induced by latent transcription factors, so protein synthesis is not required for their expression after a stimulus (Hawk and Abel, 2017). Not surprisingly, there has been a massive use of IEGs in neuroscience because their near-instantaneous activation provides a molecular link between experience and subsequent modification of the brain, especially those with the fastest induction: Arc, c-fos, Zif268 and Npas4 mRNA levels peak after stimulation is usually within 30 minutes in vivo (Sun and Lin, 2016). Thus, IEGs expressions are strongly interpreted as a marker of neural activity: a positive correlation has been found between IEG expression levels and average neural calcium activity, and even higher with maximum calcium activity (Mahringer et al. 2019).

Once the neuronal candidates for learning have been identified, Josselyn's group proceeded with the first "necessity" study at the level of a cell ensemble (2009), ablating only these cells and testing the effect on the fear memory expression. Using a combination of approaches, they infected LA to overexpress

CREB and they confined to CREB-enhanced neurons the expression of the receptor for the diphtheria toxin (DT), a neural toxin that induces a rapid apoptotic cell death: once administered, diphtheria specifically targeted and killed only these cells, leaving the others unaffected (Figure 5a). This selective deletion permanently erased the expression of the fear memory: the observed amnesia was «specific, robust, persistent and not due to a disruption in either reconsolidation or overall LA function» (Han et al., 2009). Also, deleting a similar portion of randomly selected LA neurons via the toxin had no effect on freezing behavior, showing a causal link between neurons with high CREB levels and the fear expression (Figure 5b).

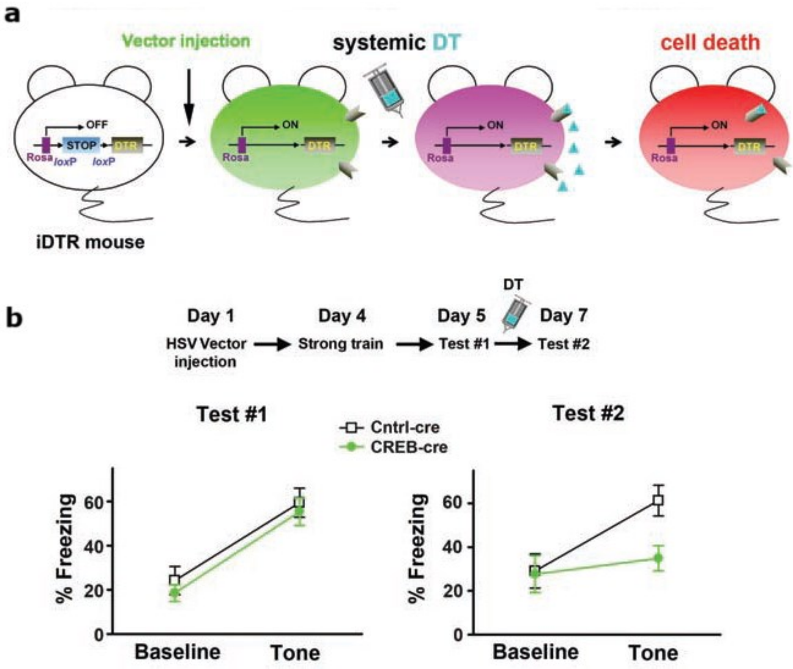

Figure 5. Ablating LA CREB-overexpressing neurons, but not a similar portion of random neurons, erases a fear memory. a) In white, iDTR transgenic mice (see Buch et al., 2005), able to express DT receptors (DTRs) in a Cre-recombinase (cre)-inducible manner, expressed DTR under control of a loxPflanked STOP cassette (see Bapst et al., 2020). In green, LA is injected with CREB-vector (CREB-cre), or a control vector that induces apoptosis in similar portion of not fear-activated neurons (Cntrl-cre). In pink, injected DT binds DTRs, which are expressed as cre removes the STOP cassette. In red, DT-driven cellular apoptosis. **b**) During test 1, which occurs before DT injection, the Cntrl-cre and CREB-cre mice exhibit similar levels of freezing in response to an auditory fear conditioning; in test 2, which occurs after the injection, only CREB-cre mice (and not Cntrl-cre mice) show significantly lower freezing levels than those shown in the previous test. (Modified from Han et al., 2009)

A few years later (2012), the group led by Susumu Tonegawa performed the first "sufficiency" experiment, labeling and reactivating a specific population of neurons activated by learning. First, they injected a viral vector in DG to express channelrhodopsin-2 (ChR2) under a tetracycline-responsive element (TRE, see below) promoter in the DG area of the hippocampus, fused to an enhanced yellow fluorescent protein (EYFP). When exposed to light of a specific wavelength (usually blue light), the ChR2 protein undergoes a conformational change that forms a pore across the cell membrane, allowing positive ions to depolarize the neuron. This constitutes an extraordinary control tool in the now "classic" field of optogenetics (Mahmoudi et al., 2017). For this reason, an optical fiber was implanted over DG by the authors to be able to activate ChR2 with light. They also took advantage of a c-fos-tTA transgenic mouse: the c-fos promoter controlled the expression of the tetracycline transactivator (tTA), that is the principal component of a Tet-off system for doxycycline-inducible gene expression (for a review, see Das et al., 2016): in this specific configuration, the administration of doxycycline (dox) antibiotic inhibited c-fos promoter-driven tTA from binding its TRE target, preventing ChR2-EYFP expression in neurons (Figure 6a).

During the first behavioral phase, habituation in a context A, mice were kept on dox; subsequently, dox was removed for the fear conditioning phase in a context B, in order to allow ChR2-EYFP expression in activating neurons. Finally, dox was introduced again for the recall phase in the context A, in order to prevent other neurons from expressing ChR2: cells that were part of the hippocampus index during conditioning could be identified and now reactivated with light (Figure 6b). Mice, that were safe in the context A (which had never been associated with the shock), exhibited high levels of freezing while the blue light was on; on the contrary, these dramatically decreased when the light was off, indicating a strong light-induced fear memory recall (Figure 6c). If there was no footshock during the conditioning phase (Figure 6d), or if the injected construct lacked ChR2 (Figure 6e), mice did not show any light-induced fear memory response. «This is the first demonstration that directly activating a subset of cells involved in the formation of a memory is sufficient to induce the behavioral expression of that memory» (Liu et al., 2012).

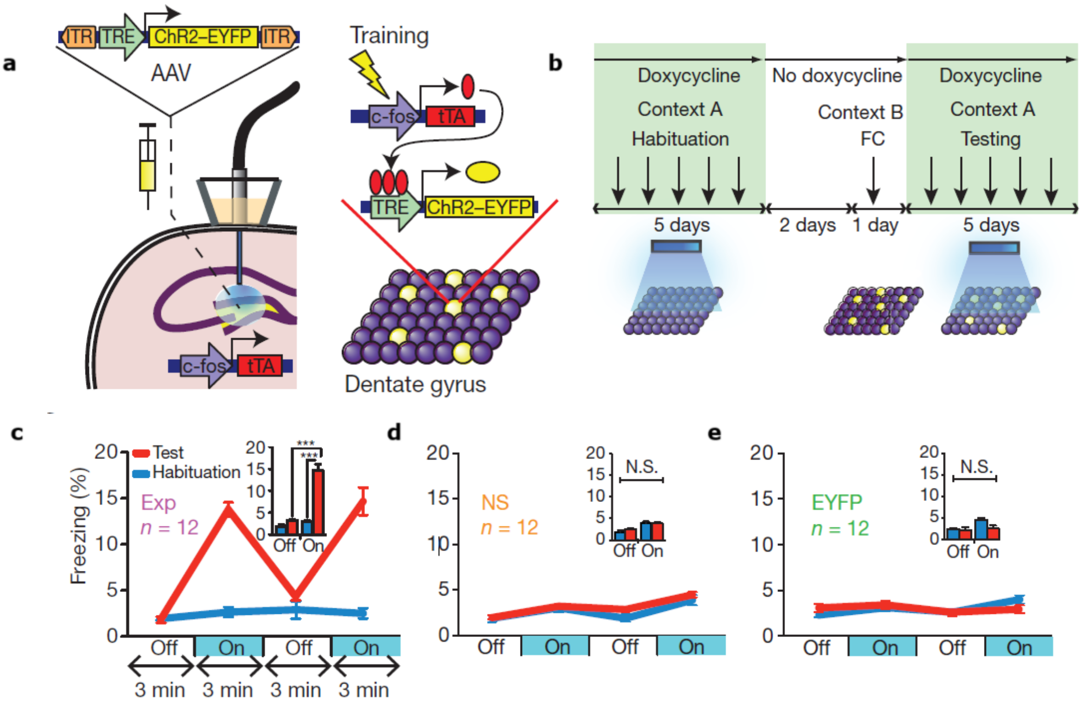

a
ITR
TRE
ChR2–EYFP
ITR
AAV
c-fos
tTA
Training
c-fos
tTA
TRE
ChR2–EYFP
Dentate gyrus
b
Doxycycline
Context A
Habituation
No doxycycline
Context B
FC
Doxycycline
Context A
Testing
5 days
2 days
1 day
5 days
c
Freezing (%)
Test
Habituation
Exp
n = 12
***
***
Off On
Off
On
Off
On
3 min
3 min
3 min
3 min
d
NS
n = 12
N.S.
Off On
Off
On
Off
On
e
EYFP
n = 12
N.S.
Off On
Off
On
Off
On

Figure 6. Reactivating DG cells, active during a memory encoding, is sufficient to establish a memory recall. a, left) c-fos-tTA transgenic mice are injected with AAV9-TRE-ChR2-EYFP and implanted with an optical fibre; **right**) only by removing doxycycline (dox) from the system, training activity can induce expression of tTA, which binds its target TRE and allows to label training-activated neurons by ChR2-EYFP. **b**) Mice are habituated for 5 days with both light and dox on in a context A; then, dox is removed for 2 days and, on the third, mice are fear-conditioned in a context B; finally, mice are tested for 5 days in context A while on dox. **c**) Light-on phases of the recall test show significantly higher levels of freezing than the light-off phases, **d**) while no difference if a different group (NS) does not undergo the shock during training, **e**) or if another group (EYFP) is injected with a construct in which Chr2 is absent. (Modified from Liu et al., 2012)

Ramirez and colleagues (2013) took this work and this procedure to the next level, resulting in a fear conditioning association with a context in which the US was never even delivered. To realize this, hippocampal neurons that were active during the exploration of a context A were labeled with ChR2 and a fluorescent red protein (mCherry); then, after interrupting the labeling window with doxycycline, mice were fear-conditioned in a different context B and neurons that had been active during exploration of the context A were reactivated via photostimulation. Fear memory was finally tested in either the original context A or a completely novel context C (Figure 7a): mice displayed freezing in context A (even though they had never been shocked in that context) but not in context C, indicating that freezing was context-specific: they literally created a “false” fear memory in the hippocampus (Figure 7b).

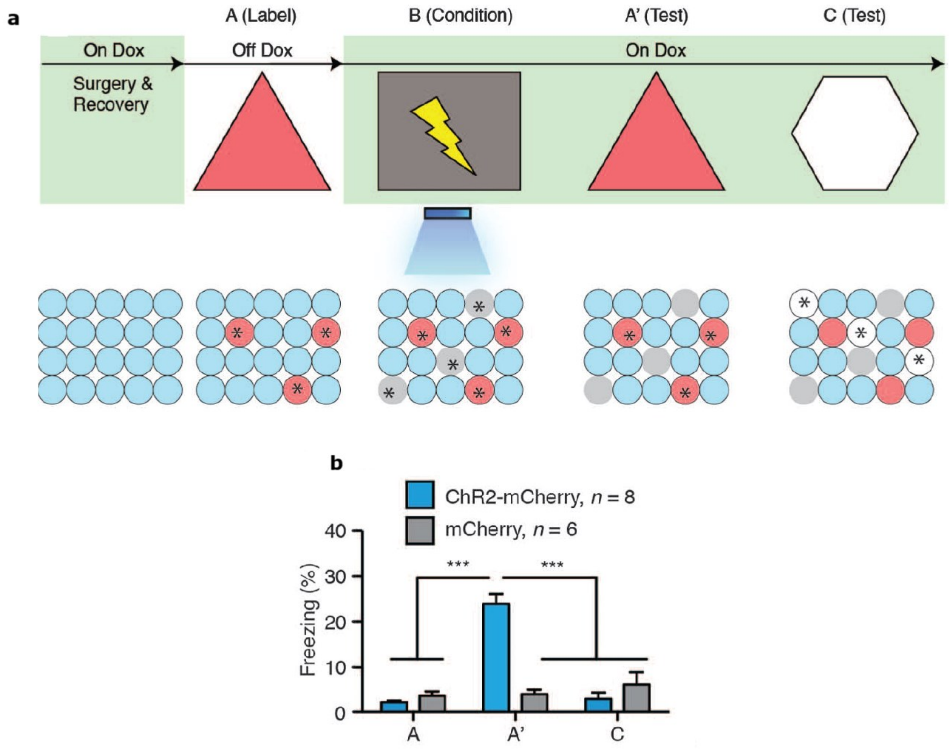

Figure 7. A false contextual fear memory can be induced by light reactivation. a) After the vector injection, mice were habituated in a context A while off dox, in order to let DG neurons be labeled by ChR2-mCherry; then, mice were put on dox and conditioned in a context B along with delivery of light pulses. Finally, freezing was tested in context A and in a completely novel context C. In red, ChR2-mCherry neurons encoding context A; in gray, neurons encoding context B; in white, neurons encoding context C; marked with asterisks, neurons activated by context exposure or light stimulation. **b**) Freezing dramatically increased in context A but not in context C for the experimental mice (Chr2-mCherry); no difference for the control mice (mCherry). (Modified from Ramirez et al., 2013).

The Frankland lab recently pushed this approach to the extreme, showing that an appropriate neural stimulation allows to create a memory even in the total absence of natural stimuli. To build a mnestic trace without the need of sensory experience, Vetere and colleagues (2019) chose to pair photostimulation of an olfactory glomerulus (to mimic a specific odor, which serves as CS), with photostimulation of distinct neural projections that mediate either aversion or reward (to mimic the valence of the stimulus, which serve as US. Figure 8a-b). Only the presentation of an odor that corresponded to the targeted olfactory glomerulus (and not another odor) induced memory recall, and mice either approached or avoided this odor depending on the valence of the US pathway they stimulated during training: mice behaved as if they had experienced a specific past sensory event (Figure 8c-d). Also, levels of c-Fos expression assessed in the central olfactory system regions and in the regions implicated in associative memory were highly correlated between both natural (real odor memory) and artificial conditions (glomerulus photostimulation), suggesting that the two types of memory engaged similar neural circuitry (Figure 8e).

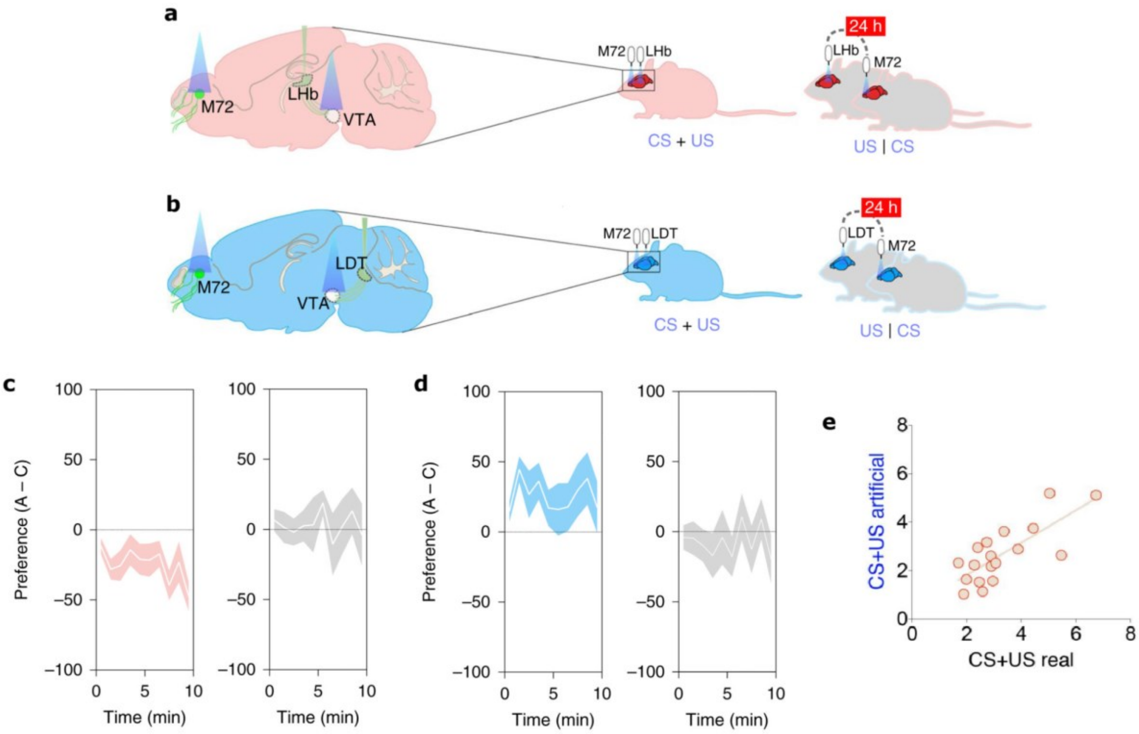

Figure 8. Two photostimulations can replace US and CS in the creation of a conditioned memory. **a**) During training, photostimulation of lateral habenula (LHb) - medial ventral tegmental nucleus (VTA) projections, known to mediate aversion (Lammel et al., 2012), is paired (CS+US) or not (CS|US) with photostimulation of M72 olfactory sensory neurons (Jiang et al., 2015); 1 day later, preference for M72-activating odorant (acetophenone) is tested. **b**) The same is done in another group, by photostimulating laterodorsal tegmental nucleus (LDT) - lateral VTA projections, known to mediate attraction (Lammel et al., 2012). **c**) LHb-VTA CS+US mice (pink) avoided acetophenone, but not the CS|US mice (grey); **d**) LDT-VTA CS+US mice (sky blue) are attracted to acetophenone, but not the CS|US mice (grey). **e**) Post-training C-Fos levels are assessed in 18 brain regions, including associative memory regions: they are highly correlated between both real (acetophenone presentation) and artificial (M72 photostimulation) conditions. (Modified from Vetere et al., 2019).

Together, all these experiments show that, despite a great difference in terms of nature and purpose, informations are equally engraved somewhere into the brain as physical memory traces: engrams (from Greek, ἐν «in» + γραμμα «letter»), as formulated from Richard Semon in the early last century (1921). They are all "written" in a book made of neural cells, that are able to rapidly change itself and to preserve the effects of the experience over time, be it remote (long term memory, LTM) or just passed (short term memory, STM. See Atkinson and Shiffrin, 1968). Thus, operatively, we properly refer to "learning" as the process of acquiring these informations, and to "memory" as the persistence of learning in a state that can be revealed at a later time (Squire, 1987): the first writes the engrams on the book, while the second reads them for us. An efficient and continuous reiteration of this sequence in specific populations of cellular engrams tunes our behavior to our environment and, ultimately, makes us who we are. Very recently, Roy and colleagues (2022) have provided the most comprehensive mapping available of cellular engrams and high-probability engram–holding regions. Their multiple approach, drawn on c-fos brain-wide activity mapping, natural memory recall and optogenetic reactivation-based memory recall, allowed to identify additional brain regions as holders of CFC engram cell ensembles (brainstem, hypothalamus, thalamus, cortex and midbrain): an unexpected list of 117 brain regions in which c-fos was activated during contextual fear conditioning. Even more interesting, the simultaneous chemogenetic reactivation of multiple engram ensembles mimicked the same levels of natural memory recall, something never achieved in optogenetic reactivation studies of a single engram ensemble, in which animal freezing is significant but lower than that expressed in presence of natural recall cues. This strongly suggests that a memory is stored not just in a single engram cell ensemble, but in a functionally connected engram ensembles' complex distributed broadly across the brain; this is also consistent with the multiple trace theory (Nadel and Moscovitch, 1997), that assumes that the redundancy of a mnestic trace, shared by the activity of distributed neurons that serve as an index, protects an old memory from disruption and from partial damage of a neural region (as the hippocampus).

The acquisition and recall of a given memory necessarily involves some change in the existing status of neurons, thus implying a strong relationship with functional and structural synaptic plasticity phenomena.

1.4 Activity-dependent synaptic plasticity

Timothy Bliss and Terje Lomo in 1973 intelligently took advantage of the hippocampal synaptic circuitry to stimulate a set of fibers in a subfield while monitoring activity in the region where these fibers terminated. Specifically, they applied stimulation to the perforant path and they recorded the evoked responses in the DG. After determining that a stronger stimulus from the stimulating electrode (presynaptic fibers of the perforant path) evoked a stronger response from the recording electrode (postsynaptic cells of DG), they proceeded to admister a high-frequency sequence (HFS) of stimuli to the perforant path. A test stimulus (single-pulse stimulation), which remained the same before and after stimulation, evoked a stronger response after the tetanic stimulation compared to before, and this effect endured for several hours of recording.

So, the electrical stimulation of the perforant path dramatically amplified the activity of the DG granular neurons; similar findings are observed when the Schaffer collateral fibers are stimulated and the response of the pyramidal cells in the CA1 subfield is recorded (Figure 9a): a brief, high-frequency train of stimuli causes a long-lasting increase in the excitatory postsynaptic potential (EPSP) amplitude. The EPSP, detected by the recording electrode, measures the rate at which sodium (Na+) ions are leaving the recording field and depolarizing synapses on the postsynaptic neurons. As the number of ions flowing into the postsynaptic neurons increases, so does the strength of connections linking the pre- and the postsynaptic neurons.

This phenomenon, that clearly shows how synaptic strength can be functionally modified by neural activity, is known as long-term potentiation (LTP) and relies on a remarkable convergence of actions occurring through the N-methyl-D-aspartate receptors (NMDAr) of the postsynaptic cell. These ionotropic receptors are responsible for the primary excitatory neurotransmitter in the central nervous system: the glutamate. When the glutamate is released from the presynaptic terminal, it binds to the postsynaptic NMDAr, allowing a substantial influx of CA^{2+} ions that triggers LTP. However, calcium cannot enter the cell unless magnesium is removed from the pore of the channel: at the same time, the glutamate must bind to α-amino-3-hydroxy-5-methyl-4- isoxazolepropionic acid receptors (AMPAR), allowing an influx of sodium ions (Na^+) and producing a depolarization in the synapse. If, and only if these two events occur together, we observe a change in the conformation of the NMDA receptor and incoming calcium can potentiate a synapse (Figure 9b). So, if NMDA receptors are critical for the initial induction of LTP, AMPA receptors are critical for the NMDA receptors and for the expression of LTP (for a review, see Lüscher and Malenka, 2012). Indeed, the application of an NMDAr antagonist (such as APV) before a high-frequency stimulation prevents the induction of LTP but has no effect if the application takes place after LTP has been induced; in contrast, an AMPAR antagonist (such as CNQX) blocks both the induction and expression of LTP (Collingridge et al., 1983).

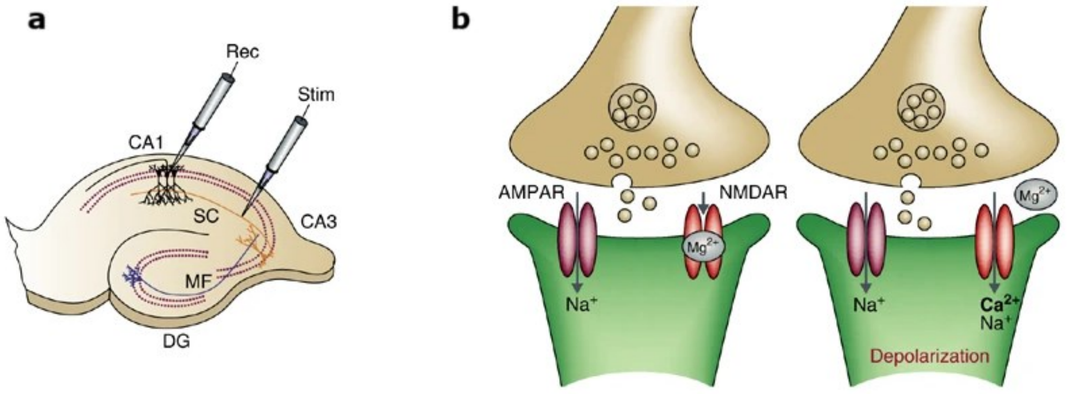

Figure 9. NMDAr-dependent LTP in the CA1 region of the hippocampus. a) A typical electrodes placement for studying LTP: a stimulating electrode (Stim) is placed in the Schaffer collateral fibers (SC); resulting EPSPs are recorded from a recording electrode (Rec) in CA1. **b**) Representative model of the induction dynamics of LTP at excitatory synapses: during basal activity (left), glutamate binds both the NMDARs and AMPARs. Na+ pass through the AMPAR channel but not through the NMDAR channel, blocked by Mg2+. Depolarization of the postsynaptic cell (right) removes the block, allowing an influx of both Na+ and Ca2+ into the spine. The increase of Ca2+ is determinant for triggering subsequent events of synaptic plasticity.(Modified from Citri and Malenka, 2007)

LTP exhibits three interesting and recurring properties: it requires the cooperative stimulation of different pathways, as it happens for the aforementioned Schaffer collateral fibers; it shows associativity, which means that a weak (and insufficient) stimulation of a single pathway can still lead to LTP if facilitated with concurrent activation of other synapses; finally, LTP is input specific, i.e. restricted to synapses activated by a strong stimulation and not spreading to the other synapses that contact the same neurons. In learning and memory, the first property results in the fact that only events that trigger sufficient inputs can result in memory storage; the second represents a mechanism of associative learning; the last one ensures the accuracy of memory storage (Hao et al., 2018). Everything can be reduced to a general operating principle, of which LTP is a specific biological manifestation: “cells that fire together wire together” (Shatz, 1992).

However, synaptic plasticity is not unidirectional and experience not only can strengthen synaptic connections but can also weaken them: if Schaffer collaterals are subjected to low frequency stimulation (LFS) for extended time periods, the response evoked by the test stimulus is markedly reduced (Dudek and Bear, 1993. Figure 10). This long-term depression (LTD), again, depends on NMDAr activation and postsynaptic Ca2+ entry, in particular, Ca2+ triggers LTD at low concentrations and triggers LTP at high concentrations (Bear, 1995). Based on the BCM model (Bienenstock et al., 1982), there is a certain threshold below which the result is LTD and above is LTP, depending on the level of postsynaptic response and on the average amount of postsynaptic activity. This regulation plays a fundamental role in allowing the neuron to maintain a variable range of output, based on the previous history of activation of the single synapses: if they were only reinforced, they would become static and dysfunctional: LTP can be “saturated” by repeated induction episodes (Cao and Harris, 2014). So, especially if the synapse has already been subject to LTP, the threshold is raised, increasing the probability that an additional calcium influx will provoke LTD to maintain synaptic plasticity (Bear, 1995). This “plasticity of synaptic plasticity” is named metaplasticity and it is manifest as a change in the ability to induce subsequent synaptic plasticity, such as LTP or LTD (Abraham and Bear, 1996); it can occur homosynaptically, if the effects of synaptic activity are specifically confined to the previously activated synapses, or heterosynaptically, if they extend to neighboring non-activated synapses, beyond those synapses that were initially involved.

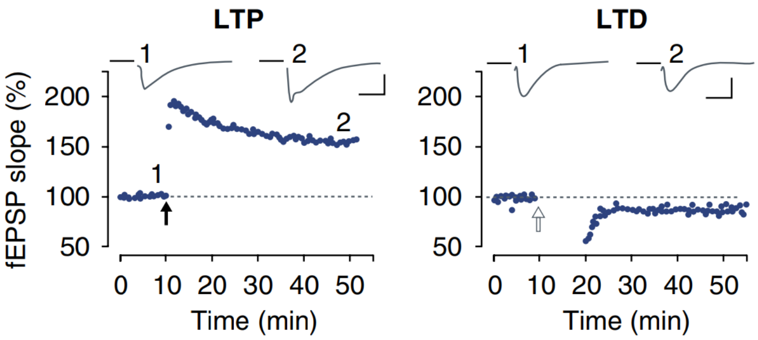

Figure 10. Induction of LTP and LTD in the CA1 region of the hippocampus. Field excitatory postsynaptic potentials (fEPSPs) are plotted as a function of time. On the left, a high-frequency stimulation (1 s of 100 Hz stimulation; black arrow) is applied to elicit LTP; on the right, low-frequency stimulation (twice 3 min of 5 Hz stimulation, 3 min interval; white arrow) is applied to elicit LTD. The steepness of the slopes represent the amount of synaptic depolarization around the recording electrode (Modified from Citri and Malenka, 2007).

Both LTP and LTD can be considered activity-dependent forms of Hebbian plasticity, named after the psychologist who first postulated the adaptation of neural activity in learning processes (1949), synthesized in the adage "Neurons that fire together, wire together".

Of note, strong stimulation of synaptic circuits potentially leading to LTP may provoke positive feedback loops (to which the hippocampus is intrinsically prone because of its reverberant internal connectivity) of activity-dependent changes: once LTP is induced, as above, synapses can enter a cycle that leads to further potentiation, ultimately resulting in hyperexcitability. But also LTD, if it occurs in an unrestrained manner, could lead to pathological synapse silencing and elimination (Collingridge et al. 2010). In order to prevent this, neurons are also able to sense their own excitability and trigger negative-feedback homeostatic mechanisms to restrain synaptic activity within a physiological range (Fernandes and Carvalho, 2016): the most extensively studied form of homeostatic plasticity at excitatory synapses, known as synaptic scaling, occurs through postsynaptic mechanisms of regulation of AMPAR abundance at the synapse (see section 1.6). By adjusting the number of AMPARs, synaptic scaling helps restore the balance between excitation and inhibition and it is of particular importance in sustaining synaptic plasticity of the Hebbian type.

Together, these synaptic strengthening dynamics (and their “control” mechanisms) are functional correlates of memory: when we learn new information or acquire new skills, systems of cells (or cell ensembles) are repeatedly active at the same time, synapses between them strengthen and they form circuits in which the activity of one neuron facilitates activity in the other (Hebb, 1949). These circuits represent the substrate of a certain, particular learning experience: as memories are recalled, the same neural circuits are reactivated, and this process strengthens the synaptic connections even further, making the memory more robust and easier to recall in the future. On the other hand, if some neurons are rarely or never activated together, the synaptic connection weakens, leading to reduced communication between them and the loss of their content.

So, different cell ensembles - in different brain regions - may support different aspects of an experience: hippocampal cells ensembles may represent the context (Ghandour et al., 2019), amygdala cells ensembles may represent valence information (Redondo et al., 2014), cortical cell ensembles may represent distinct sensory information (Sacco and Sacchetti, 2010).

1.5 Structural substrates of activity-dependent synaptic plasticity

Synapses reveal an amazing capacity to reconfigure their strength in response to different patterns of neural activity; in fact, the same stimuli that induce LTP and LTD can also trigger structural modifications in the underlying neural architecture. For instance, LTP-enhanced activity can lead to the growth of new synaptic contacts and dendritic structures that host them, while reduced activity during LTD can prompt their retraction or elimination (Holtmaat and Svoboda, 2009; Bosch and Hayashi, 2012; see also section 1.7). In turn, formation of these new structures can provide additional sites for synaptic connections, facilitating the expression of synaptic plasticity mechanisms, while their elimination can refine neuronal networks, preventing excessive synaptic noise and optimizing the specificity of synaptic signaling.

Evolution has selected an elegant and dynamic structure to host the majority of postsynaptic excitatory synapses in the brain: the dendritic spine, a sub-micrometer membrane protrusion that covers the surface of neuronal dendrites. Ranging in volume from 0.001 to 1 μm^3 (Hotulainen and Hoogenraad, 2010), spines are composed by a thin and cylindrical segment (neck) that connects the dendritic shaft to the portion at the tip of the spine (head), where organelles, receptors, and the synaptic machinery involved in receiving and processing signals from other neurons is contained (see section 1.6). Both components are extremely variable in shape and size and dendritic spine morphology can change in response to neuronal activity to an extent that is correlated with the strength of excitatory synapses (Adrian et al., 2014).

In response to the high-frequency stimulus that produces LTP, a cascade of biochemical processes increases the head volume, while the neck becomes shorter and wider: the spine becomes potentiated (Figure 11). The enlargement of the spine head is accompanied by increased exposure of AMPARs at the postsynaptic membrane, ultimately resulting in a higher sensitivity to glutamate

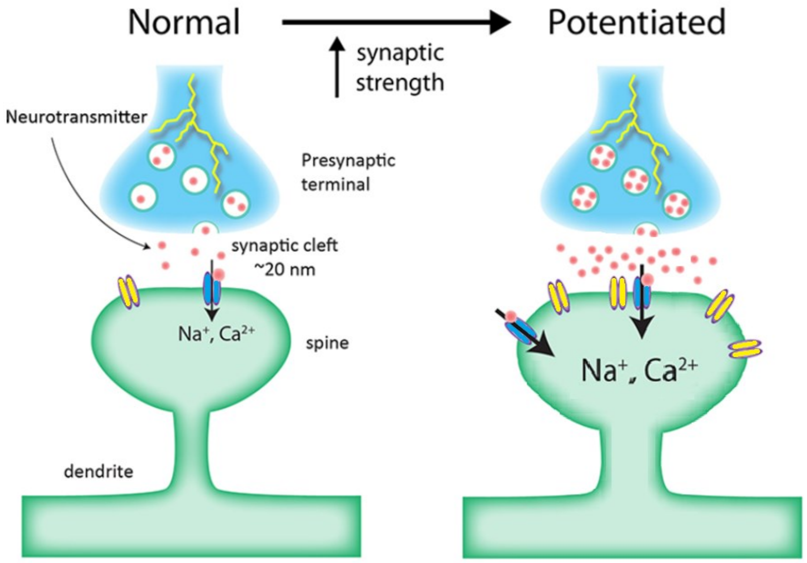

Figure 11. Simplified representation of a dendritic spine potentiation: a high-frequency stimulation induces biochemical processes that change a spine morphology, by broadening its neck and increasing its head volume, and leads to a massive insertion of AMPArs (in yellow) at the postsynaptic membrane, much more sustained manner then NMDArs (in sky blue). (Modified from Woodruff et al., QBI).

(Matsuzaki et al., 2001; Holtmaat and Svoboda, 2009). Similarly, LTD causes spine head shrinkage (Zhou et al., 2004). This mobility is allowed by the presence of different and separate pools of actin filaments along the structure, which become more dynamic as you get to the head of the spine (Honkura et al., 2009); the initial induction of LTP requires a rapid disassembling of actin filaments, followed by a rapid reassembling in order to initially trap new AMPA receptors (Rudy, 2014; see section 1.6).

Since spine volume is proportional to its age and probability of lasting in time (Yasumatsu et al., 2008), these activity-dependent changes in geometry are thought to be necessary to make the structure resistant over time and less susceptible to further modification. In a smaller spine, Ca^{2+} accumulates in the head in sufficient quantity to initiate the biochemical cascades needed to alter synaptic strength: as the neck is narrow, calcium hardly diffuses towards the dendrite and the only way out is via Ca^{2+} extrusion pumps located in the head; conversely, potentiated spines remove Ca^{2+}faster so that increases in its concentration become more moderate and transient, making the spine less susceptible to Ca^{2+}-induced plasticity processes (Noguchi et al., 2005; Hayashi and Majewska, 2005). Also, larger spines are more successful than smaller spines in both attracting and maintaining diffusing key proteins, as PSD-95 (Gray et al., 2006; see section 1.6). For these reasons, larger and mushroom-shaped spines can persist for long periods of time: they are less plastic, but more stable, “memory” spines. By contrast, thin spines are mostly transient, emerging and disappearing over a few days (Holtmaat et al., 2005); they maintain enough structural flexibility to be able to widen and then stabilize, or to shrink and then be dismantled. Containing many NMDArs, but few AMPARs, they are ready for potentiation via their addition, making them ideal candidates as "learning" spines (Bourne and Harris, 2007).

By virtue of these features, changes in the formation, elimination, and remodeling of spines have been extensively studied and manipulated with a large variety of methods and behavioral paradigms as a marker of synapses formation and activity-dependent connectivity (Runge et al., 2020). These studies gathered information on spine dynamics in basal and specific experimental contexts, like motor tasks (Xu et al., 2009) or sensory deprivations (Keck et al., 2008). Fear conditioning, for example, induces spine elimination in the frontal association cortex (Lai et al., 2012) and in the primary motor cortex (Xu et al., 2019), while an increase in spine formation in the auditory cortex (Lai et al., 2018), in BLA (Heinrichs et al., 2013), in the hippocampus and in the anterior cingulate cortex (Restivo et al., 2009). *In vivo* imaging studies also revealed specific spatial rules of dendritic spine disposition along the dendrites: Yang and colleagues (2014) found that spine formation is branch-specific: rates of spine formation on sibling dendritic branches (i.e., two branches split from the same branch) significantly differed after a training. Also, a learning task led to a rapid spine formation in clusters: a second new spine tends to form in close proximity to a first stable neighbor, in contrast with a baseline activity condition in which new spines appear to avoid existing stable spines on the same dendritic branch; in addition, within the same cluster, formation of a second spine is accompanied by the head enlargement of the first one (Fu et al., 2012). Further, clusters actively promote the survival of new spines, that is significantly lower in non-clustered spines even 4-6 weeks after (Frank et al., 2018).

It is now clear why most of the processes underlying plasticity have place at these functional sites. Now let’s take a look at the “control center” of the spine, located at the top of its head, which serves as both a signaling apparatus and a protein scaffolding for neurotransmitter receptors: the postsynaptic density (PSD).

1.6 The postsynaptic density: a moving mosaic

Potentiating a synapse depends on a rapid increase in the levels of Ca^{2+} and Na^+ ions within the spine. This stimulation-dependent boost in the amount of these ions, in turn, depends on increasing the number of AMPAR on the plasma membrane via activity-dependent changes in AMPAR trafficking (Malenka and Bear, 2004). Enhanced AMPAR exocytosis occurs during synaptic potentiation around the postsynaptic membrane, but also in extrasynaptic membrane away from synapses: extrasynaptic AMPARRs possesses a high mobility and, trough their lateral movement, they can be trapped and translocated to postsynaptic membrane (Hirano, 2018). Also, upon fast synaptic stimulation, lateral diffusion of extrasynaptic AMPARs allows a fast exchange of desensitized receptors with fresh functional ones, contributing to the fine regulation of synaptic efficacy (Kopach and Voitenko, 2013).

The LTP-produced rearrangement results in as many immobilized AMPARs as possible in the postsynaptic density (PSD), a membrane thickening that, under the electron microscope, appears as «a dense lamina just beneath the postsynaptic membrane» (Dosemeci et al., 2016. Figure 12a). This region

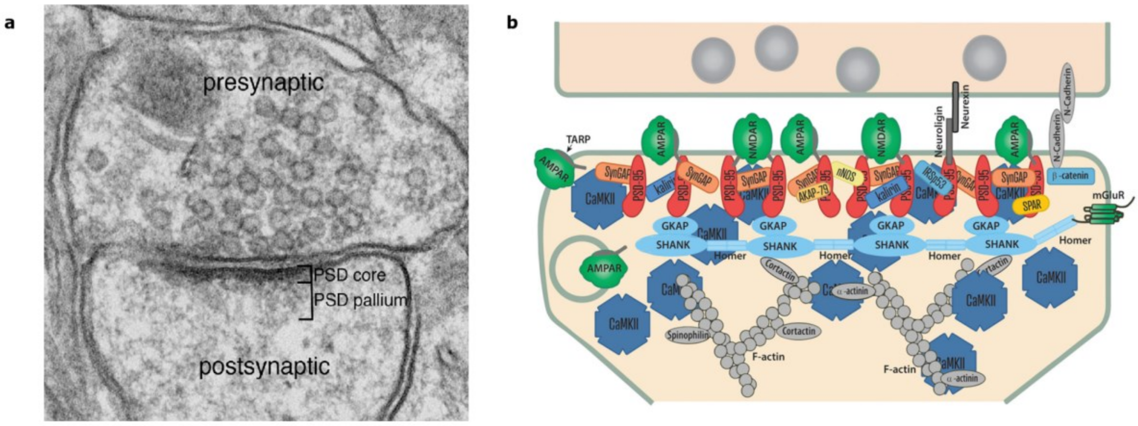
a
presynaptic
PSD core
PSD pallium
postsynaptic
b
TARP
AMPAR
NMDAR
Neuroligin
Neurexin
N-Cadherin
β-catenin
SynGAP
PSD-95
kalirin
nNOS
AKAP-79
IRSp53
SPAR
CaMKII
GKAP
SHANK
Homer
mGluR
Cortactin
α-actinin
Spinophilin
F-actin

Figure 12. Outside and inside the post-synaptic density. a) This is how PSD looks under the electron microscope; going towards the synaptic cleft, a PSD pallium and a PSD core region can be distinguished. (From Dosemeci et al., 2016). **b**) Cartoon representing a fraction of PSD protein mosaic organization. Listing a few from the base, the actin filaments of the spine (F-actin); in the middle, signaling and scaffolding proteins (PSD-95, SHANK, Homer, SynGAP, CAMKII); at the membrane, neurotransmitter receptors and adhesion proteins (AMPAr, NMDAr, mGlur, Neuroligin). (From Kennedy, 2018).

contains several hundreds of proteins that expose and align these glutamate receptors with the presynaptic neurotransmitter release zone (Figure 12b), representing both the best position to respond to incoming glutamate and the first processing station once information converges on the dendrite. For these reasons, the primary function of the PSD is to position proteins involved in plasticity-related signaling close to glutamate receptors, in order to fine-tune the strength of synaptic transmission. First of all Ca^{2+}, acting as a second messenger (Siegelbaum et al., 2000), plays a pivotal role in targeting these PSD proteins and starting a series of intracellular signaling cascades; once entered through the NMDAr, Ca^{2+} first binds to the ryanodine receptors (RyRs), contained by the smooth endoplasmic reticulum (ER) region that protrudes into the spine, releasing additional Ca^{2+} from the ER and amplifying the overall availability of Ca^{2+} in the spine (Berridge, 1998).

This increase in calcium activates the calcium/calmodulin dependent protein kinase II (CaMKII) which, in turn, changes the channel properties of the AMPAR: phosphorylating the Ser 831 site of the GluA1 subunit, CAMKII allows AMPAR to influx Ca^{2+} as well as Na^{+}. Calcium-permeable AMPARs (CP-AMPARs) mostly consist of GluA1-containing AMPA receptors and support acute synaptic potentiation, but are less stable at the synapse; calcium-impermeable AMPARs (CI-AMPARs) make up for most of the basal synaptic transmission and are more stable at the synapse, because of their interactions through the GluA2 subunit (Derkach et al., 2007). Accordingly, LTP involves early increases in GluA1-containing AMPARs, which are gradually replaced by GluA2-containing AMPARs (Shi et al., 2001).

Other kinases can phosphorylate other AMPAR serine sites, to provoke other effects: protein kinase A (PKA), activated by the second messenger Cyclic adenosine monophosphate (cAMP), phosphorylates the Ser 845 site, moving the receptors contained in intracellular endosomes to the extrasynaptic region; protein kinase C (PKC), activated by Ca^{2+}, phosphorylates the Ser 818 site, helping to anchor the receptor to the PSD (for a review, see Bredt and Nicoll, 2003). To ultimately immobilize the AMPA receptors in the PSD, CAMKII phosphorylates the serine residues of the Stargazin protein, that forms a complex with AMPAR: this releases Stargazin from the membrane and facilitates its binding with the PDZ domains of the Postsynaptic density protein of 95 kDa (PSD-95), which forms potential “slots” for trapping AMPA receptors that are laterally diffusing through the PSD (Opazo et al., 2010; Figure 13a).

PSD-95 is a member of the membrane associated guanylate kinase (MAGUK) family (which also includes PSD-93, SAP97 and SAP102); it is the most abundant scaffold protein in the PSD of the excitatory neurons (Cheng et al., 2006) and one of the most widespread throughout the brain. Its structure includes an SH3 domain, a guanylate kinase-like domain (GK) and three PDZ domains that bind to the C-termini of a broad repertoire of partners beyond AMPAR, including the aforementioned NMDAr, stargazin, and Neuroligin (Figure 13b). Dosemeci and

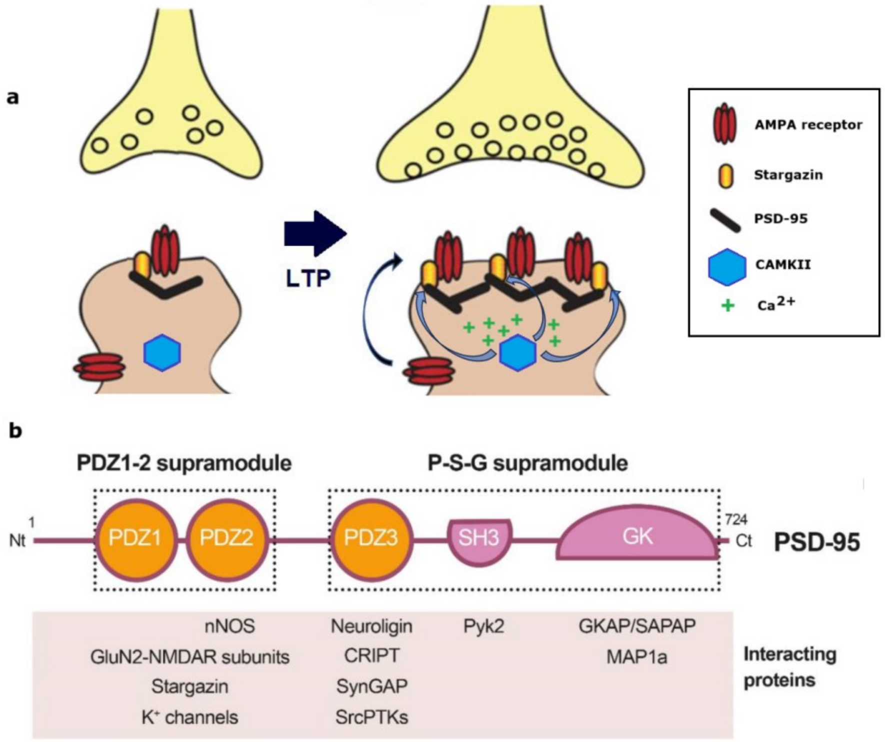
a
LTP
AMPA receptor
Stargazin
PSD-95
CAMKII
+ Ca^{2+}
b
PDZ1-2 supramodule
P-S-G supramodule
1
Nt
PDZ1
PDZ2
PDZ3
SH3
GK
724
Ct
PSD-95
nNOS
GluN2-NMDAR subunits
Stargazin
K$^+$ channels
Neuroligin
CRIPT
SynGAP
SrcPTKs
Pyk2
GKAP/SAPAP
MAP1a
Interacting proteins

Figure 13. PSD-95: scaffolding function and protein domains. a) PSD-95 PDZ domains (shown in b) indirectly interact with AMPARs through PDZ-ligands of AMPAR auxiliary proteins, such as stargazin/transmembrane AMPAR regulatory proteins (TARPs). LTP-inducing stimuli increase calcium into the spine, that activates CAMKII; this kinase, in turn, phosphorylates serine residues on Stargazin terminal (blue arrows), releasing terminal from the membrane and facilitates binding to PSD-95 complex. This allows to trap laterally diffusing AMPARs in the PSD (black arrow). (Modified from Keith and Hel-Husseini, 2008). **b**) PSD-95 protein structure is organized in different protein domains: three PDZ domains (PDZ1–PDZ3) followed by a Src homology 3 (SH3) domain and a guanylate kinase-like (GK) domain, distinguishable in two supramodules. Under each domain, some relative direct PSD interactors. (From Ugalde-Triviño and Díaz-Guerra, 2021).

colleagues (2007) tried to map the whole interactome of PSD: analyzing large, affinity-purified PSD-95 complexes derived from the synapse, a subset of the identified proteins were selected as likely to be consistent, integral components of the complex. Let's briefly describe some of them, starting from key scaffolding PSD proteins as Shank and Homer, that together form a mesh-like matrix structure, which serves as a binding platform for other synaptic proteins (Hayashi et al., 2009). The former, encoded by three genes SHANK1, SHANK2, and SHANK3, is involved in different synaptic functions, including spine morphogenesis, synapse formation, glutamate receptor trafficking and activity-dependent neuronal signaling; mutations in these genes are strongly associated with autism spectrum disorders (ASD; see Sala et al., 2015). The second ones also have isoforms belonging to three gene families, Homer 1, 2, and 3; among the different functions and implications in neurological disorders (see Szumlinski et al., 2006), Homer proteins are responsible in regulating the activity of metabotropic glutamate receptors (mGluRs), equally included in the list provided by Dosemeci (2007): along with AMPARs and NMDARs, mGluRs also mediate glutamatergic neurotransmission. mGluRs are G-protein coupled receptors that transduce signals via the interaction of intracellular G proteins, after their large extracellular N-terminal domain binds glutamate. Binding their C-terminus, Homer bridges mGluRs with inositol trisphosphate receptors (IP3Rs) to release calcium from the ER in the dendritic compartment (Tu et al., 1998). That represents an important second source of intracellular calcium recruited by an LTP-inducing high-frequency stimulation (Raymond and Redman, 2002), in addition to the aforementioned one mediated by the RyRs. Among the various isoforms of Homer, Homer1a is an IEG that is increased by synaptic activity through the ERK1/2 pathway, while Homer1b/c are constitutively expressed. A negative loop, in which Homer1a activity-dependent increases inhibit the scaffolding ability of Homer1b/c, diminishes synaptic strength by modulation of dendritic spine morphology and AMPA/NMDA receptors activity (Stephens et al., 2017).

Another critical protein of the complex, neuroligin, is a cell adhesion protein involved in the initial establishment of synapses during development. Phosphorylated by CAMKII (Bemben et al., 2014), it binds to neurexins on the presynaptic side, which are another family of cell adhesion molecules, promoting the trans-synaptic connectivity of the pre- and postsynaptic components by the Ca2+-dependent interaction of their alternatively spliced extracellular domain. This ensures the proper alignment of neurotransmitter release sites and receptors (Araç et al., 2007).

SynGAP is a GTPase-activating protein (GAP) which specifically targets Ras G-proteins that, in turn, are essential for activation of the mitogen-activated protein kinase (MAPK) cascade by growth factors or by intracellular Ca^{2+} (Fukunaga and Miyamoto, 1998). The first MAPK to be discovered is the extracellular signal-regulated kinase (ERK) 1/2 cascade, that has strongly been shown to be involved in the induction and maintenance of LTP (Thomas and Huganir, 2004; Wortzel and Seger, 2011).

Finally, protein kinase M zeta (PKMζ) is a constitutively active kinase that facilitates the release of non-synaptic pools of GluA2 AMPAR for insertion in the PSD and disrupting the normal endocytosis that normally removes these receptors from the synapse, maintaining the number of AMPAR required to support a potentiated response to glutamate (Sacktor, 2011).

By organizing all these signaling and structural proteins into complexes and trapping AMPARs at the postsynaptic membrane, PSD-95 plays a key role in synaptic transmission (Pedersen et al., 2017) and in stabilization of young synaptic contacts (Taft and Turrigiano, 2013). A knockdown of PSD95 arrests the morphological development of glutamatergic synapses: although early LTP is unaffected, spine morphological changes are reduced and spines are less stable over the time (Ehrlich, 2007); loss of PSD95 function also impairs learning, formation and expression of fear conditioning memories (Fitzgerald et al. 2015).

Formation of late-phase LTP involves enduring structural changes, including expansion of the PSD and enlargement of the dendritic spine head (Yang et al., 2008; see also section 1.5). These structural changes, in turn, depend on actin accumulation as well as new protein synthesis (Bramham et al., 2008): concerning the former, one of the major regulators of actin dynamics in spines is cofilin, an actin side-binding protein. At its normal, unphosphorylated state, cofilin depolymerizes actin filaments; vice versa, phosphorylated cofilin no longer interferes with actin polymerization, leading to elongation or stabilization of filaments, and this is strongly implicated in spine enlargement at a late phase of LTP (Bosch et al., 2014). Concerning the latter, consolidation of synaptic changes strictly depends on the generation of new proteins: protein synthesis inhibitors (such as anisomycin) block the development of a long-lasting LTP (Frey et al., 1988). These new proteins can derived from genomic signaling cascades (synapse-to-nucleus and soma-to-nucleus signaling, see Adams and Dudek, 2005), in which second messengers or their kinase targets enter the nucleus to phosphorylate transcription factors, such as the cAMP-responsive element-binding (CREB) protein, which binds to the cAMP response element (CRE) of its target gene promoters to initiate transcription. But new proteins also come from local translation of mRNAs that is already present in the dendritic spine region: translation machinery (ER, Golgi elements, ribosomal assemblies) is also directly present in the local dendritic region (Steward and Schuman, 2001). This process involves the regulation of a class of mRNAs located in the dendritic spine region called terminal oligopyrimidine tracts (TOP) mRNAs, that encode for proteins that are part of the translational machinery. Synthesis of TOP mRNAs is regulated by the mammalian target of rapamycin (mTOR) kinase: preventing the activation of mTOR selectively impairs the late phase of LTP, without influencing the initial induction (Tang et al., 2002). The brain-derived neurotrophic factor (BDNF), in turn, plays a critical role in activating the mTOR-TOP pathway, binding to Tropomyosin receptor kinase (TrkB) receptors, that are co-localized with NMDA receptors in the PSD (Bramham and Messaoudi, 2005).

The synaptic tagging, or tag-and-capture theory (Frey and Morris, 1998), which will be detailed in the next paragraph, effectively explains how all these products, necessary for a late phase of LTP (L-LTP) and its maintenance, may be targeted to a specific set of synapses; it also allows to understand why the synapse, rather than the neuronal nucleus, is the truly fundamental unit of long-lasting neuronal plasticity (Martin, 2009).

1.7 Synaptic tagging and capture

It is now clear that allocation of memory to specific engram cells is anything but random: the excitability of a cell is one of the key factors in determining whether or not it will participate in the “engram game” (see section 1.3). However, in the same way as neurons, not all synapses are recruited and respond identically to a given stimulation pattern (Varga et a., 2011). Activation of synapses that are proximal to the cell body has a relatively large effect on the likelihood of a cell to generate an action potential; on the contrary, the activity of single distal synapses, that is far from the cell body, has a small effect on somatic excitability. It’s the synchronous activation of groups of distal synapses, arranged in spatial proximity, that can lead to a significant and sustained depolarization of the soma (Major et al., 2013).

In the sequence memory model described by Hawkins and Ahmad (2016), neurons have unique benefits by assigning unique roles to the different synaptic integration zones: their pyramidal neuron model is directly activated only by patterns detected on proximal synapses, whereas it maintains longer lasting sub-threshold depolarization for patterns detected on basal and apical synapses. So, both neuronal and synaptic allocation, sharing also the same molecular mechanisms (for example, CREB signaling), function hand-in-hand to determine where memories are stored in neural circuits (Rogerson et al. 2014).

Within the same neuron, some subsets of synapses may appear more “competent” than others in participating in long-lasting forms of plasticity. In a study with the Aplysia culture system (Martin et al., 1997), the group led by Eric Kandel set up an in vitro preparation in which a single Aplysia sensory neuron forms synaptic contacts with two separate motor neurons. Five pulses of serotonin were applied to the connections made onto one of the motor neurons, resulting in an increase in the EPSP at that connection, but no change at the opposite connection. Microinjection of anti-CREB antibodies into the sensory neuron blocked this branch-specific facilitation produced by local serotonin application, showing that the EPSP increase was dependent on CREB-mediated transcription in the nucleus, but also restricted to a single set of synapses: only the latter, and not those at the opposite connection had used the neuronal plasticity-related products (PRPs). Moreover, even a single subthreshold serotonin pulse, if administered to the opposite connection within a certain time window (both before and after) from the five pulses, was able to generate a long-lasting increase in EPSP, "capturing" that transcription-dependent increase in synaptic strength. In contrast, long-term facilitation could not be captured if the single pulse was administered 4h before or 4 h after the five pulses (Martin et al., 1997; Casadio et al., 1999).

The same "capture" phenomenon was observed also during hippocampal LTP by Frey and Morris (1997, 1998), exploiting the fact that separate sets of Schaffer collateral fibers synapse on different territories of the dendritic arbor of of CA1 neurons. They applied strong stimuli to one input (S1) to CA1, in order to produce a sustained, protein synthesis-dependent L-LTP, then weak stimuli to a second

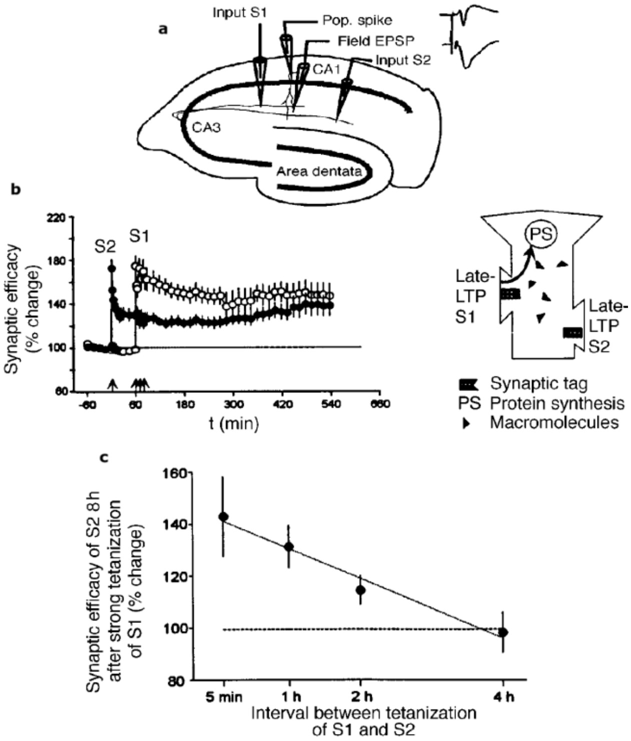

Figure 14. A weakly stimulated pathway can "capture" the L-LTP from a second strongly stimulated pathway. a) Two electrodes are placed in two independent inputs (S1 and s2) of an hippocampal slice, converging on the same CA1 neuronal population. **b, left**) An "early-before-late paradigm": if S2 E-LTP-inducing stimulation is administered 5 to 60 minutes before S1 L-LTP-inducing stimulation, S2 E-LTP is transformed into L-LTP. **right**) This happens because a synaptic tag in S2 is able to sequester plasticity-related macromolecules produced by SA1 L-LTP. (**c**) This effect diminishes if the interval between the "weak" and the strong tetanization is 2h; it is completely abolished after 4h. (Modified from Frey and Morris, 1998)

input (S2) that normally would produce only an early phase LTP (E-LTP; Figure 14a). As long as the stimuli to S1 and S2 were delivered within a certain time window (Figure 14c), L-LTP was observed both at S1 and S2: the weaker stimulus “hijacked” the PRPs generated by the strong stimulus (Figure 14b).

Together, these findings have led to the elaboration of the "synaptic tagging and capture" hypothesis (Frey and Morris, 1998), according to which the PRPs reach all of the synapses, both active and inactive, but they can only be captured and used productively at those synapses that have been tagged by local activity (Alarcon et al., 2006). The capability of weakly stimulated synapses to undergo LTP, if a second pathway had been strongly stimulated, was interpreted by the authors of the theory as a sign of tagging: that “tag” allowed these synapses to capture PRPs even though they had not been responsible for triggering their synthesis (as strongly stimulated synapses had been able to do) (Frey and Morris, 1998).

Strikingly, synaptic tagging and capture-like phenomena have been shown to occur at individual dendritic spines: LTP induced at one spine can affect the LTP-inducing probability at a nearby spine in response to subthreshold stimulation (Harvey et al., 2008). This is inversely related to time between stimuli and inter-spine distance, with no synaptic tagging if spines are located more than a certain distance on the same dendritic branch or on different dendritic branches (Govindarajan et al., 2011). Also, E-LTP at one spine can be converted to L-LTP: this protein synthesis-dependent process can take place if L-LTP was previously induced at a nearby spine (Govindarajan et al., 2011). These dynamics also concern the clustering of spines, as a result of synaptic allocation mechanisms: clustering of potentiated synapses happens in close proximity to previously activated synapses (Fu et al., 2012; see also section 1.5). Finally, induction of LTP at two nearby spines causes a reduction in spine growth rate (that indicates synaptic potentiation), suggesting a competition between them for a limited supply of PRPs (Govindarajan et al., 2011).

The CAMKII-CREB pathway is critical for the synthesis of the PRPs shared between tagged synapses. These proteins include GluR1, Homer1a, PKMζ, ARC (see section 1.6). Due to its properties, the latter will now be discussed in detail.

1.8 Arc

The immediate-early gene (IEG) Arc (also called Arg3.1; see also section 1.3) is one of the most sensitive genes to sensory, learning and memory inputs (Minatohara, 2016). Arc transcription is strongly induced by synaptic activity and newly synthesized Arc mRNA tends to localize close to synapses that have been subjected to a pattern of activity capable of activating NMDA receptors (Steward et al., 2015). In CA1, for example, Arc RNA appears in neuronal nuclei within 2 minutes of a new experience (like exploring a novel context), and, within about 15-20 minutes, processed Arc mRNA translocates from the nucleus to the cytoplasm (Guzowski et. al. 2001, Figure 15). Transport of Arc in dendrites can reach the speed of 65 μm per minute, thus reaching - from the nucleus - the synapses on the distalmost dendritic branches in just a handful of minutes (Dynes and Steward, 2007).

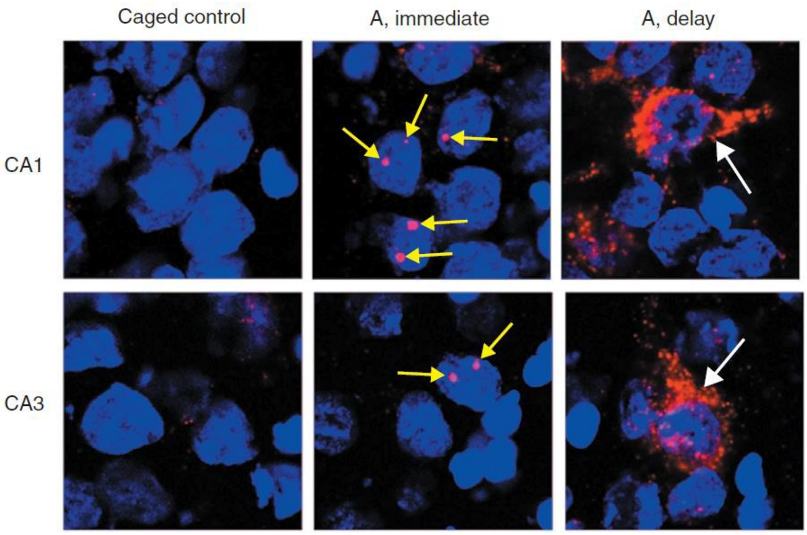

Figure 15. CA1 and CA3 Arc RNA induction by exploration of a novel environment. Within 2 minutes of activation (A, immediate), Arc RNA (stained with CY3 fluorochrome, in red) appears in the nuclei (stained with DAPI, in blue). These intranuclear foci (yellow arrows) disappear after 16 min from the removal of stimuli (A, delay), indicating that neural activation occurs during this interval (2-16 min) before the sacrifice of the animal. 20-45 min after the induction, processed ARC mRNA accumulates in the cytoplasm (white arrows). (From Guzowski et al., 2001)

Okuno and colleagues (2012) showed that Arc is also captured at inactive or less active synapses, finding a specific accumulation of Arc at post-synapses that were opposed to pre-synapses inhibited through tetanus toxin. During the late phase of LTP, Arc protein transported into dendritic regions is initially delivered into both the potentiated and non-potentiated synapses, then is gradually lost from the active synapses and accumulates in the non-potentiated synapses: this phenomenon, called inverse synaptic tagging, may serve to alter the inducibility of synaptic plasticity at later periods (Okuno et al., 2018). This Arc accumulation in the inactive synapses is mediated by selective interaction with the inactive form of CaMKII, and plays a key role in increasing AMPAR removal from the postsynaptic membrane (Okuno et al., 2012).

Activation of NMDAr and ERK are necessary for Arc transcription following LTP induction; Arc is also induced pharmacologically in hippocampal neurons by BDNF (for a review, see Bramham et al., 2010). To get to their destination, Arc mRNAs are packaged into messenger ribonucleoprotein (mRNP) complexes, which are transported by the motor protein complex kinesin along dendritic microtubule tracks to their target synapses; Arc 3' untranslated region (UTR) also contains two cis-acting dendritic targeting elements (DTE) required for a specific dendritic localization (Kobayashi et al., 2005).

Giorgi and colleagues (2007) found that Arc is a natural target for a process known as nonsense-mediated RNA decay (NMD), needed for rapidly downregulating aberrant mRNAs: an exon-junction complex (EJC), made by an RNA-binding tetrameric core, can target Arc due to the presence of two introns in the 3'UTR of the gene and then be removed after the first round of translation, leading Arc mRNA to be destructed upon translation: following a BDNF treatment, more than half of the Arc mRNA transport beads in dendrites colocalize with one of the EJC proteins, suggesting that Arc is translationally silent prior to reaching the dendrite.

Very interestingly, recent publications showed that Arc protein can bind Arc mRNA forming virus-like capsids (closely matching those of Human Immunodeficiency Virus, HIV) that can be transferred extracellularly between neurons via extracellular vesicles. The transferred Arc mRNA can undergo activity-dependent translation in the target cells (Pastuzyn et al., 2018) and, if this trans-synaptic transport is disrupted, synaptic plasticity is blocked (Ashley et al., 2018). Such a mechanism could complete or even make unnecessary a tagging dynamic to direct the arc mRNAs to such activated sites (Budnik and Thomson, 2020).

The systematic work by Messaoudi and colleagues (2007) clearly highlights how Arc behaves a multifunctional hub protein (Nikolaienko et al., 2018), showing its dual role in the consolidation of the LTP: regulation of local actin polymerization and activity-induced gene expression. Concerning the former, L-LTP is associated with marked hyperphosphorylation of cofilin (see section 1.6) and Arc is directly responsible for this: infusion of Arc antisense oligodeoxynucleotides (AS-ODNs), 2 h after LTP induction, results in rapid dephosphorylation of cofilin and a corresponding large loss of new actin filaments available. Concerning the latter, a pretreatment with AS-ODNs reverses a well established HFS inducing-LTP when applied up to 160 minutes, but not when applied 280 minutes after the induction; the same happens with a BDNF inducing-LTP, rapidly reversed by AS-ODNs treatment at 2 h (but not 4 h) after BDNF infusion. This finding strongly links the BDNF→mTOR→TOP pathway signaling (see section 1.6) to the synthesis of Arc and to long-lasting synaptic changes that support potentiated synapses (Bramham et al., 2010; Rudy, 2014): this pathway, in turn, regulates postsynaptic localization of PSD-95 (Yoshii and Paton, 2014) and translation of many dendritic spine mRNAs (Bramham and Messaoudi, 2005), placing Arc as a central piece of the PSD mosaic. Cao and colleagues (2013) found that even abnormal levels of Arc can disrupt BDNF signaling, interfering with BDNF-induced recruitment of PSD-95, whose association with TrkB - in turn - is critical for an intact BDNF signaling.

1.9 Analyzing plasticity at the single-synapse resolution

We have seen in paragraph 1.3 that researchers, taking advantage of IEGs as Arc, have devised creative ways to manipulate cellular engrams *in vivo*, up to creating a false memory, or even an “experience without experience”.

Now, consider that the volume of a young adult mouse hippocampus is - on average - 19 mm^3 (Peirce et al., 2003) and that there are more than 2 synapses for each cubic micron of tissue (Santuy et al., 2020): only this microscopic region of the central nervous system contains more than $4x10^{10}$ synaptic connections between neurons, and each of these is subject to others’ (see section 1.7) and to its own (see section 1.4) synaptic plasticity events. Thus, shifting the study of memory engrams from the cellular to the synaptic level becomes a crucial point to extend our perspective of the “neural algebra” at the basis of learning and memory. Studying and manipulating synaptic engrams represents the starting point of this conceptual and methodological change of perspective. In this regard, investigating whether and how memory is allocated at specific subsets of synapses of a given neuron has remained a major puzzle, owing to the lack of fully appropriate methodologies for manipulating individual synapses *in vivo* (Gobbo and Cattaneo, 2020; Ma and Zuo, 2022).

A first step to fill this gap has been the pioneering work by Hayashi-Takagi and colleagues (2015), who created a genetically encoded tool for the manipulation of dendritic spines activated by behavioral learning: an Activated Synapse-targeting Photoactivatable Rac1 (AS-PaRac1). This fusion protein took advantage of a photoactivatable version of Rac1 (PaRac1, Wu et al., 2009), a small GTPase that normally induces phosphorylation of cofilin to promote actin polymerization and spine remodeling (see section 1.6): an aberrantly increased activity of Rac1, on the opposite, inhibits cofilin and led to spine shrinkage and elimination (Pyronneau, 2017). In this way, light stimulation could selectively erase the AS-PaRac1-expressing spines in the primary motor cortex (M1), when the construct was injected. Activity-dependent expression of this photoprobe was regulated by Synaptic Activity Responsive Elements (SARE) in the Arc gene promoter, whose activation is dependent on synaptic Ca2+ influx through NMDARs (Inoue et al., 2010). Finally, localization specificity at the activated synapses (AS) was ensured by fusing this photoprobe to DTE of Arc mRNA, for dendritic input specificity, and to a shortened PSD-95 (i.e., deletion of two PDZ domains), which is known to concentrate at the PSD but cannot bind with the major PDZ binding proteins (which it minimizes undesirable effects of PSD-95 overexpression. First, thanks to the presence of a yellow fluorescent protein (Venus) in the construct (Figure 16a), spines that had recently been activated by a motor skill test were labeled; then, a selective shrinkage of these spines disrupted the acquired motor learning (Figure 16b). Very interestingly, this acquired learning was not affected by an identical manipulation of spines evoked

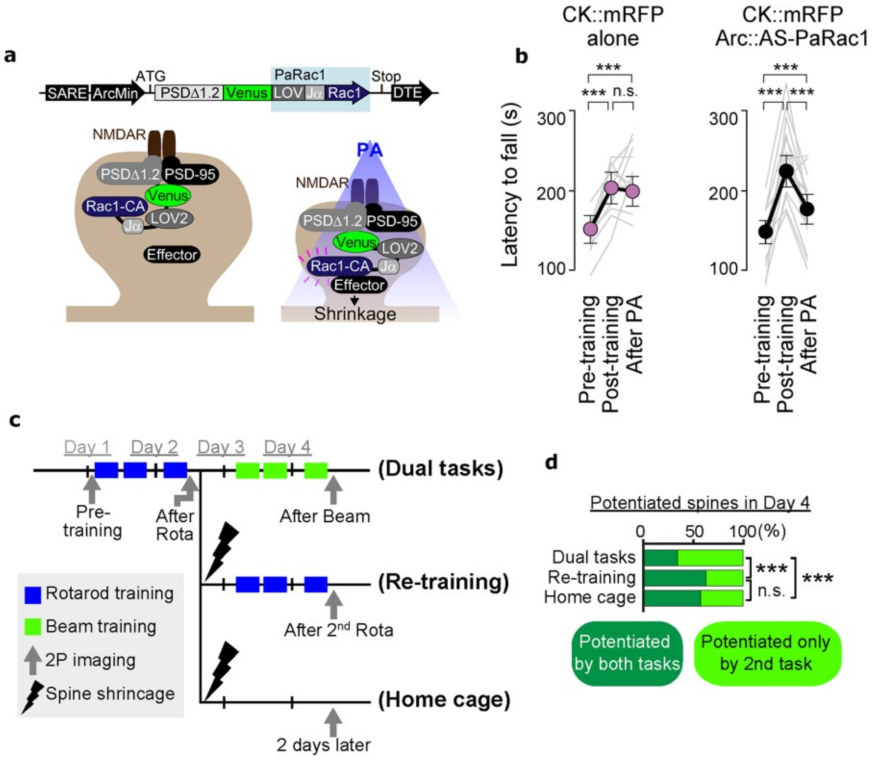
a
SARE
ArcMin
ATG
PSDΔ1.2
Venus
PaRac1
LOV
Jα
Rac1
Stop
DTE
NMDAR
PSDΔ1.2
PSD-95
Venus
Rac1-CA
LOV2
Jα
Effector
PA
NMDAR
Shrinkage
b
CK::mRFP alone
CK::mRFP Arc::AS-PaRac1
***
*** n.s.
*** ***
Latency to fall (s)
300
200
100
Pre-training
Post-training
After PA
c
Day 1
Day 2
Day 3
Day 4
(Dual tasks)
Pre-training
After Rota
After Beam
(Re-training)
After 2nd Rota
(Home cage)
2 days later
Rotarod training
Beam training
2P imaging
Spine shrincage
d
Potentiated spines in Day 4
0
50
100(%)
Dual tasks
Re-training
Home cage
***
n.s.
***
Potentiated by both tasks
Potentiated only by 2nd task

Figure 16. Selectively labeling and eliminating activated spines by AS-PaRac1. a) AS-PaRac1 is transcribed under control of the synaptic activity-responsive element (SARE) and the Arc minimal promoter (Arc min); LOV2 domain binds the N-terminus of Rac1 constitutively active form (Rac1-CA), blocking Rac1 effector binding site until blue light undocks LOV Ja helix (for a review on LOV systems, see Czapiński et al., 2017). This allows an optical control (by photoactivation, PA) of spine shrinkage. **b**) Both two groups of mice, one infected with the experimental and a filler construct CAMKII:mRFP (monomeric red fluorescent protein) and the other with the filler alone, show a better rotarod performance after training (Post-training), but only AS-PaRac1 group fall much more (latency of falling) after administration of light (after PA). **c**) M1 neurons are sparsely transduced with Arc::AS-PaRac1-Venus and CAG::mRFP and mice undergo different training protocols: in the dual task protocol, they sequentially learn a rotarod and a beam task in the first and the latter 2 days, respectively. Re-training group is subjected to the rotarod task in the first 2 days, learning-potentiated spines are shrinkaded by PA, then rotarod task is re-trained. Finally, home cage group is subjected to the rotarod task and subsequent PA, then mice are not manipulated for 2 days. **d**) Proportion of newly potentiated spines, that have not undergone potentiation in the first 2 days, significantly increases only in the dual task group. (Modified from Hoshiba et al., 2017)

by a second, different motor task in the same cortical region; also, more than half of the synaptic ensembles activated for the second task had not been potentiated by the first task, strongly suggesting that distinct tasks induced potentiation of distinct subsets of spine (Figure 16c and 16d).

This innovative approach was limited by the fact that shrinking via photoablation was an irreversible process that prevented subsequent manipulation of potentiated spines, thus allowing to demonstrate only the necessity of spine potentiation for motor learning, while the sufficiency of the activation of potentiated spines for memory recall could not be addressed. With this purpose in mind, the group led by Antonino Cattaneo designed an approach to image and activate potentiated synapses, named SynActive (SA, Gobbo et al., 2017), once again benefiting from the extraordinary advantages conferred by Arc UTRs: they expressed a variant of the optogenetic probe Channelrhodopsin (ChETA, Gunaydin et al., 2010), fused to the red fluorescent protein mCherry, between Arc 5'- and 3'- UTRs (Sa-Ch). Also, they fused to the C-terminus of ChETA-Cherry a short bipartite SYN tag, composed of the NMDAR C terminus and the PSD95-PDZ-binding consensus, in order to confer synaptic retention of SA-Ch protein (Figure 17a). To test a synapse-specific and protein-synthesis-dependent SA-Ch expression, they first demonstrated in culture that the number SA-Ch-positive spines dramatically increased with L-LTP-inducing treatments, while it decreased with NMDAR inhibition via AP5; also, translation inhibition with geneticin G418 blocked a BDNF effect on SA-Ch expression, demonstrating its dependence on novel protein synthesis (Figure 17b). Furthermore, glutamate uncaging induced SA-Ch expression at stimulated synapses, but not at neighboring synapses or at other synapses on the same dendrite (Figure 17c), paralleled by a long-lasting volume spine increase; both were blocked by a translation inhibition with anisomycin. Finally, light activation of expressed SA-Ch was sufficient to elicit calcium transients in most stimulated spines, but not when light was omitted: this mimicked the physiological activity of synapses, with an enrichment of CAMKII at Sa-Ch positive spines (Figure 17d).

Then, researchers expressed SA-Ch *in vivo* under the TRE promoter in the hippocampus of electroporated mice. Taking advantage of rtTA and the Tet-on

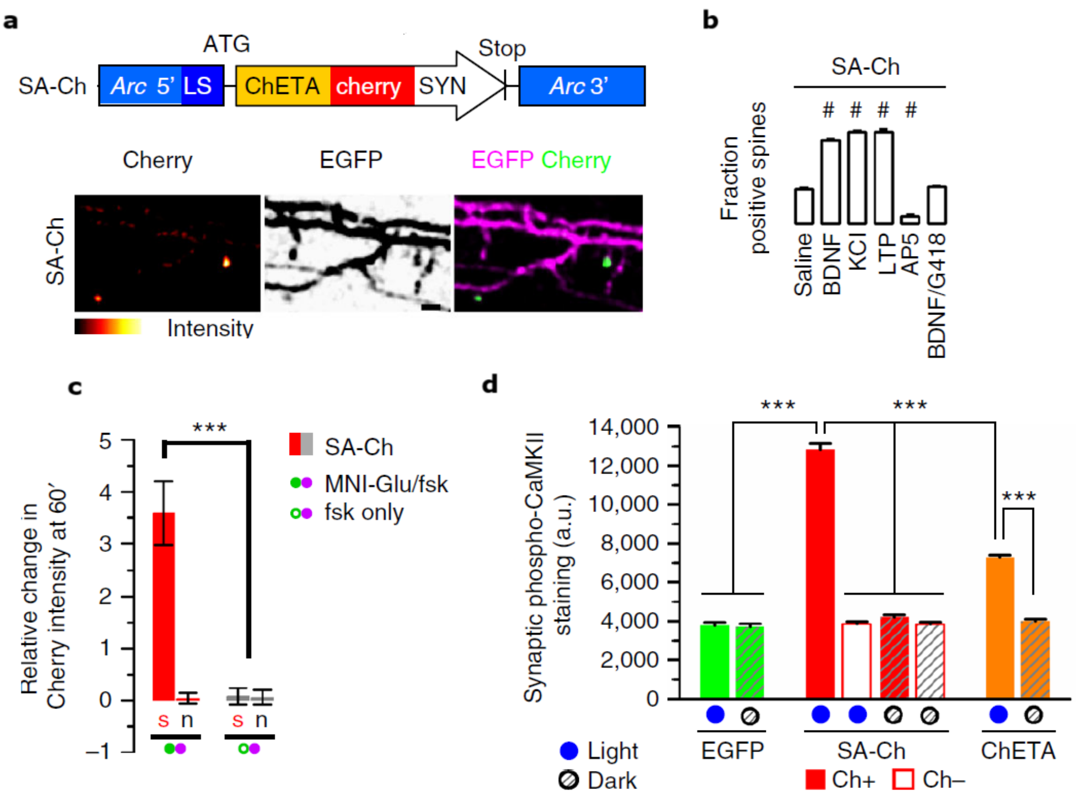

Figure 17. In vitro synapse-specific and protein synthesis-dependent SA-Ch expression. a) Expressed SA-Ch construct and patterns of dendritic expression for ChETA-Cherry (on the left), EGFP filler (in the centre) and merge (on the right). **b**) Fraction of SA-Ch-positive spines dramatically increases with L-LTP-inducing treatments (KCl, BDNF, NMDA-induced LTP), while it decreases with NMDAR inhibition via AP5, or blocking BDNF with geneticin G418 **c**) Glutamate uncaging induces SA-Ch expression only at stimulated synapses (s), measured as the change of mCherry intensity, but not at neighboring synapses (d); when MNI-glutamate is not present in the medium (fsk only), there is no Sa-Ch expression. **d**) Following a 3h pretreatment with CNQX, AP5 and TTX to reduce CAMKII background activation, neurons are light-stimulated, fixed and stained for phospho-CAMKII, that is significantly increased in Sa-Ch-expressing spines. Neurons with no Cherry signal (Ch-) are no different in expression respect to the neurons kept in dark and those expressing only EGFP; an increase is present in untargeted ChETA-Cherry-expressing neurons, that remains lower than that in Sa-Ch-expressing neurons. (Modified from Gobbo et al., 2017)

system (see Sun et al., 2007 for a review; see also section 1.3 for a Tet-off system), they were able to express Sa-Ch in a doxycycline-dependent restricted time window, almost exclusively at spines of electroporated neurons: an exposure to a novel context increased the number of SA-Ch spines along the dendrites of both CA1 and DG regions (Figure 18a), following a solid clustered distribution that was significantly more likely to express SA-Ch than a random one (Figure 18b and 18c).

Together with other reporters (Gobbo and Cattaneo, 2020), both AS-PARac1 and SA-Ch provide live access to potentiated synapses *in vivo*. However, SA-Ch appears to be more versatile, thanks to its non-destructive approach on potentiated spines. Also, SA-Ch seems to exhibit a more pronounced dependence on the translation control, facilitated by a larger segment of Arc 5’ UTR, which employs an internal ribosome entry site (IRES)-dependent translation initiation that considerably increases translation in dendrites (Gobbo and Cattaneo, 2020; Pinkstaff et al., 2001). Finally, the SynActive system allows to express virtually any reporter protein in a synaptic activity-dependent manner by only modifying the cDNA sequence translated into protein. The project illustrated below was built on these advantages and on the potential of this synaptic tool.

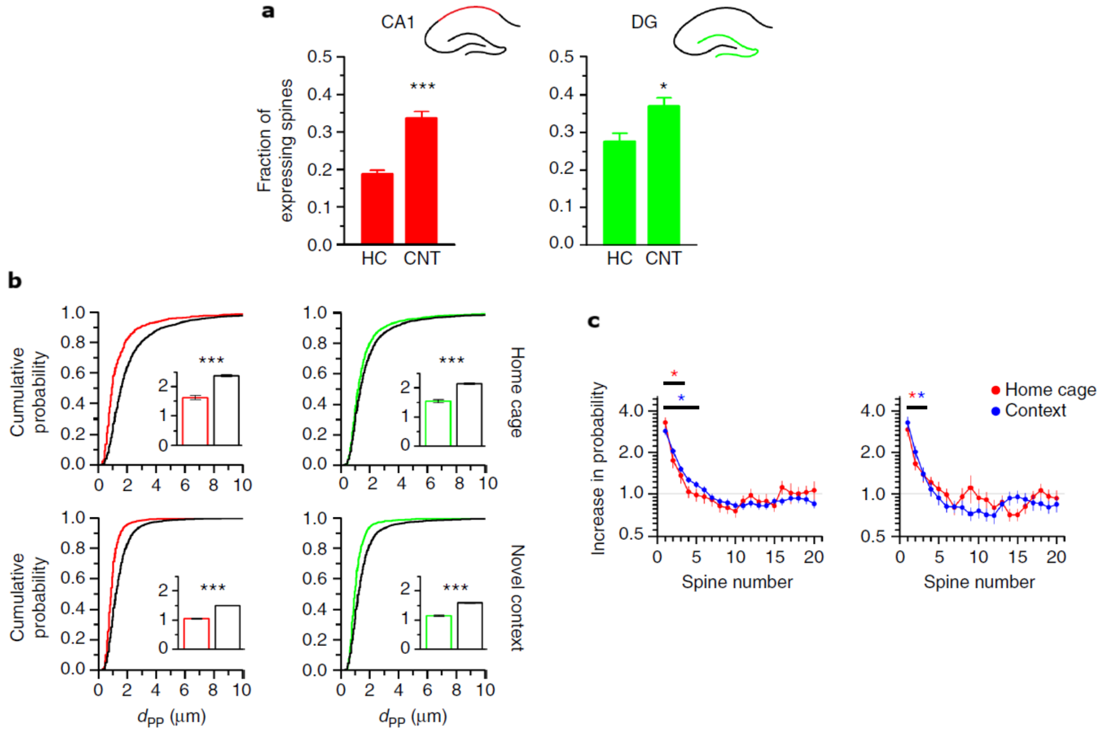

Figure 18. In vivo electroporation with TRE:SA-Ch and hippocampal spines analysis. a) Electroporated mice with TRE:SA-Ch exposed to a novel context (CNT) show both in CA1 and DG a significantly higher fraction of SA-Ch positive spines than mice kept in the home cage (HC). **b**) The distribution of first neighbor spine distance (dPP) shows that two Sa-Ch-expressing spines (red lines for CA1 on the left, green for DG on the right) are closer together than calculated if their position along the dendrite were random (black lines). **c**) The probability to express SA-Ch for the first 20 neighboring spines of a potentiated spine is higher with respect to a uniform (and random) distribution (CA1 on the left, DG on the right). (Modified from Gobbo et al., 2017)

2. Aims of the project

With the general goal of fully exploiting the capabilities of the SynActive toolbox (see section 1.9), the first objective of this work focused on setting up tools for imaging and proteomics of synapses undergoing activity-dependent potentiation through the use of Adeno Associated Viral vectors (AAVs). The AAV-SynActive toolbox was then exploited in two parallel directions:

- SynActive-assisted mapping of potentiated synapses (SA-Map)
    - Only recently research on learning-driven neural activity moved from a cellular (Josselyn et al., 2009; Liu et al., 2012; Ramirez et al., 2013) to a synaptic level (Hayashi-Takagi et al., 2015; Gobbo et al., 2017). In order to increase our knowledge on the synaptic ensembles activated by learning tasks, this study exploited the advantages provided by the SynActive toolbox (SA, Gobbo et al., 2017) to create an *in vivo* hippocampal topography of synaptic potentiation in mice.
    - Goals: tagging, imaging and analyzing CA1 and DG dendritic spines hosting the potentiated synapses (i.e., expressing a SA-controlled reporter) that support the encoding of a contextual fear memory.

- Initial testing of a SynActive-based tool for molecular characterization of potentiated synapses (SA-Mol)
    - The postsynaptic density (PSD) plays a crucial role in synaptic function by anchoring neurotransmitter receptors, signaling and scaffolding proteins (Dosemeci et al., 2016); one of the most important is PSD-95, whose interactors have been identified thanks to the proteomic analysis (Dosemeci et al., 2007; Fernández et al., 2009). However, there are currently no studies describing PSD-95 interactome in response to synapse potentiation. To fill this gap, this study employed the SA toolbox to study PSD-95 interactome of *in vivo* potentiated hippocampal synapses.

- Goal: validating activity-dependent expression of SA-driven proteomic probe in CA1 dendritic spines, following the encoding of a contextual fear memory.

For both sets of experiments, SA-constructs were stereotaxically injected into the hippocampus and, after a sufficient expression period, a contextual fear conditioning protocol was performed.

For the SA-Map aim, doxycycline was administered to limit the expression of construct to the time-window during the formation of contextual fear memory; then, tissue was fixed, signal was boosted through immunofluorescence and several factors were evaluated through confocal microscopy: fraction of SA-positive spines, distribution within and between CA1 and DG, spine head dimensions, possible clusterization, correlational measurements with behavioral responses.

For the SA-Mol first goal, tissue was fixed following CFC; signal was boosted through immunofluorescence and rate of expression was assessed through confocal microscopy.

3. Materials and methods

3.1 Animals and surgical procedures

C57BL/6J male mice (2 months old) were used for all investigations. Stereotaxic injection procedures were performed on anesthetized mice, by intraperitoneally injecting a mixture of zoletil (100 mg/kg) and xylazine (10mg/kg). Body temperature was kept constant throughout the procedures at 36°C by a closed loop temperature control system (Harvard Apparatus). Before surgery, the scalp was treated with topical anesthetic (Luan cream 2.5% lidocaine). Two holes were opened in the skull using a microdrill (Silfradent® Falcon), in order to insert heat-pulled micropipettes fabricated from calibrated glass capillaries (BLAUBRAND intraMark) filled with a cocktail of adeno associated viral (AAV) vectors stereotaxic microinjections were performed by adapting the procedures described in Di Garbo et al. (2011) and in Marchetti et al. (2019).

For the SA-Map experiment, 1 µl of a solution containing equal amounts of (i) SynActive AAV2/5 construct pTRE3g::Arc5'UTR-PSD95Δ1.2-mVenus-HA-Arc3'UTR (4.8x10^{11} vg/ml) and (ii) neuronal filler AAV2/5 construct pSynapsin:: rtTA - IRES – TdTomato (2.7x10^{11} vg/ml) was injected into hippocampal CA1 (−2.0 mm AP, ±1.9 mm ML and −1.4 mm DV relative to bregma; hemisphere 1) and hippocampal DG (−2.0 mm AP, ±1.55 mm ML and −1.8 mm DV relative to bregma; hemisphere 2) of mice belonging to both experimental groups (CFC, N=7; home cage, N=5) using a microinjector (CellTram® 4r Oil) at a rate of 0.1 µl/min.

For SA-Mol, two different AAV2/5 cocktails were injected: (i) pESARE::Arc5'UTR-PSD95-HAT-TEV-FLAG-Arc3'UTR (5.4x10^{11} vg/ml) and h-Synapsin::rtTA-IRES–TdTomato (2.7x10^{11} vg/ml) (N=14), or (ii) h-Synapsin::PSD95 – HAT – TEV – FLAG (4.7x10^{11} vg/ml) and h-Synapsin::rtTA - IRES – TdTomato (2.7x10^{11} vg/ml) (N= 14). Injection was in the CA1 area using the same procedure and total injection volume used for SA-Map

After the injection procedure, the micropipette was kept in place for 10 min to prevent spillover of the virus during subsequent retraction. Finally, the wound was cleaned and sutured. Mice received Tramadol:Paracetamol in drinking water and 21 days were allowed to let the mice recover and to achieve steady-state expression of the AAVs .

3.2 Contextual fear conditioning and doxycycline injections

All behavioral experiments were performed using a computerized fear-conditioning system (Ugo Basile ANYmaze). A testing chamber with electrified grid floor, was placed into a white sound-attenuating box (48.5x38.5x48.5cm) equipped with loudspeaker, a ventilation fan and a camera mounted on the ceiling. A high-contrast pattern was attached to the walls of the chamber to characterize the context (conditioning stimulus, CS) where the electric shock (unconditioned stimulus, US) was to be delivered. On day 1 (habituation phase), mice were acclimated to the behavioral testing room for 30 minutes. Then, they were exposed to the conditioning context for 5 min, in order to avoid novelty effects during the following phase. On day 2 (association phase), after habituation to the room, mice were exposed to the same conditioning context, where they were subjected to 5 foot shocks (0.5 mA, 1 sec; 25 sec inter-shock interval) during the first 3 minutes; then, 2 minutes were allowed for further exploration of the context. Three hours later, mice were subjected to histological fixation (please see below, section 3.3) (Figure 19a).

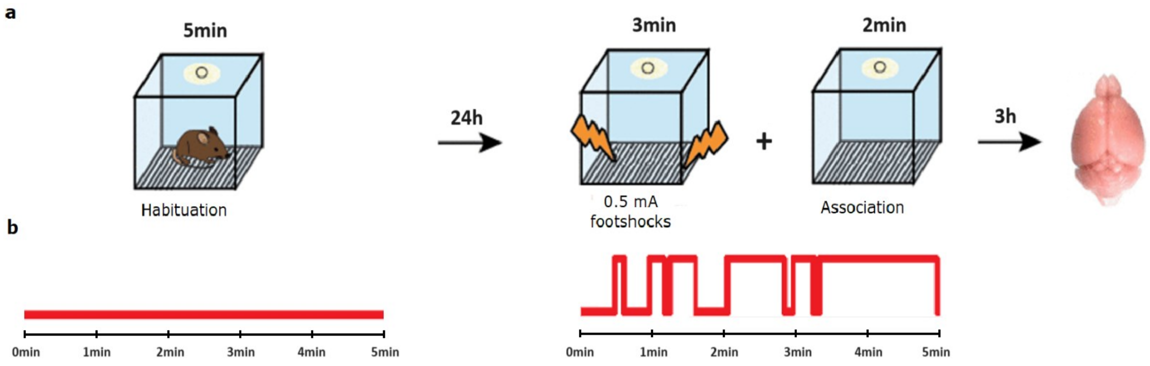

Figure 19. Contextual fear conditioning protocol. a) On day 1, 5 minutes of habituation to the context; On day 2, 3 minutes of exposure to footshocks followed by 2 minutes for additional exploration of the context. **b**) Representative plot showing the progressive increase in the time spent freezing during the association phase.

Freezing behavior, considered as the complete absence of voluntary movements, was automatically scored by the AnyMaze software (CFC group, for SA-Map N= 7 mice, for SA-Mol N=14 mice). During the last 2 minutes of testing, freezing behavior dramatically increased, which can be used to qualitatively assess the animal's capability to form a CS-US association (Figure 19b. See also section 1.1). As a control group, mice were kept in their home cage (hoca group, for SA-Map N=5 mice, for SA-Mol N=14 mice).

Only for SA-Map, 2 h after the habituation phase, mice received an i.p. doxycycline injection (1.5 mg/mouse) to activate the Tet-ON system and the transcription of the SA construct. An additional injection was performed 24 hours after the end of the habituation phase.

3.3 Histological fixation

Mice were overdosed with chloral hydrate (10% W/V), then the heart was exposed and the left ventricle was cannulated using a 27G needle connected to silicone tubing passing through a peristaltic pump (Gilson). After cutting the wall of the right atrium, perfusion was started at a flow rate and were transcardially perfused at a of 18.5 ml/min. First 30-35 ml of ice-cold phosphate-buffered saline (PBS) pH 7.4 were passed to clear tissues from blood, followed by at least 25 ml of paraformaldehyde solution (PFA) (4% W/V in 0.1 M, pH 7.4 phosphate buffer, PB). Brains were extracted from the skull and postfixed in 4% paraformaldehyde solution for 2-6 hours. Samples were finally transferred to 30% W/V sucrose in 0.1 M PB and maintained at 4°C for at least 3 days, or until they sank to the bottom of the tube, for cryoprotection.

3.4 Immunofluorescence and confocal imaging

Brains were quickly frozen in dry ice, then coronal sections were cut using a sliding microtome (80 µM, using Leica SM2010R), then they were processed for antigen retrieval, in citrate buffer (pH 6.0, 10 mM) for 12 minutes at 80°C.

For SA-Map, slices were treated with blocking solution (10% normal goat serum and 0.3% Triton X-100 in PBS) for 2 hours at room temperature, then incubated with primary antibody solution (1% normal goat serum, 0.3% Triton X-100, 1:500 rabbit α-mCherry antibody AbCam ab167453, 1:3000 chicken α-HA antibody AbCam ab9111, in PBS 1x) overnight at 4°C. After washing 3 times, 10 min each (1 time with 0.3% Triton X-100 in PBS 1x, 2 times with PBS 1x), tissue was stained with secondary antibody solution (1% normal goat serum, 0.1% Triton X-100, 1:400 goat α-chicken Alexa Fluor 488 Invitrogen A-11039, 1:400 goat α-rabbit Invitrogen Alexa Fluor 555 A-21428, in PBS 1x). Then, slices were washed 3 times again, 10 min each (1 time with 0.1% Triton X-100 in PBS 1x, 2 times with PBS 1x).

For SA-Mol**,** slices were treated with blocking solution (10% normal goat serum and 0.3% Triton X-100 in PBS 1x) for 2 hours at room temperature, then incubated with primary antibody solution (1% normal goat serum, 0.3% Triton X-100, 1:1000 chicken α-mCherry antibody AbCam ab205402, 1:1600 rabbit α-FLAG antibody Sigma F7425 in PBS 1x) overnight at 4°C. After washing 3 times, 10 min each (1 time with 0.3% Triton X-100 in PBS 1x, 2 times with only PBS 1x), tissue was stained with secondary antibody solution (1% normal goat serum, 0.1% Triton X-100, 1:400 goat α-chicken Alexa Fluor 555 Invitrogen A-21437, 1:400 goat α-rabbit Alexa Fluor 488 Invitrogen A-11008 in PBS 1x). Then, slices were washed 3 times again, 10 min each (1 time with 0.1% Triton X-100 in PBS 1x, 2 times with PBS 1x). Finally sections mounted onto microscope slides using an antifade medium (Vectashield H-1000, Vector Labs). In the postsynaptic control triple immunofluorescence (see section 4.7), guinea pig α-homer SySy 160 025 was added in the primary antibody solution (1:300) and goat α-guinea pig Alexa Fluor 647 Invitrogen A-21450 was added in the secondary antibody solution (1:400).

Images were acquired with a confocal microscope (Zeiss LSM 900), using either a 40x objective with 1x zoom in confocal mode), or a 63x objective with 2.4x zoom in Airyscan mode).

3.5 Image post-processing

To enhance the fluorescence signal-to-noise ratio, as well as the spatial resolution of acquired images, a combination of two post-processing techniques (2D image deconvolution and background subtraction) were performed using Fiji software (Schindelin et al., 2012), version 1.53f and related plugins (Diffraction PSF 3D, Dougherty 2005; DeconvolutionJ, Linnenbrügger 2002) for both SA-Map and SA-Mol.

First, given the conditions of our specific acquisition hardware (microscope, camera and associated light), a Point Spread Function (PSF) was generated to calculate the target image in the absence of the distortion effects (Giannini and Giannini, 2016). Then, based on the PSF, a deconvolution algorithm was employed to process each image of the acquired confocal z-stacks. Finally, a background correction was performed. This approach resulted in more detailed and sharper images (Figure 20) and in better detection of dendritic spines compared to the original raw image (Figure 21). The same software settings were used for all conditions (see Figure 20).

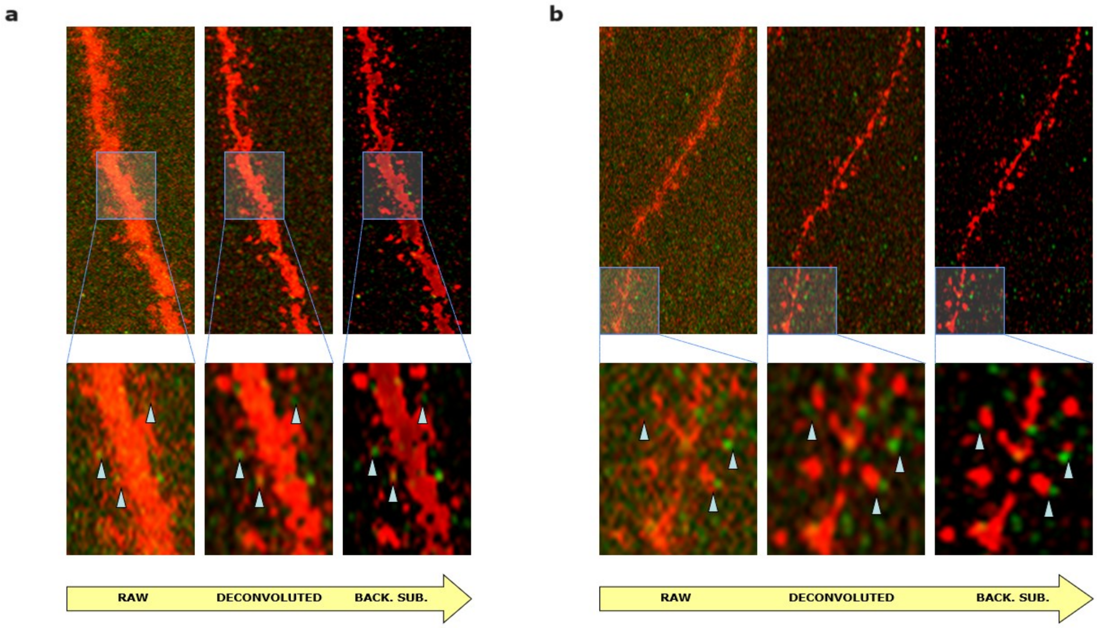

Figure 20. Representative images showing the workflow for image postprocessing. For both the DG (**a**) and CA1 (**b**), deconvolution followed by background subtraction resulted in improved signal-to-noise ratio of immunofluorescence signals. White arrows indicate SA-positive puncta (green) apposed to TdTomato dendritic spines (red). Point-spread function (PSF) parameters: index of refraction of the media = 1.510; numerical aperture, n*sin(theta) = 1.40; longitudinal spherical aberration = 0; image pixel spacing = 64nm; w/h = 1024x1024; normalization = 1. Deconvolution parameters: resizing = no resizing; complex number precision = single precision; regularization parameter (gamma) = 0.0001.

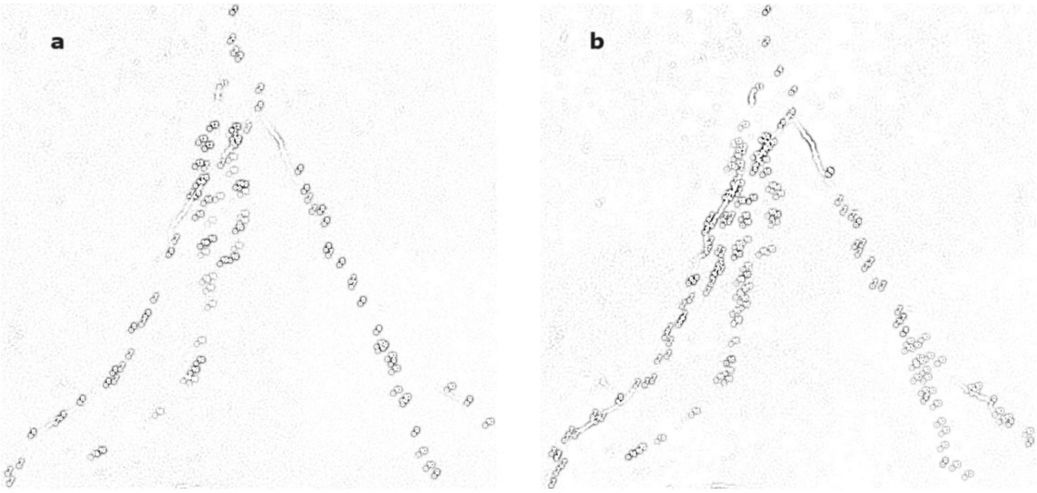

Figure 21. Representative tracings for the same image before (**a**) and after (**b**) image postprocessing showing the increase in the number of detected SA-positive puncta.

3.6 Slice quantifications

All immunofluorescence counts were manually performed using Fiji software (Schindelin et al., 2012), version 1.53f.

For SA-Map, a spine was considered SA-positive only if the signal corresponding to the HA tag (i.e., emitted by AlexaFluor488, displayed as green) colocalized with the TdTomato signal (i.e., emitted by AlexaFluor555, displayed as red) corresponding to dendritic spines; green puncta that were apposed to but did not overlap with the red head of the spine were not considered to belong to that spine (Figure 22). Consequently, red spines with no colocalizing green signal were considered to be SA-negative.

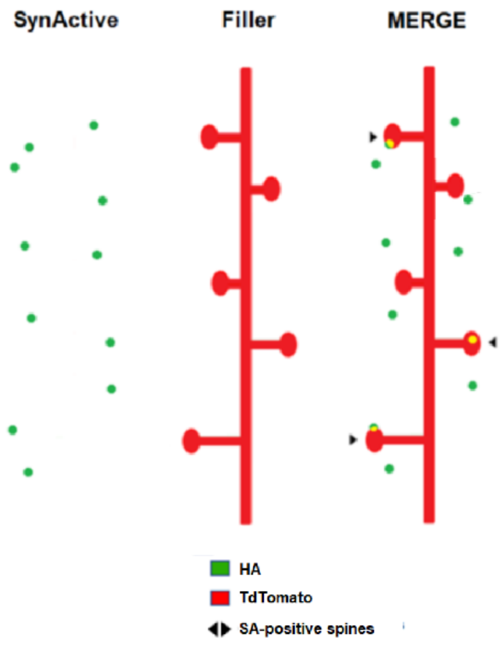

Figure 22. SA-Map quantification. Scheme showing the criterion for counting an HA-immunoreactive punctum as belonging to a given tdTomato-immunoreactive dendrite (black arrows).

For SA-Mol, a spine was considered to be positive for the expression of the SA-PSD95-FLAG protein (labeled by AlexaFluor488, displayed in green) only if colocalization with the TdTomato signal (labeled by AlexaFluor555, displayed in green) corresponding to dendritic spines was observed; green puncta dots that were apposed to but did not overlap with close but not touching the red head of the spine were not considered to belong to that spine (Figures 23a-b). Consequently, red spines with no colocalized green signal were considered to be FLAG-negative.

The number of FLAG-positive spines was normalized on the length of their parent dendrite to obtain a linear density [spines/μm].

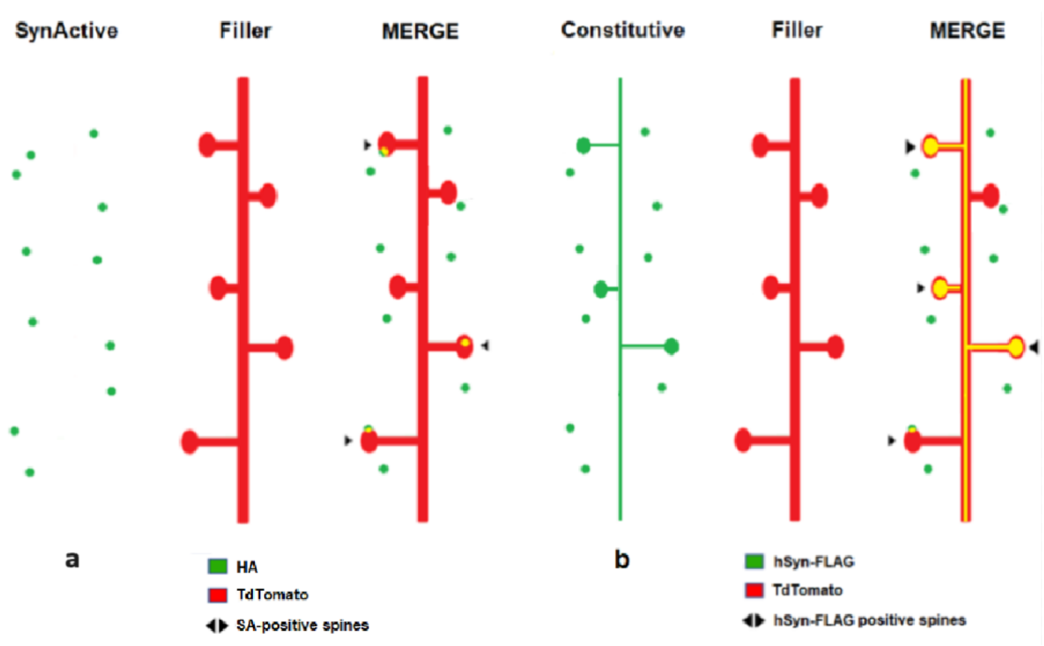
SynActive
Filler
MERGE
Constitutive
Filler
MERGE
a
🟩 HA
🟥 TdTomato
◀▶ SA-positive spines
b
🟩 hSyn-FLAG
🟥 TdTomato
◀▶ hSyn-FLAG positive spines

Figure 23. SA-Mol quantification. a) SynActive (left), filler (center) and merged (right) configurations. **b**) Constitutive (left), filler (center) and merged (right) configurations. For both, on merged, black arrows indicate which spine is considered valid

3.7 Statistical analyses

Dendritic spine properties were compared using two-way ANOVA or two-way repeated measures ANOVA (Figure 24, factor 1 = spine response to the SynActive tool (SA-positive/negative), factor 2 = dendritic branching order; Figure 25, factor 1 = hippocampal region (CA1/DG), factor 2 = spine response to the SynActive tool (SA-positive/negative); Figure 26, factor 1 = behavioral treatment (CFC/hoca), factor 2 = dendritic branching order; Figure 27, factor 1 = hippocampal region (CA1/DG), factor 2 = dendritic branching order; Figure 28, factor 1 = behavioral treatment (CFC/hoca), factor 2 = dendritic branching order; Figure 29, factor 1 = hippocampal region (CA1/DG), factor 2 = dendritic branching order; Figure 33, factor 1 = type of AAV construct (ESARE/hSyn), behavioral treatment (CFC/hoca)) and all pairwise multiple comparison procedures (Bonferroni post-hoc test or Holm-Sidak post-hoc test). All these tests were performed using SigmaPlot software, version 12.0; graphs were elaborated using OriginPro software, version 2019b.

Dendritic spine cumulative distributions on the corresponding branching dendritic orders (Figures 30-31) were compared using the Kolmogorov-Smirnov test via OriginPro software, version 2019b.

Correlational measures between time spent by the animals in freezing and the spine head volumes (R squared coefficient), together with the related graphs (Figure 32), were performed using GraphPad Prism software, version 7.00.

4. Results

4.1 SA-Map: labeling and imaging of dendritic spines and translation-dependent structural potentiation

The first objective of this thesis was to find the experimental conditions for the best titer of AAVs, for imaging of the SA-signal, for balancing the whole dendrite staining by the filler and the post-synaptic signaling, and for a quantification of the SA-signal. This preparatory activity, fundamental to carry out the whole project and also for the more general use of the AAV-SynActive toolbox by the lab and by the scientific community at large, led to the experimental conditions outlined in the methods section above.

Co-injection of the two AAVs coding for synapsin::tdTomato and TRE3g::SynActive-PSD95Δ1.2-mVenus-HA (see section 3.1) resulted in sparse labeling of entire hippocampal neurons, including their dendritic arbor, along with a punctate pattern that colocalized with dendritic spine heads.

Even before a quantification of HA-immunoreactive puncta was performed (see section 4.3), it was readily apparent from visual inspection of images that brains corresponding to mice exposed to contextual fear conditioning (CFC group) showed an intense signal that colocalized with the spine heads for each dendrite (Figure 24a, rows 1 and 3), indicated by the white arrows in hippocampal CA1 (Figure 24b, row 1) and DG (Figure 24b, row 3). In home cage (hoca group) mice, the absence of exposure to a specific cognitive task was associated with a less intense HA signal and fewer green dots colocalizing with spine heads (Figure 24a, rows 2 and 4), reflecting the intrinsic baseline rate of synaptic potentiation in CA1 (Figure 24b, row 2) and DG (Figure 24b, row 4).

If doxycycline was not injected to activate the transcription of TRE3g::SynActive-PSD95Δ1.2-mVenus-HA in CA1 (Figure 24c, row 1) and in DG (Figure 24c, row 2), no HA immunoreactivity could be detected upon exposure to CFC, with only a few dots resulting from tissue autofluorescence. Similarly, if the primary antibody against the filler protein TdTomato and HA was omitted during the immunofluorescence procedure (see section 3.4), the secondary antibodies did not show significant signal neither in CA1 (Figure 24d, row 1) nor in DG (Figure 24d, row 2). Finally, if no AAVs had been injected before

CFC, no significant signal appeared either in the red or green channels (CA1, Figure 24e row 1; DG, Figure 24e row 2).

Of note, the presence of HA-immunoreactive dots that did not colocalize with labeled dendritic spines can correspond to neurons expressing insufficient levels of the tdTomato filler, while maintaining levels of the rtTA transactivator adequate for triggering transcription of TRE3g-controlled SynActive-PSD95Δ1.2-mVenus-HA. This can be explained by the tdTomato coding sequence being cloned downstream of an internal ribosome entry site (IRES), which may result in lower translation with respect to the upstream coding sequence corresponding, in our case, to rtTA. However, this had the advantage of achieving a sparse labeling of hippocampal neurons, required to perform accurate mapping of individual dendritic arbors. Moreover, the "no-doxycycline" and "no-AAV" controls demonstrate that the green puncta labeling originated from TRE3g- and Synactive-dependent expression of PSD95Δ1.2-mVenus-HA.

These results show that the expression of TRE3g::SynActive-PS095DΔ1.2-mVenus-HA (i) can be controlled using the TetON doxycycline-dependent system and (ii) correlated with hippocampal activation triggered by exposure to CFC.

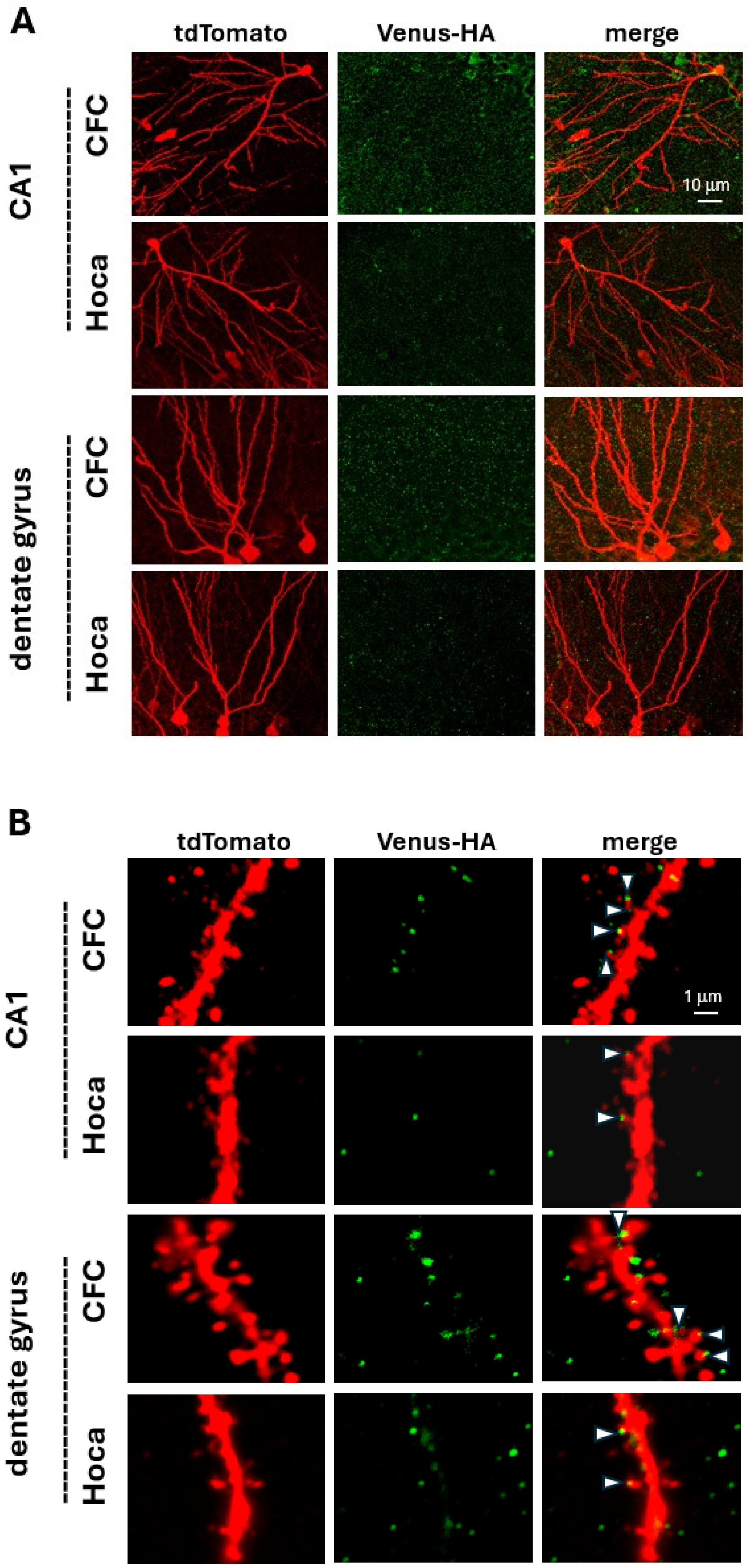
A
tdTomato
Venus-HA
merge
CA1
CFC
Hoca
dentate gyrus
CFC
Hoca
10 µm
B
tdTomato
Venus-HA
merge
CA1
CFC
Hoca
dentate gyrus
CFC
Hoca
1 µm

Figure 24. SA-Map representative images. Representative low- (**A**) and high-magnification (**B**) images from the hippocampi of mice expressing synapsin::rtTA-IRES-tdTomato and TRE3g::SynActive-PSD95Δ1.2-mVenus-HA. Continued on next page.

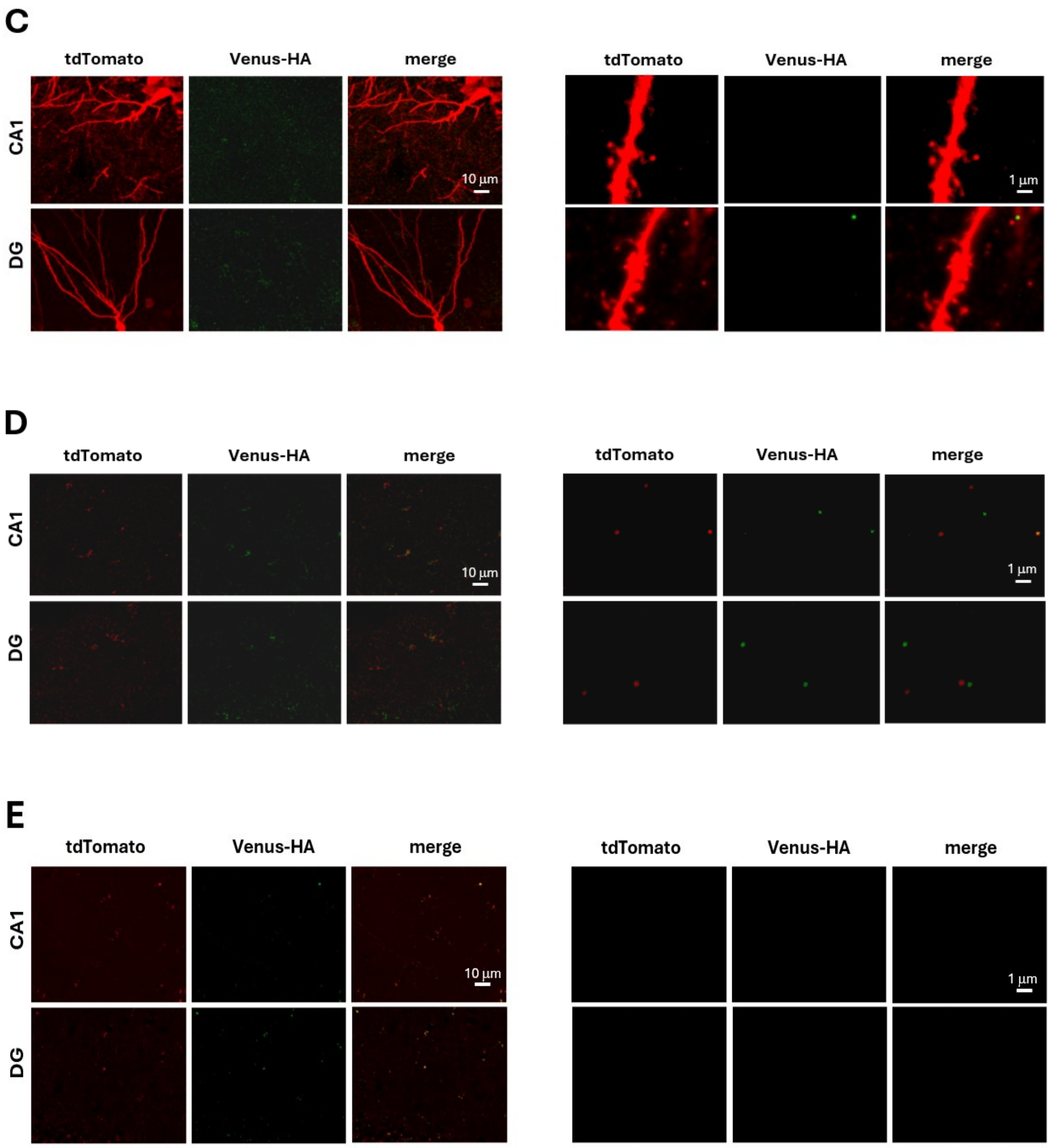
C
tdTomato
Venus-HA
merge
tdTomato
Venus-HA
merge
CA1
DG
10 µm
1 µm
D
tdTomato
Venus-HA
merge
tdTomato
Venus-HA
merge
CA1
DG
10 µm
1 µm
E
tdTomato
Venus-HA
merge
tdTomato
Venus-HA
merge
CA1
DG
10 µm
1 µm

Figure 24. Continued from previous page. C) Omitting doxycycline injection results in undetectable expression of PSD95Δ1.2-mVenus-HA. **D**) Omitting the primary antibodies against tdTomato and HA from the immunofluorescence procedure abolishes detection of both antigens, thus ruling out that signals are generated by aspecific reactivity of the secondary antibodies. **E**) Omitting AAV injection results in undetectable immunoreactivity for both tdTomato and HA. On the left low-magnification panels, on the right high-magnification panels.

4.2 SA-Map: labeling spines showing structural potentiation

The volume of a dendritic spine is considered proportional to the size of its postsynaptic density (PSD), glutamate receptors availability and, consequently, synaptic strength (Matsuzaki et al., 2001; Holtmaat and Svoboda, 2009; see sections 1.5 and 1.6). For these reasons, changes in the volume of dendritic spines, before and after a potentiation-inducing event, are considered as a structural proxy for functional synaptic potentiation. To observe whether our SA tool was capable of selectively labeling potentiated spines showing a significant increase in volume (compared to non-potentiated ones), SA-positive and SA-negative spines head volumes were compared, focusing on the CA1 and dentate gyrus. In addition, CFC and home cage mice were also compared. Finally, the dendritic branching order was also considered from the first to the third order.

The volume of each spine was calculated approximating their shape as if it were generated by the rotation of a perfect ellipsoid (we approximated two of the dimensions as equal):

$$\frac{4}{3}\pi\, a\, b^2$$

where a is the semi-major axis of the ellipsoid and b the semi-minor axis (also equal to the third dimension).

Comparing SA-positive and SA-negative spines on the same dendritic order, in the animals exposed to contextual fear conditioning (CFC group) CA1 SA-positive spines had a larger volume than negative ones, but regardless of the branching order (Figure 24a). A similar, statistically significant trend was observed in the DG where, in addition, third-order spines showed a significantly larger volume than first-order spines (Figure 24b).

Similarly, in mice kept in their home cage (hoca group), SA-positive spine head volumes for both the CA1 (Figure 24c) and DG (Figure 24d) were significantly larger than SA-negative spines.

Finally, if considered independently of their dendritic order, the head volumes of both SA-positive and SA-negative spines were always larger in the dentate gyrus than in CA1, whether the treatment was CFC (Figure 25a) or home cage (Figure 25b).

Taken together, these results show that – regardless of the behavioral treatment and the hippocampal region – SynActive-controlled PSD95Δ1.2-mVenus-HA labels spines showing structural potentiation.

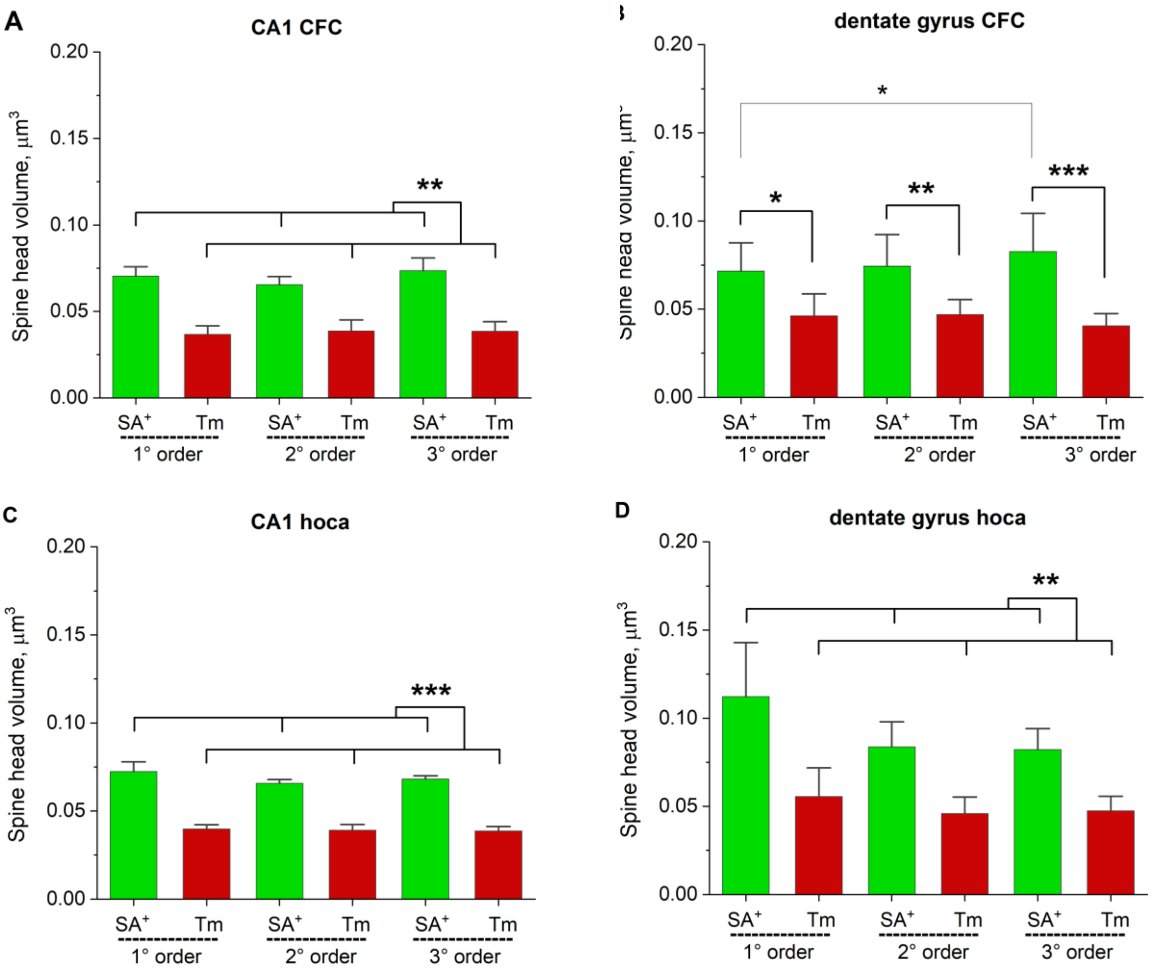

Figure 24. Synactive-PSD95Δ1.2-mVenus-HA labels structurally potentiated dendritic spines in the CA1 and DG. A) Exposure to CFC results in CA1 SA-positive dendritic spines showing a larger volume than SA-negative dendritic spines, regardless of the branching order (repeated measures ANOVA-2 with factor 1 = SA-positive/negative and factor 2 = branching order; factor 1, F = 38.467; p = 0.002; factor 2, F = 0.503; p = 0.619; interaction, F = 1.695; p = 0.232. **B)** Exposure to CFC results in DG SA-positive dendritic spines showing a larger volume than SA-negative dendritic spines, with a more pronounced effect on third-order dendritic spines (repeated measures ANOVA-2 with factor 1 = SA-positive/negative and factor 2 = branching order; interaction, F = 4.412, p = 0.042; Holm-Sidak post-hoc test, SA-positive vs SA-negative first order, t = 3.128; *p = 0.015; second order, t = 3.399; **p = 0.010; third order, t = 5.210, *p = 0.001; SA-positive, third order vs. first order, t = 2.777, *p = 0.035). (**C, D**) A similar trend was observed for the home cage (hoca) condition, in both the CA1 (factor 1, F = 226.209, ***p < 0.001; factor 2, F = 2.080; p = 0.187; interaction, F = 1.368, p = 0.368) and DG (factor 1, F = 73.759; ***p = 0.003; factor 2, F = 2.691, p = 0.146; interaction, F = 3.810, p =0.085). The analysis was conducted on the average value for each mouse; CFC, N=7 mice, CA1 N=12 neurons, DG N=15 neurons; hoca, N=5 mice, CA1 N=6 neurons, DG N=6 neurons.

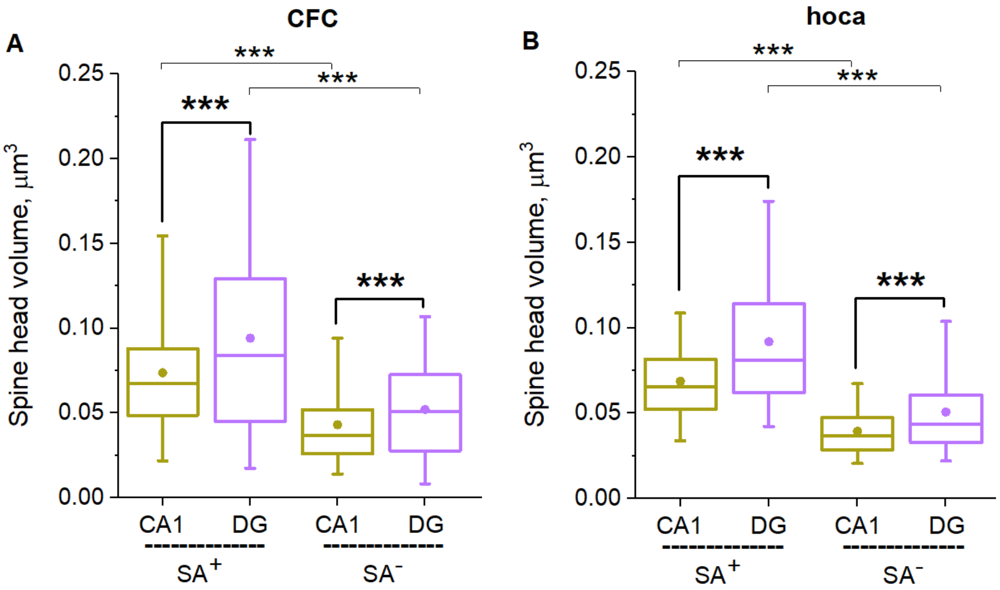

Figure 25 Comparison of SA-positive and SA-negative dendritic spine volumes between the CA1 and DG regions. Both SA-positive and SA-negative dendritic spines show a larger volume in DG than in CA1. This is true for both behavioral treatments: (**A**) CFC (ANOVA-2 with factor 1 = CA1/DG and factor 2 = SA-positive/negative; interaction, F = 22.995, $p < 0.001$; Bonferroni post-hoc test, DG SA-positive spines vs CA1 SA-positive spines, t = 9.821, ***$p < 0.001$; DG SA-negative spines vs CA1 SA-negative spines, t = 7.815, ***$p < 0.001$; SA-positive spines vs SA-negative spines within DG, t = 27.467, ***$p < 0.001$; SA-positive spines vs SA-negative spines within CA1, t = 16.814, ***$p < 0.001$) and (**B**) home cage (hoca, interaction, F = 40.784, $p < 0.001$; Bonferroni post-hoc test, DG SA-positive spines vs CA1 SA-positive spines, t = 13.286, ***$p < 0.001$; DG SA-negative spines vs CA1 SA-negative spines, t = 16.836, ***$p < 0.001$; SA-positive spines vs SA-negative spines within DG, t = 29.884, ***$p < 0.001$; SA-positive spines vs SA-negative spines within CA1, t = 23.246, ***$p < 0.001$). The analysis was conducted on all the spine head volumes, independently from branching order: CFC, DG SA-positive N=801 spines, CA1 N=524 spines, DG SA-negative N=2173 spines, CA1 N=1953 spines; hoca, DG SA-positive N=352 spines, CA1 N=440 spines, DG SA-negative N=2813 spines, CA1 N=2535 spines.

4.3 SA-Map: detection of synaptic potentiation triggered in tha CA1 and dentate gyrus by exposure to contextual fear conditioning

As seen in section 4.2, hippocampal dendritic spines that were SynActive-positive showed a larger head volume than spines that did not express our construct. It was therefore reasonable to expect that the number of potentiated spines (and, possibly, their local density) increased in response to exposure to a behavioral task known to trigger hippocampus-dependent learning and memory, in our case CFC, as far as the spatial context component of the task is concerned. To test this, the number of SA-positive spines was normalized on the total number of spines and compared between CFC and home cage mice to obtain the density of potentiated spines for the three dendritic orders considered. In both CA1 (Figure 26a) and dentate gyrus (Figure 26b), the density of SA-positive spines was significantly higher in conditioned (CFC) mice compared to home cage (hoca) controls.

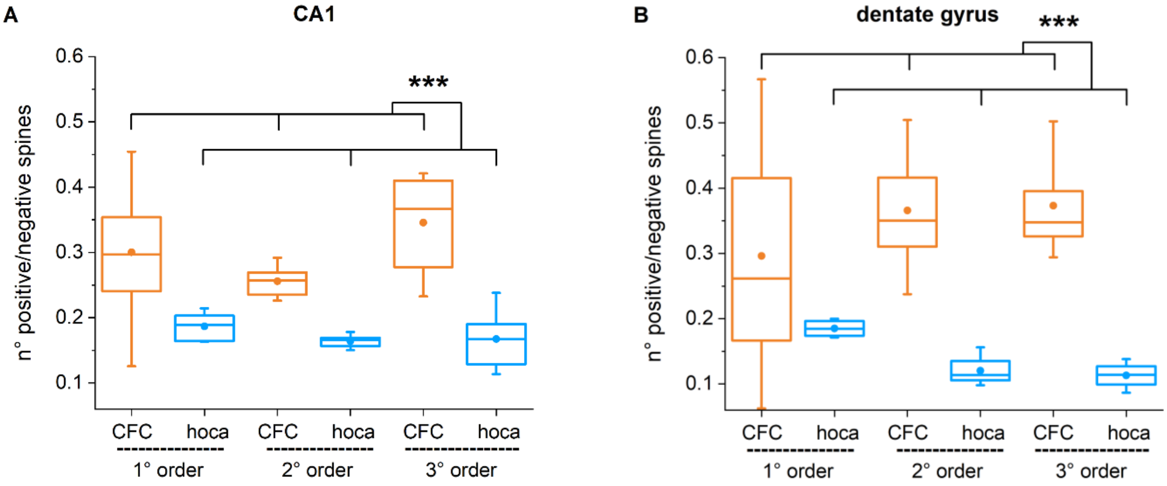

Figure 26. Comparison of the fraction of structurally potentiated dendritic spines in the CA1 and DG. Significant differences were observed for both the **A**) CA1 (factor 1, CFC or hoca; factor 2, branching order; repeated measures ANOVA-2, factor 1, F = 52.246, ***p < 0.001; factor 2, F = 1.429, p = 0.246; interaction, F = 1.177, p = 0.330) and **B**) DG (factor 1, F = 22.768, ***p = 0.001; factor 2, F = 0.0188, p = 0.981; interaction, F = 2.437, p = 0.119). N for each group are the same as for figure 24.

Comparing the SA-positive spines fraction between the two hippocampal regions did not show any differences in CFC mice (Figure 27a); however, in home cage mice, CA1 showed a higher overall density of SA-positive spines than the DG (Figure 27b).

Taken together, these results show that in both CA1 and DG the number of SA-positive spines, relative to the number of SA-negative spines, increases in an learning-dependent manner; after exposure to CFC, there are no significant differences between the fraction of SA-positive spines between the two regions, while the CA1 shows a higher baseline (home cage) fraction of potentiated spines than the DG.

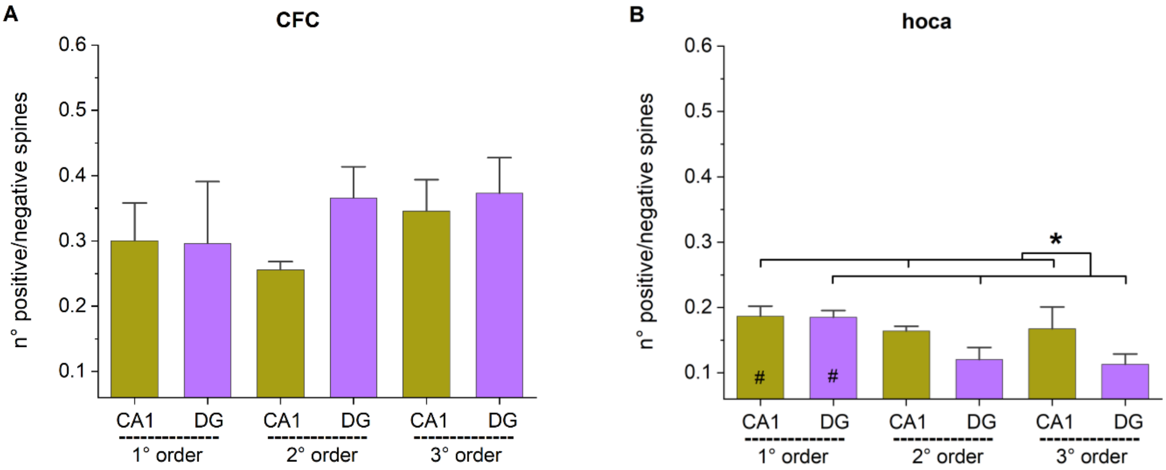

Figure 27. Comparison of the fraction of structurally potentiated dendritic spines in CFC and hoca mice between CA1 and DG. A) No significant difference was observed in CFC-exposed mice (factor 1, CA1 or DG; factor 2, branching order; repeated measures ANOVA-2, factor 1, F = 1.339, p = 0.297; factor 2, F = 2.516, p = 0.125; interaction, F = 0.756, p = 0.497) **B**) In the home cage (hoca) condition, the fraction of structurally potentiated spines was larger in the CA1 compared to the DG for all branching orders (factor 1, F = 14.860, *p = 0.031; factor 2, F = 8.553, #p = 0.018; interaction, F = 4.287, p = 0.070). N for each group are the same as for figure 24.

4.4 SA-Map: calculation of nearest neighbor distance

Modeling studies have shown that potentiated synapses may show a tendency to group in clusters along the dendrites (Kastellakis and Poirazi, 2019; see sections 1.5 and 1.7). Since the SynActive tool allows to label synapses that have been potentiated following the learning phase of a CFC task, it was of interest to investigate the spatial arrangement of SA-positive synapses.

To investigate this aspect, the nearest neighbor distance (NND) was calculated for SA-positive spines as a measure of spine clusterization.

No significant differences were detected in NND for SA-positive spines in the CA1 between CFC and home cage (hoca) groups (Figure 28a). On the contrary, in the DG, SA-positive spines, in third order dendritic branches, were found to be closer to each other, than SA-negative spines (Figure 28b).

Vice versa, SA-negative spines showed a significantly shorter NND in the home cage condition, both in the CA1 (Figure 28c) and the DG (Fig 28d).

When NND was compared between the CA1 and the DG, no statistically significant difference emerged for SA-positive spines in the CFC group. On the other hand (Figure 29a), SA-positive spines showed a significantly shorter NND in the CA1 than in the DG for home cage mice (Figure 29b). For SA-negative spines, no significant differences were observed when comparing the CA1 and DG of CFC mice, but spines located on second-order dendrites of the CA1 had a significantly shorter NND than first- and third-order spines (Figure 29c). Finally, SA-negative spines in the DG show a significantly shorter NND in home cage than in CFC groups (Figure 29d).

The above described NND analysis indicates that in the DG (in distal dendritic branches), but not in the CA1, SA-positive dendritic spines tend to group together in response to a behavioral task triggering associative learning. Moreover, structurally potentiated spines tended to be closer in DG than in CA1 in a baseline behavioral condition.

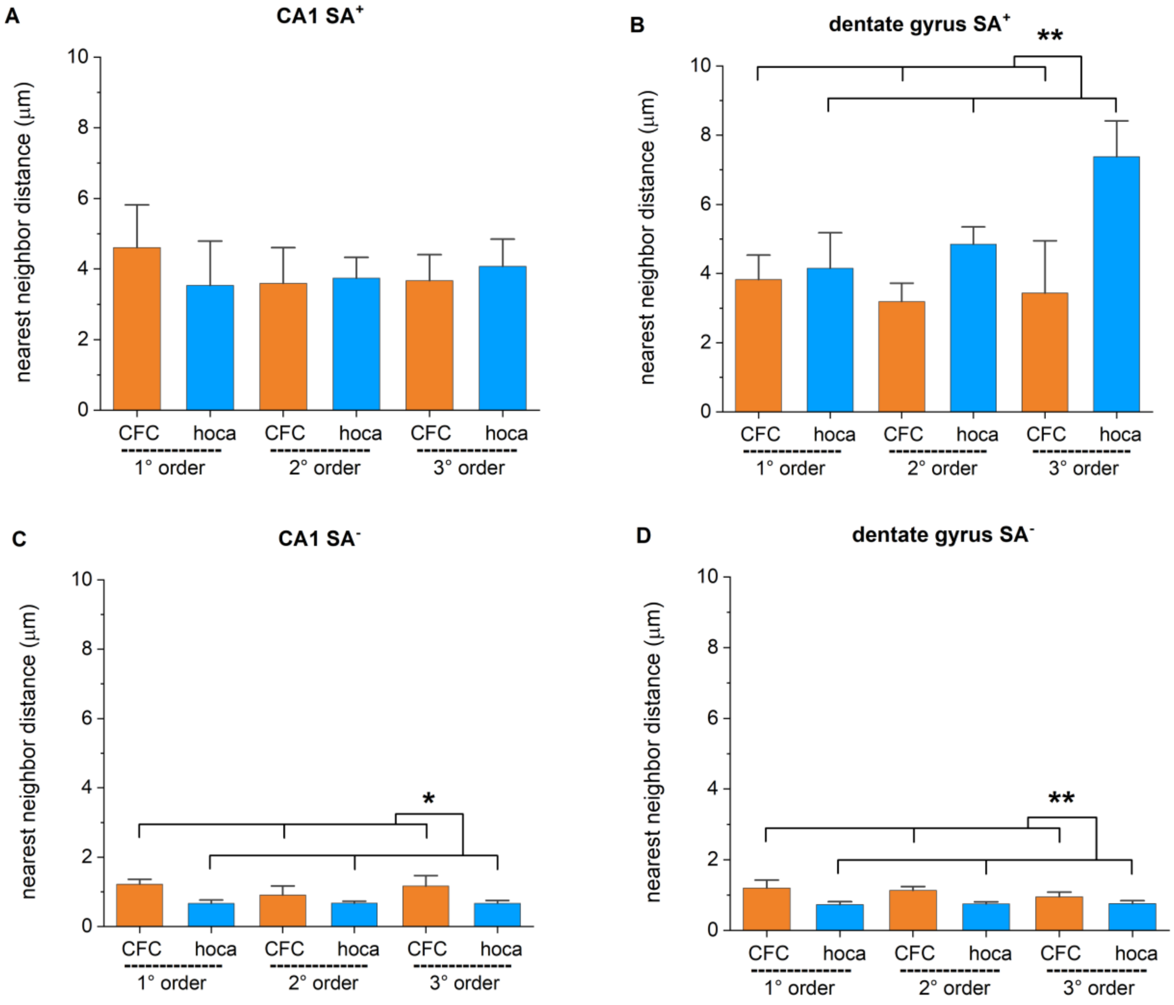

Figure 28. Nearest neighbor analysis for SA-positive and SA-negative dendritic spines in the CA1 and DG. A) No significant difference in the nearest neighbor distance (NND) of SA-positive dendritic spines was detected for the CA1 in CFC vs. hoca mice (repeated-measures ANOVA-2, factor 1, CFC or hoca; factor 2, branching order; factor 1, F = 0.110, p = 0.747; factor 2, F = 0.277, p = 0.761; interaction, F = 0.830, p = 0.451). **B)** In the DG, NND was significantly shorter in CFC mice compared to hoca controls (factor 1, F = 15.475, **p = 0.004; factor 2, F = 3.045, p = 0.076; interaction, F = 2.726, p = 0.096). **C-D)** For both the CA1 (factor 1, F = 7.875, **p = 0.019; factor 2, F = 2.661, p = 0.096; interaction, F = 2.804, p = 0.086) and DG (factor 1, F = 10.626, **p = 0.01; factor 2, F = 0.484, p = 0.624; interaction, F = 0.827, p = 0.454), the NND of SA-negative dendritic spines was significantly higher in CFC mice compared to hoca controls. N for each group are the same as for figure 24.

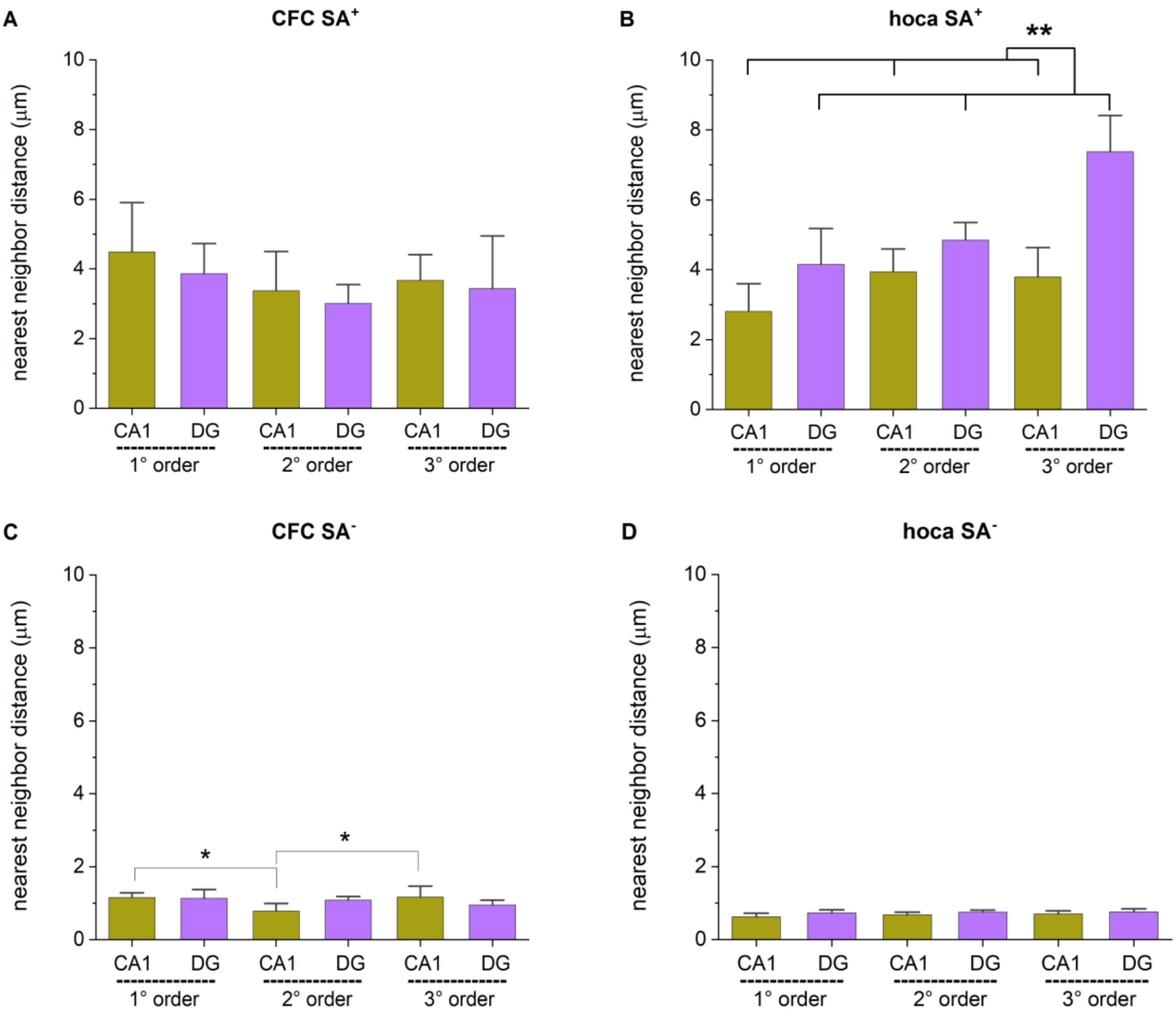

Figure 29. Comparison of nearest neighbor distances between CA1 and DG for SA-positive and SA-negative dendritic spines in CFC and hoca mice. **A**) No significant difference in the nearest neighbor distance (NND) of SA-positive dendritic spines was detected for the CFC mice in CA1 vs. DG (repeated-measures ANOVA-2, factor 1, CA1or DG; factor 2, branching order; factor 1, F = 0.248; p = 0.639; factor 2, F = 0.929; p = 0.246; interaction, F = 0.0235; p = 0.977). **B**) For hoca mice, NND for SA-positive dendritic spines was significantly shorter in the CA1 vs. DG (factor 1, F = 36.760; p = **0.009; factor 2, F = 6.315; p = 0.033; interaction, F = 2.666; p = 0.148). **C**) SA-negative dendritic spines of CFC mice showed in the CA1 a significant difference among branching orders (interaction, F = 5.606; p = 0.023, followed by Holm-Sidak post hoc test, first order vs. second order, t = 2.760; *p = 0.026; third order vs. second order, t = 2.818, *p = 0.034). **D**) For hoca mice, no significant differences were detected for SA-negative spines between the CA1 and DG (factor 1, F = 1.625; p = 0.292; factor 2, F = 0.865; p = 0.468; interaction, F = 0.300; p = 0.752). N for each group are the same as for figure 24.

4.5 SA-Map: mapping of dendritic spine density along the dendritic arbor

To investigate whether the position of SA-positive and SA-negative spines varies along the apical dendritic tree of CA1 and DG neurons, the cumulative distributions of distances between dendritic spines and their corresponding dendritic branching points were compared, in the different experimental groups.

No statistically significant differences in the distribution of SA-positive versus SA-negative dendritic spines were detected for the first branching order of apical dendrites in both the CA1 and DG of CFC mice.

At the level of the second branching order, SA-positive spines showed a statistically significant shift toward more distal positions compared to SA-negative spines (Figure 30b). A statistically significant, opposite trend was observed in the CA1 for second branching-order SA-positive spines in the CA1, which were located at more proximal locations than SA-negative spines (Figure 30e). Concerning the third branching order, no significant differences were observed in the DG (Figure 30c), while in the CA1 a both-ends shift emerged (Figure 30f), i.e. SA-positive spines were localized preferentially closer to the branching point or far from it.

When a similar analysis was conducted on the home cage group, no significant differences were detected except for the 3rd order of CA1 apical dendrites (Figure 31f), where SA-positive spines were shifted proximally respect to SA-negative spines.

Taken together, these results show that SA-positive synapses are not distributed uniformly along the different dendrite sections of the same neuron.

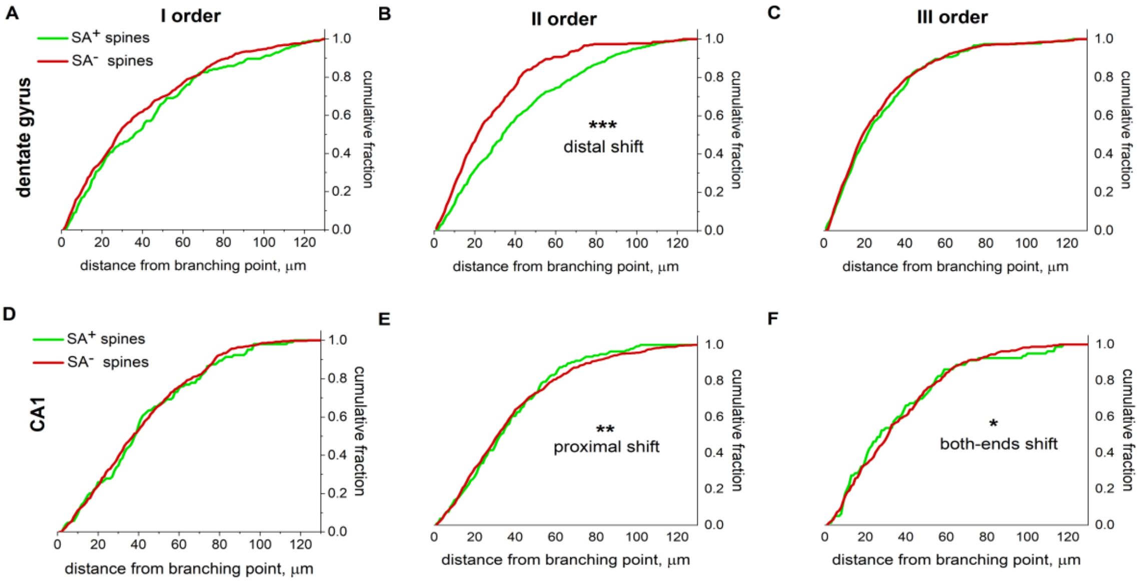

Figure 30. Comparison of the spatial distribution of SA-positive and SA-negative dendritic spines along the dendritic tree of CA1 and DG neurons of CFC mice. In the DG, **A**) No significant difference was detected for the first branching order (Kolmogorov-Smirnov two-sample test, D = 0.14615; p = 0.10082). **B**) For second-order dendrites, SA-positive spines were located at significantly more distal (i.e., farther from the upstream branching point) positions than SA-negative spines (D = 0.25385; ***p < 0.001). **C**) No significant difference was detected in the DG for the third branching order (D = 0.1; p = 0.4652). In the CA1, **D**) No significant difference was detected in the DG for the first branching order (D = 0.10769; p = 0.37625). **E**) For second-order dendrites, SA-positive spines were located at significantly more proximal (i.e., closer to the upstream branching point) positions than SA-negative spines (D = 0.2; **p = 0.00828). **F**) For third-order dendrites, SA-positive spines were located at either more proximal or more distal positions than SA-negative spines (D = 0.19231; * p = 0.0124). CFC-CA1, N = 2477 spines; hoca-CA1, N = 2975 spines; CFC-DG, N = 3230 spines; hoca-DG, N = 3165 spines.

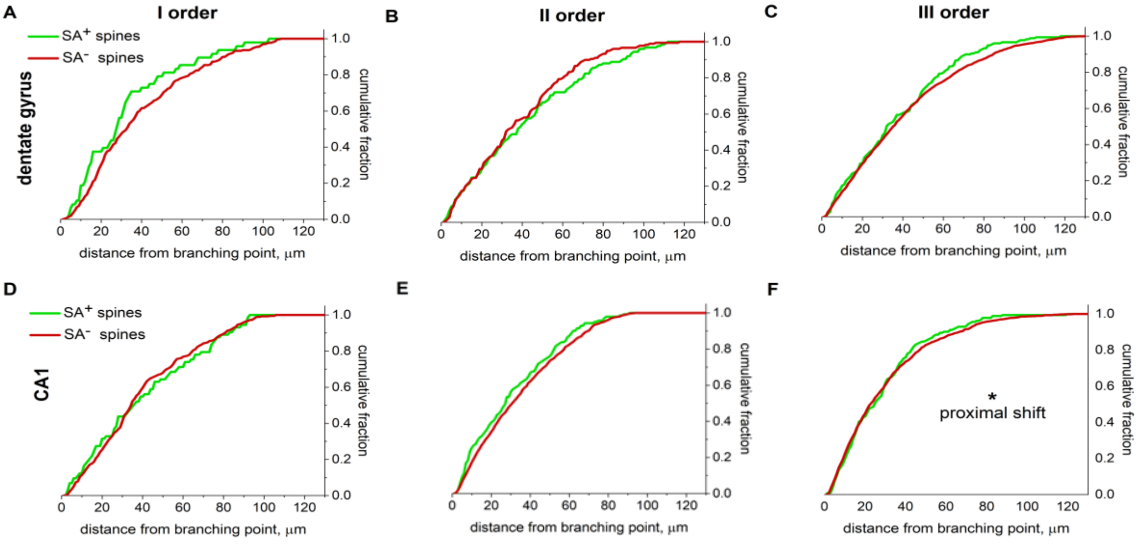

Figure 31. Comparison of the spatial distribution of SA-positive and SA-negative dendritic spines along the dendritic tree of CA1 and DG neurons in hoca mice. In the DG, **A-C**) No significant differences were detected in any branching order for the first branching order (Kolmogorov-Smirnov two-sample test, first order, D = 0.13077, p = 0.17917; second order, D = 0.15385, p = 0.07389; third order, D = 0.13846, p = 0.13545). In the CA1, no significant differences were detected for **c**) first- and **D**) second-order dendrites (first order, D = 0.1, p = 0.4652; second order, D = 0.06154, p = 0.93251). **E**) For the third branching order, for SA-positive spines a small, but significant proximal shift was detected in comparison to SA-negative spines (D = 0.19231; * p = 0.0124). N are the same as figure 30.

4.6 SA-Map: correlation of synaptic structural potentiation labeling with the expression of CFC-related behavior

The amount of time each mice spent in freezing behavior can be considered as an indicator of the intensity of learning during exposure to the association phase of CFC (see section 1.1). On the other hand, potentiated spine volume can be considered as an index of the strength of synaptic structural potentiation (see sections 1.5 and 1.6). To establish a relationship between these measures, a linear regression analysis was performed.

For both CA1 (Figure 32a) and DG (Figure 32b) we found a statistically significant correlation between the time spent in freezing and the average volume of SA-positive spines; on the opposite, no significant correlation existed for SA-negative spines (Figure 32c, Figure 32d).

These data point to a direct relationship between the degree of physical synaptic potentiation in the CA1 and DG and the strength of expression of a hippocampus-dependent behavior, based on associative learning.

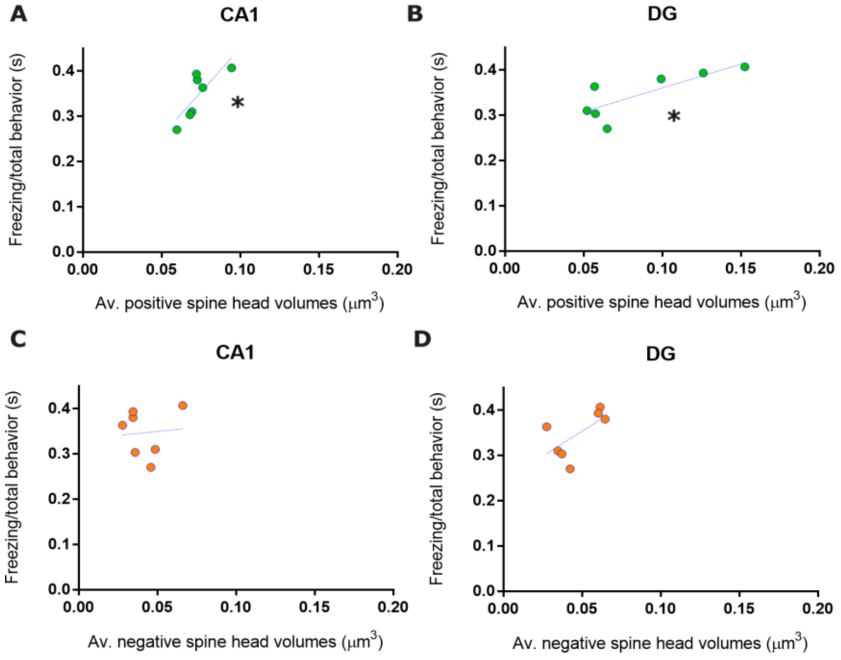

Figure 32. Direct relationship between the time spent in freezing and the strength of structural potentiation. A-B) Significant correlation between the time spent in freezing and the volume of SA-positive dendritic spines in the CA1 (linear regression analysis, R^2 = 0.6346, *p = 0.0320) and DG (R^2 = 0.6395, *p = 0.0309). **C-D)** No significant correlation could be detected between the time spent freezing and the volume of SA-negative dendritic spines for either the CA1 (R^2 = 0.007611, p = 0.8525) and the DG (R^2 = 0.4066, p = 0.1234). CFC, N = 7 mice, CA1, N=15 neurons, DG, N=12 neurons; hoca, N = 5 mice) For CFC condition, CA1, N=6 neurons, DG, N=6 neurons.

4.7 SA-Mol: validation of the *in vivo* expression pattern of constructs for the analysis of the PSD-95 interactome at potentiated synapses

The results obtained from the SA-Map set of experiments sparked the question of determining the changes in the synaptic proteome associated with synaptic potentiation induced by a specific learning task. To this end, we took inspiration from the PSD-95 proteomic bait described by Férnandez et al. (2009), and expressed specifically at potentiated synapses, under SynActive control, a construct for the isolation of the interactome of the postsynaptic hub protein PSD-95 via co-immunoprecipitation.

More in detail, PSD-95 was fused to a sequence allowing for tandem affinity purification using sequential immunoprecipitation against the FLAG and 6×His tags, separated by the consensus sequence for cleavage by the tobacco etch virus (TEV) protease (Férnandez et al., 2009). This coding region was flanked by 5' and 3' UTR regions of the Arc mRNA, and controlled by the synthetic activity-dependent promoter ESARE (Kawashima et al., 2013), to obtain ESARE::SA-PSD95-6×His-TEV-FLAG. As a control construct, the same PSD95-6×His-TEV-FLAG coding region was placed under the control of the constitutive synapsin promoter to obtain hSyn::PSD95-6×His-TEV-FLAG (see also section 3.1). The DNA constructs were delivered to the brain via Adeno Associated Vectors and used for the co-immunoprecipitation of the SA-PSD-95 proteomic bait with the synaptic proteins interacting, directly or indirectly, with the endogenous PSD-95 (PSD-95 interactome) and their subsequent identification via mass spectrometry.

Before embarking in the co-immunoprecipitation of the SA-PSD-95 proteomic bait with thePSD-95 interactome and in its subsequent identification via mass spectrometry, the pattern of expression of the two constructs was verified, by injection of AAVs coding for either one of them, along with hSyn-driven tdTomato filler, to visualize the neuronal morphology. Imaging of sections stained for immunofluorescence against FLAG and tdTomato showed a sparse labeling of neurons (TdTomato signal), surrounded by green puncta (FLAG signal, Figures 33 a-b). A further immunofluorescence was done also against Homer 1b/c, to control for FLAG colocalizing with postsynaptic elements (Homer-1 signal, Figure

33d). Finally, if primary antibodies were omitted during the immunofluorescence procedure (Figure 33e), or no AAVs were injected (Figure 33f), no significant signal appeared neither from the red nor from the green channel.

For both ESARE::SA-PSD95-6×His-TEV-FLAG and hSyn::PSD95-6×His-TEV-FLAG conditions, mice exposed to CFC and home cage (hoca) controls were analyzed. Quantification of FLAG-positive synaptic puncta along apical dendrites of CA1 neurons showed that, for ESARE::SA-PSD95-6×His-TEV-FLAG-expressing mice, exposure to CFC was accompanied by a significant increase in their linear density [puncta/μm] compared to home cage mice. On the contrary, hSyn::PSD95-6×His-TEV-FLAG-expressing mice did not show any significant differences between the CFC and home cage conditions (Figure 33c).

These results show that only SynActive-controlled PSD95-6×His-TEV-FLAG responds to behavioral induction of learning and to the ensuing synaptic structural potentiation with a rise in its expression. This supports the use of ESARE::SA-PSD95-6×His-TEV-FLAG for identifying the potentiation-specific PSD-95 interactome using a comparative approach.

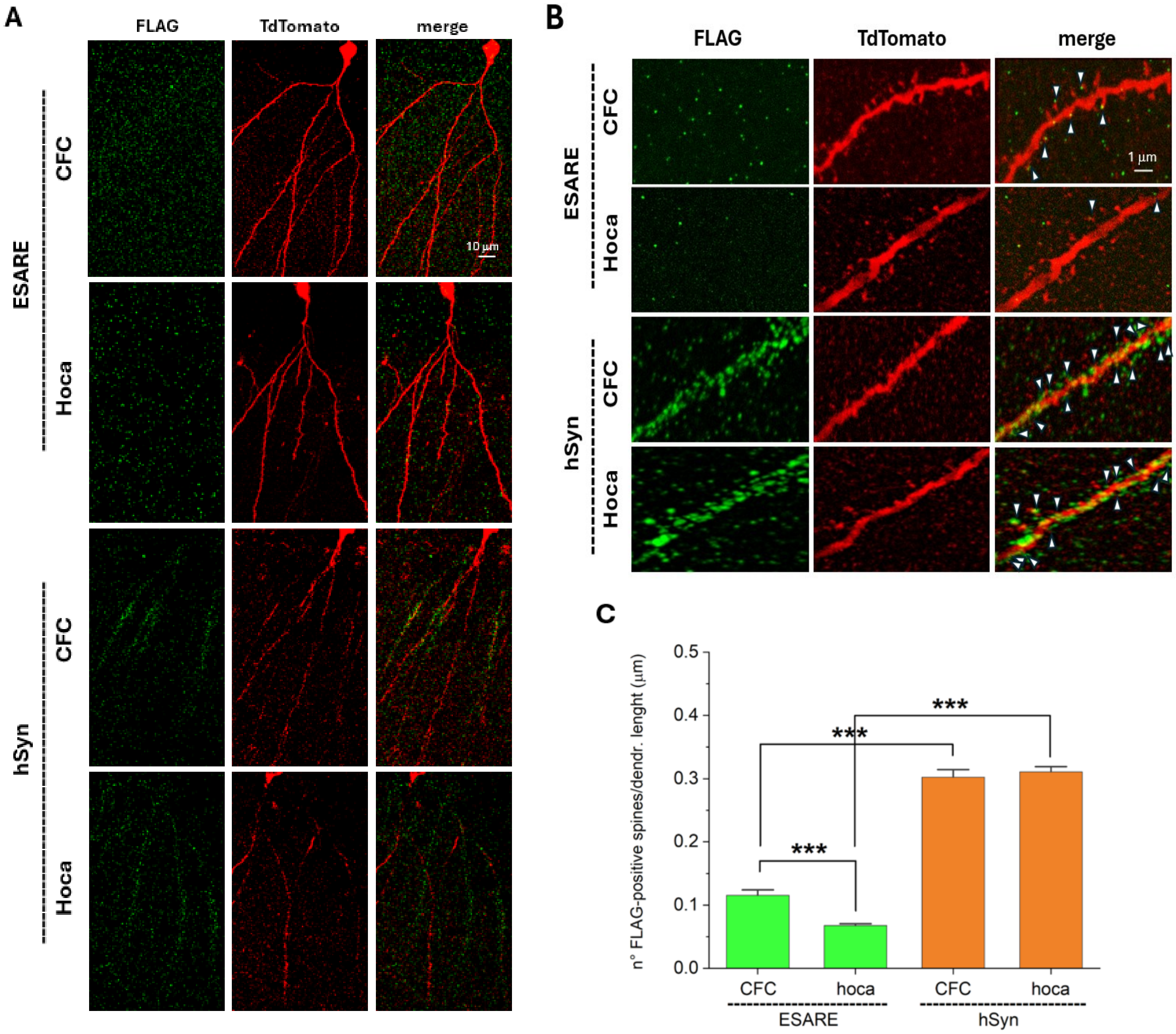
A
FLAG
TdTomato
merge
ESARE
CFC
Hoca
hSyn
CFC
Hoca
10 µm
B
FLAG
TdTomato
merge
ESARE
CFC
Hoca
hSyn
CFC
Hoca
1 µm
C
n° FLAG-positive spines/dendr. lenght (µm)
0.5
0.4
0.3
0.2
0.1
0.0
***
***
***
CFC
hoca
CFC
hoca
ESARE
hSyn

Figure 33. Representative images and quantification of the density of PSD95-FLAG-positive puncta in mice expressing ESARE::SA-PSD95-6×His-TEV-FLAG or hSyn::PSD95-6×His-TEV-FLAG in the CA1. Representative low- (**A**) and high-magnification (**B**) images from the CA1 of mice expressing ESARE::SA-PSD95-6×His-TEV-FLAG or hSyn::PSD95-6×His-TEV-FLAG. **C)** Exposure to CFC resulted in increased density of PSD95-FLAG-positive puncta in comparison to hoca only for mice expressing the SA-controlled version of the construct (ESARE), while constitutive expression of the construct (hSyn) resulted in lack of responsiveness to learning activity, in addition to labeling a significantly higher number of dendritic spines (ANOVA-2, factor 1 = type of construct, factor 2 = CFC or hoca; interaction, F = 24.369, ***$p<0.001$, followed by Bonferroni post hoc test, ESARE-CFC vs. ESARE-hoca, t = 5.935, ***$p < 0.001$; hSyn-CFC vs. ESARE-CFC, t = 23.211, ***$p < 0.001$; ESARE-hoca vs. hSyn-hoca, t = 30.192, ***$p < 0.001$; hSyn-CFC vs. hSyn-hoca, t = 1.046, p = 0.306). ESARE-CFC, N=7 mice and 15 neurons; ESARE-hoca, N=7 mice and 15 neurons; hSyn-CFC, N=7 mice and 15 neurons; hSyn-hoca, N=7 mice and 15 neurons. Continued on next page.

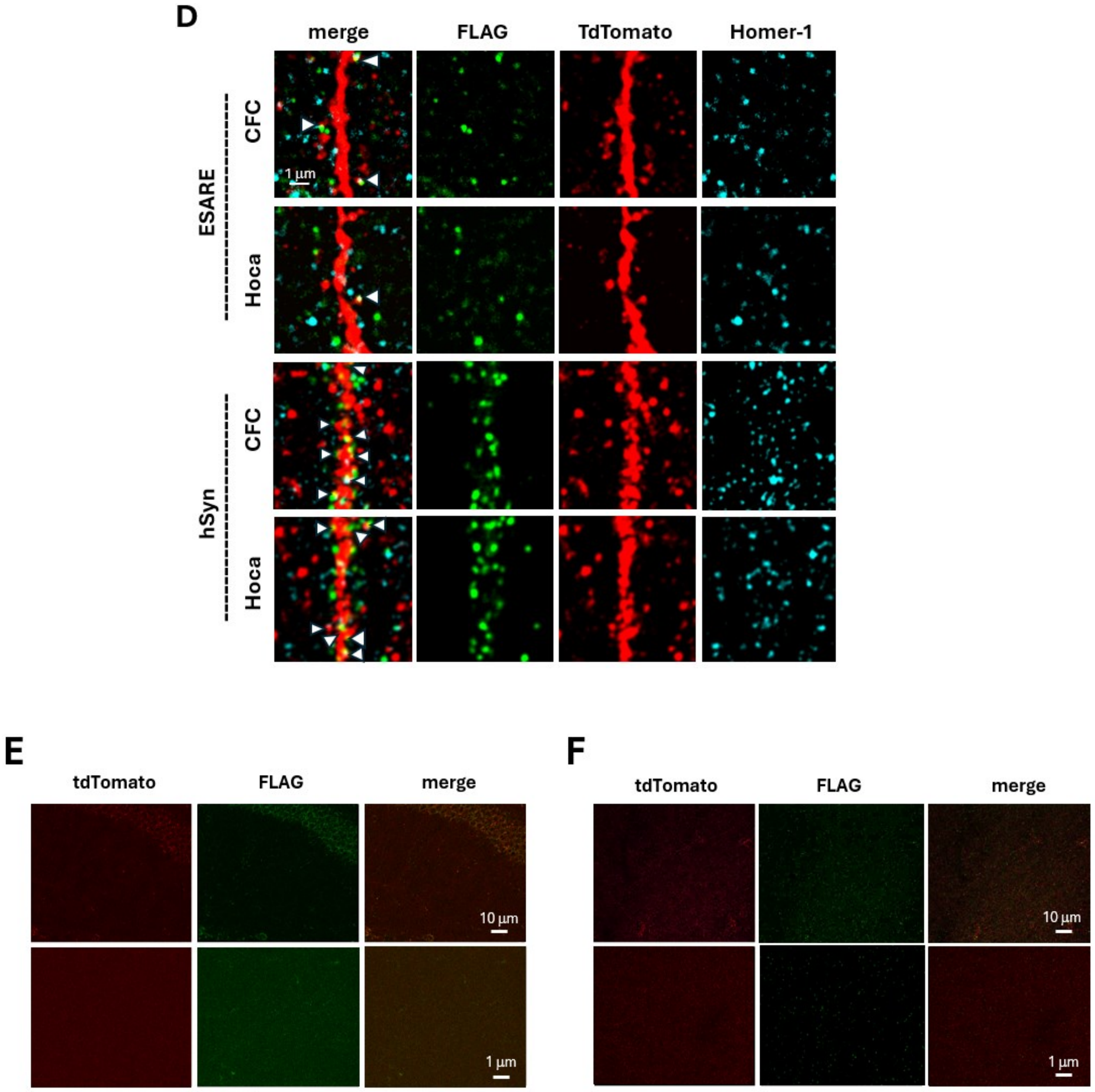
D
merge
FLAG
TdTomato
Homer-1
ESARE
CFC
Hoca
hSyn
CFC
Hoca
1 µm
E
tdTomato
FLAG
merge
10 µm
1 µm
F
tdTomato
FLAG
merge
10 µm
1 µm

Figure 33. Continued from previous page. D) High magnification of CA1 dendrites signal colocalizing with postsynaptic Homer 1b/c. **E)** Omitting the primary antibodies against tdTomato and FLAG from the immunofluorescence procedure abolishes detection of both antigens; **F)** omitting AAV injection results in undetectable immunoreactivity for both tdTomato and FLAG.

5. Discussion

Despite a strong consensus has been reached about the existence of engram cells in a variety of brain areas (Han et al., 2007; Han et al., 2009; Liu et al., 2012; Ramirez et al., 2013; Vetere et al., 2019), an additional aspect to be taken into account is that each of these engram neurons have thousands of synaptic contacts able to modify their proteic repertoire and structure to bidirectionally adapt to the strength of incoming stimuli. In order to address these questions, we have extended the ‘SynActive’ experimental strategy to facilitate the *in vivo* expression of SynActive reporters or effectors from the transgenic in utero electroporation approach, as in (SA, Gobbo et al., 2017) to the more flexible and versatile use of viral vectors. Thus, the first aim and achievement of my thesis was to exploit a set of Adeno Associated Viral vectors harboring SynActive-regulated reporter constructs. This SynActive AAV toolbox was then used to detect and characterize hippocampal potentiated spines (Sa-Map) and to validate a synaptic proteomic probe (Sa-Mol), after extensive optimization of the conditions for expression sparsity and imaging of the SA-reportes against the background of the filler staining.

For SA-Map, delivery via adeno-associated viral vectors (AAVs) of SA-based genetically encoded tools was conducted according to an experimental design that guaranteed both a spatial confinement (hippocampal injection site) and a temporal confinement of the expression of the construct (Tet-On doxycycline-dependent system), limited to a time window during which a given memory formation occurs. SA-Map imaging results confirmed these two properties of SynActive-PSD95Δ1.2-mVenus-HA fear-driven expression both in DG and CA1 (see section 4.1). Consistently with our knowledge about the activity-dependent increase of the volume of dendritic spines undergoing synaptic plasticity (Matsuzaki et al., 2001; Matsuzaki et al., 2004; Holtmaat and Svoboda, 2009), the volumes of hippocampal DG and CA1 spine heads expressing the SynActive construct were significantly larger than those of the spines that were not expressing the SynActive reporter (SA-negative), further validating that the SynActive construct was preferentially expressed at potentiated spines also via

AAV vectors (see section 4.2). Coherently, the number of SA-positive spines was greater in CFC conditioned animals compared to their mates left in their home cage (see section 4.3); also, with a view to a possible in-depth study on the basal activity of the hippocampus, it could be an interesting fact that more SA-positive spines were present in CA1 than in DG of non-conditioned mice (see section 4.3). On the other hand, the spine head volumes in DG were larger than those of CA1, regardless of the behavioral treatment and the response to the SynActive, and this already has evidence in the hippocampal microanatomy literature (Paulin et al., 2016; see section 4.2).

Regarding possible synaptic patterns of clustering, only in DG SA-positive spines tended to be closer in CFC than in resting state, while there was no difference in the nearest neighbor distance between potentiated spines in CA1. While offering important and long-waited experimental evidence for learning-dependent clustering of potentiated synapses, the finding of clustering in DG but not in CA1 may indicate subregion-specific plasticity rules which certainly deserve further investigation. Vice versa, in both regions of the hippocampus SA-negative spines tended to be closer to their neighbor in resting state (home cage) than in CFC (see section 4.4).

An important difference in the distribution of SA-positive dendritic spines, for the CFC (but not in home cage) group, regarded the 2° order dendritic branches: in DG neurons, the SA-positive spines tended to be shifted distally, respect to the SA-negative spines (so, further from the branching point of that segment and, consequently, from the soma of the neuron) while in CA1 they were distributed proximally (so, closer to the branching point of that segment and, consequently, to the soma of the neuron. See section 4.5). In terms of hippocampal connectivity (see section 1.2), even though we know that hippocampal information does not travel solely and unidirectionally through the trisynaptic loop (Yeckel and Berger, 1990), dentate gyrus first receives sensory informations from the associative area of the entorhinal cortex, and that is essential for pattern-separation and encoding of a fear memory for a new conditioned context (Hainmueller and Bartos, 2020). DG SA-positive spines further away from the soma could reflect synaptic plasticity facilitating the integration of sensory information with the emotion associated with fear, modulated by connections with the entorhinal cortex's associative area, basolateral amygdala and CA3 (Yousuf et al., 2021), towards which efferent connections from the dentate gyrus are mainly directed. In CA1, arrival station of trisynaptic information and hippocampal data integrator (Tigerholm et al., 2013; Barrientos and Tiznado, 2016), potentiated spines closer to the soma could reflect instead the strengthening of pre-existing synapses and the storage of fear-related memories. Finally, time spent by the animals in the freezing mode positively correlated with the increase of head volumes of SA-positive spines, but not of SA-negative spines (see section 4.6), in keeping with the well-established relation between functional (potentiation) and structural (spine volume increase) synaptic plasticity.

All these results, together, demonstrate that the AAV-based SynActive toolbox is able to direct the expression of virtually any reporter protein in a synaptic activity-dependent manner. Unlike most sector studies, which have long reported changes in the shape, number and distribution of entire and undifferentiated populations of dendritic spines following induced enhancement (see Runge et al., 2020 for a review), this method enables us to detect and to characterize selectively synapses undergoing potentiation in response of a behaviorally relevant, learning task, during a well defined temporal window, highlighting differences not only between different regions, but also between different sections of the same neuron.

The virally based SynActive toolbox constructed and validated in my thesis also proved to be much more flexible and versatile than the procedure exposed in Gobbo et al. (2017), whose strict dependence on in utero electroporation made it more invasive for the animal and more limited in terms of brain targeting. On the other hand, the use of intraparenchymal AAV microinjections allowed us to easily target the hippocampus, but also limited the volume of transduced neural tissue. This limitation can be overcome by packaging the SA constructs in PHP.eB serotype capsids (Chan et al., 2017), which allows easy crossing of the blood-brain barrier and, thus, could be systemically administered to transduce virtually the entire brain. This could pave the way to the creation of a brain-wide atlas of synaptic potentiation in response to the behavioral task of choice, in both physiological conditions and in pathological models of neurodevelopmental and neurodegenerative diseases.

An additional limitation of the constructs used is the need to use immunofluorescence for enhancing the signal from both fluorescent reporters, the tdTomato neuronal "filler" and mVenus-HA, localized at synapses. We will solve this problem by (i) testing the ihSyn self-reinforcing hybrid promoter (Chan et al., 2017) to drive the expression of rtTA and tdTomato and to transiently potentiate their own synthesis in response to doxycycline injection, (ii) substituting mVenus with a more stable green fluorescent protein variant. This should allow a direct visualization of the fluorescence by the SA-expressed reporters.

For SA-Mol, PSD-95-FLAG was selectively expressed at CA1 potentiated synapses: unlike the Synapsin::PSD95–HAT–TEV–FLAG construct, which expressed in a transcriptionally constitutive way by a large amount of dendritic spines and in a manner independent of the specific behavioral treatment applied, the pESARE::PSD95-HAT-TEV-FLAG construct was expressed by a limited subset of spines and in a manner strongly dependent on the behavioral treatment (see section 4.7). This enabled us to conduct with exquisite functional subcellular precision an immunoprecipitation of PSD95 and its protein-protein interactors from the hippocampal tissues of these animals following a specific behavioral learning task, using anti-flag coated paramagnetic beads; the analysis (currently in progress, Mainardi et al., 2019) of SynActive-PSD95-FLAG affinity purified proteins via mass spectrometry and comparative bioinformatics can provide a molecular fingerprint specifically of potentiated spines under learning, unlike previous proteomic approaches which have identified a variety of up and down-regulated proteins but examining mixed heterogeneous pools of synapses, not all enhanced by a specific learning task (see Dosemeci et al., 2006; Fernández et al., 2009).

In conclusion, this study provides a validation of a viral-based toolbox for the expression of SynActive reporters and takes a small step forward in the direction taken in recent years to identify the Semon’s engram: pushing this difficult search to a higher degree of resolution. The aim is to narrow the field to units that are truly sufficient and necessary for the encoding and storage of memories: from the cell to its own synapses.

6. Bibliography

Abraham, W. C., & Bear, M. F. (1996). Metaplasticity: the plasticity of synaptic plasticity. *Trends in neurosciences*, *19*(4), 126–130.

Adams, J. P., & Dudek, S. M. (2005). Late-phase long-term potentiation: getting to the nucleus. *Nature reviews. Neuroscience*, *6*(9), 737–743.

Adrian, M., Kusters, R., Wierenga, C. J., Storm, C., Hoogenraad, C. C., & Kapitein, L. C. (2014). Barriers in the brain: resolving dendritic spine morphology and compartmentalization. *Frontiers in neuroanatomy*, *8*, 142.

Akirav, I., & Richter-Levin, G. (1999). Biphasic modulation of hippocampal plasticity by behavioral stress and basolateral amygdala stimulation in the rat. *The Journal of neuroscience : the official journal of the Society for Neuroscience*, *19*(23), 10530–10535.

Alarcon, J. M., Barco, A., & Kandel, E. R. (2006). Capture of the late phase of long-term potentiation within and across the apical and basilar dendritic compartments of CA1 pyramidal neurons: synaptic tagging is compartment restricted. *The Journal of neuroscience : the official journal of the Society for Neuroscience*, *26*(1), 256–264.

Araç, D., Boucard, A. A., Ozkan, E., Strop, P., Newell, E., Südhof, T. C., & Brunger, A. T. (2007). Structures of neuroligin-1 and the neuroligin-1/neurexin-1 beta complex reveal specific protein-protein and protein-Ca2+ interactions. *Neuron*, *56*(6), 992–1003.

Ashley, J., Cordy, B., Lucia, D., Fradkin, L. G., Budnik, V., & Thomson, T. (2018). Retrovirus-like Gag Protein Arc1 Binds RNA and Traffics across Synaptic Boutons. *Cell*, *172*(1-2), 262–274.e11.

Atkinson, R.C. & Shiffrin, R.M. (1968). Human memory: a proposed system and its control processes. In K.W. Spence & J.T. Spence (Eds.), *The psychology of learning and motivation: Advances in research and theory. (Vol. 2).* New York: Academic Press. Pp. 89–195.

Bahrami, S., & Drabløs, F. (2016). Gene regulation in the immediate-early response process. *Advances in biological regulation*, *62*, 37–49.

Bapst, A. M., Dahl, S. L., Knöpfel, T., & Wenger, R. H. (2020). Cre-mediated, loxP independent sequential recombination of a tripartite transcriptional stop cassette allows for partial read-through transcription. *Biochimica et biophysica acta. Gene regulatory mechanisms*, *1863*(8), 194568.

Barrientos, S.A., Tiznado, V. (2016) Hippocampal CA1 subregion as a context decoder. *Journal of Neuroscience, 36* (25) 6602-6604.

Bear, M.F. (1995). Mechanism for a sliding synaptic modification threshold. *Neuron. 15* (1): 1-4.

Bemben, M. A., Shipman, S. L., Hirai, T., Herring, B. E., Li, Y., Badger, J. D., 2nd, Nicoll, R. A., Diamond, J. S., & Roche, K. W. (2014). CaMKII phosphorylation of neuroligin-1 regulates excitatory synapses. *Nature neuroscience*, *17*(1), 56–64.

Berridge M. J. (1998). Neuronal calcium signaling. *Neuron*, *21*(1), 13–26.

Bienenstock, E. L., Cooper, L. N., & Munro, P. W. (1982). Theory for the development of neuron selectivity: orientation specificity and binocular interaction in visual cortex. *The Journal of neuroscience : the official journal of the Society for Neuroscience*, *2*(1), 32–48.

Bliss, T. V., & Lomo, T. (1973). Long-lasting potentiation of synaptic transmission in the dentate area of the anaesthetized rabbit following stimulation of the perforant path. *The Journal of physiology*, *232*(2), 331–356.

Bosch, M., Castro, J., Saneyoshi, T., Matsuno, H., Sur, M., & Hayashi, Y. (2014). Structural and molecular remodeling of dendritic spine substructures during long-term potentiation. *Neuron*, *82*(2), 444–459.

Bosch, M., & Hayashi, Y. (2012). Structural plasticity of dendritic spines. *Current opinion in neurobiology*, *22*(3), 383–388.

Bourne, J., & Harris, K. M. (2007). Do thin spines learn to be mushroom spines that remember? *Current opinion in neurobiology*, *17*(3), 381–386.

Bouton M. E. (2002). Context, ambiguity, and unlearning: sources of relapse after behavioral extinction. *Biological psychiatry*, *52*(10), 976–986.

Bouton, M. E., & Bolles, R. C. (1979). Role of conditioned contextual stimuli in reinstatement of extinguished fear. *Journal of Experimental Psychology: Animal Behavior Processes, 5*(4), 368–378.

Bramham, C. R., Alme, M. N., Bittins, M., Kuipers, S. D., Nair, R. R., Pai, B., Panja, D., Schubert, M., Soule, J., Tiron, A., & Wibrand, K. (2010). The Arc of synaptic memory. *Experimental brain research*, *200*(2), 125–140.

Bramham, C. R., & Messaoudi, E. (2005). BDNF function in adult synaptic plasticity: the synaptic consolidation hypothesis. *Progress in neurobiology*, *76*(2), 99–125.

Bramham, C. R., Worley, P. F., Moore, M. J., & Guzowski, J. F. (2008). The immediate early gene arc/arg3.1: regulation, mechanisms, and function. *The Journal of neuroscience : the official journal of the Society for Neuroscience*, *28*(46), 11760–11767.

Bredt, D. S., & Nicoll, R. A. (2003). AMPA receptor trafficking at excitatory synapses. *Neuron*, *40*(2), 361–379.

Brewer, J. B., Gabrieli, J.D.E., Preston, A. R., Vaidya, C.J., Rosen, A.C. (2007). Chapter 5 – Memory. *Textbook of Clinical Neurology (Third Edition)*, 63-78.

Britton, J. C., Evans, T. C., & Hernandez, M. V. (2014). Looking beyond Fear and Extinction Learning: Considering Novel Treatment Targets for Anxiety. *Current behavioral neuroscience reports, 1(3)*, 134–143.

Broadbent, N. J., & Clark, R. E. (2013). Remote context fear conditioning remains hippocampus-dependent irrespective of training protocol, training-surgery interval, lesion size, and lesion method. *Neurobiology of learning and memory*, *106*, 300–308.

Buch, T., Heppner, F. L., Tertilt, C., Heinen, T. J., Kremer, M., Wunderlich, F. T., Jung, S., & Waisman, A. (2005). A Cre-inducible diphtheria toxin receptor mediates cell lineage ablation after toxin administration. *Nature methods*, *2*(6), 419–426.

Budnik, V., & Thomson, T. (2020). Structure of an Arc-ane virus-like capsid. *Nature neuroscience*, *23*(2), 153–154.

Buzsáki G. (2002). Theta oscillations in the hippocampus. *Neuron*, *33*(3), 325–340.

Cao, G., & Harris, K. M. (2014). Augmenting saturated LTP by broadly spaced episodes of theta-burst stimulation in hippocampal area CA1 of adult rats and mice. *Journal of neurophysiology*, *112*(8), 1916–1924.

Cao, C., Rioult-Pedotti, M. S., Migani, P., Yu, C. J., Tiwari, R., Parang, K., Spaller, M. R., Goebel, D. J., & Marshall, J. (2013). Impairment of TrkB-PSD-95 signaling in Angelman syndrome. *PLoS biology*, *11*(2), e1001478.

Caruana, D. A., Alexander, G. M., & Dudek, S. M. (2012). New insights into the regulation of synaptic plasticity from an unexpected place: hippocampal area CA2. *Learning & memory (Cold Spring Harbor, N.Y.)*, *19*(9), 391–400.

Casadio, A., Martin, K. C., Giustetto, M., Zhu, H., Chen, M., Bartsch, D., Bailey, C. H., & Kandel, E. R. (1999). A transient, neuron-wide form of CREB-mediated long-term facilitation can be stabilized at specific synapses by local protein synthesis. *Cell*, *99*(2), 221–237.

Chan, K. Y., Jang, M. J., Yoo, B. B., Greenbaum, A., Ravi, N., Wu, W. L., Sánchez-Guardado, L., Lois, C., Mazmanian, S. K., Deverman, B. E., & Gradinaru, V. (2017). Engineered AAVs for efficient noninvasive gene delivery to the central and peripheral nervous systems. *Nature neuroscience*, *20*(8), 1172–1179.

Cheng, D., Hoogenraad, C. C., Rush, J., Ramm, E., Schlager, M. A., Duong, D. M., Xu, P., Wijayawardana, S. R., Hanfelt, J., Nakagawa, T., Sheng, M., & Peng,

J. (2006). Relative and absolute quantification of postsynaptic density proteome isolated from rat forebrain and cerebellum. *Molecular & cellular proteomics : MCP*, *5*(6), 1158–1170.

Chevaleyre, V., & Siegelbaum, S. A. (2010). Strong CA2 pyramidal neuron synapses define a powerful disynaptic cortico-hippocampal loop. *Neuron*, *66*(4), 560–572.

Chubet, R. G., & Brizzard, B. L. (1996). Vectors for expression and secretion of FLAG epitope-tagged proteins in mammalian cells. *BioTechniques*, *20*(1), 136–141.

Citri, A., & Malenka, R. C. (2008). Synaptic plasticity: multiple forms, functions, and mechanisms. *Neuropsychopharmacology: official publication of the American College of Neuropsychopharmacology, 33*(1), 18–41.

Collingridge, G. L., Kehl, S. J., & McLennan, H. (1983). Excitatory amino acids in synaptic transmission in the Schaffer collateral-commissural pathway of the rat hippocampus. *The Journal of physiology, 334*, 33–46.

Collingridge, G. L., Peineau, S., Howland, J. G., & Wang, Y. T. (2010). Long-term depression in the CNS. *Nature reviews. Neuroscience*, *11*(7), 459–473.

Curzon, P., Rustay, N.R., Browman, K.E. (2009) Cued and Contextual Fear Conditioning for Rodents. In: *Buccafusco J.J., editor. Methods of Behavior Analysis in Neuroscience. 2nd edition. Boca Raton (FL): CRC Press/Taylor & Francis*; chapter 2.

Czapiński, J., Kiełbus, M., Kałafut, J., Kos, M., Stepulak, A., & Rivero-Müller, A. (2017). How to Train a Cell-Cutting-Edge Molecular Tools. *Frontiers in chemistry*, *5*, 12.

Das, A.T., Tenenbaum, L., Berkhout, B. (2016) Tet-On Systems For Doxycycline-inducible Gene Expression. *Curr Gene Ther. 16*(3):156-67.

Denny, C. A., Lebois, E., & Ramirez, S. (2017). From Engrams to Pathologies of the Brain. *Frontiers in neural circuits*, *11*, 23.

Derkach, V. A., Oh, M. C., Guire, E. S., & Soderling, T. R. (2007). Regulatory mechanisms of AMPA receptors in synaptic plasticity. *Nature reviews. Neuroscience*, *8*(2), 101–113.

Di Garbo, A., Mainardi, M., Chillemi, S., Maffei, L., & Caleo, M. (2011). Environmental enrichment modulates cortico-cortical interactions in the mouse. *PloS one*, *6*(9), e25285.

Dosemeci, A., Makusky, A. J., Jankowska-Stephens, E., Yang, X., Slotta, D. J., & Markey, S. P. (2007). Composition of the synaptic PSD-95 complex. *Molecular & cellular proteomics : MCP*, *6*(10), 1749–1760.

Dosemeci, A., Weinberg, R. J., Reese, T. S., & Tao-Cheng, J. H. (2016). The Postsynaptic Density: There Is More than Meets the Eye. *Frontiers in synaptic neuroscience*, *8*, 23.

Dougherty, B (2005). www.optinav.info/Diffraction-PSF-3D.htm

Dudek, S. M., & Bear, M. F. (1993). Bidirectional long-term modification of synaptic effectiveness in the adult and immature hippocampus. *The Journal of neuroscience: the official journal of the Society for Neuroscience*, *13*(7), 2910–2918.

Duncan K, Ketz N, Inati SJ, Davachi L (2012) Evidence for area CA1 as a match/mismatch detector: a high-resolution FMRI study of the human hippocampus. *Hippocampus 22*:389–398.

Dynes, J. L., & Steward, O. (2007). Dynamics of bidirectional transport of Arc mRNA in neuronal dendrites. *The Journal of comparative neurology*, *500*(3), 433–447.

Ehrlich, I., Klein, M., Rumpel, S., & Malinow, R. (2007). PSD-95 is required for activity-driven synapse stabilization. *Proceedings of the National Academy of Sciences of the United States of America*, *104*(10), 4176–4181.

Eichenbaum, H., Yonelinas, A. P., & Ranganath, C. (2007). The medial temporal lobe and recognition memory. *Annual review of neuroscience*, *30*, 123–152.

Einhauer, A., & Jungbauer, A. (2001). The FLAG peptide, a versatile fusion tag for the purification of recombinant proteins. *Journal of biochemical and biophysical methods*, *49*(1-3), 455–465.

Feldman, D.E. (2009) Developmental Synaptic Plasticity: LTP, LTD, and Synapse Formation and Elimination. *Encyclopedia of Neuroscience, Academic Press*, 495-501.

Fernandes, D., & Carvalho, A. L. (2016). Mechanisms of homeostatic plasticity in the excitatory synapse. *Journal of neurochemistry*, *139*(6), 973–996.

Fernández, E., Collins, M. O., Uren, R. T., Kopanitsa, M. V., Komiyama, N. H., Croning, M. D., Zografos, L., Armstrong, J. D., Choudhary, J. S., & Grant, S. G. (2009). Targeted tandem affinity purification of PSD-95 recovers core postsynaptic complexes and schizophrenia susceptibility proteins. *Molecular systems biology*, *5*, 269.

Fitzgerald, P. J., Pinard, C. R., Camp, M. C., Feyder, M., Sah, A., Bergstrom, H. C., Graybeal, C., Liu, Y., Schlüter, O. M., Grant, S. G., Singewald, N., Xu, W., & Holmes, A. (2015). Durable fear memories require PSD-95. *Molecular psychiatry*, *20*(7), 901–912.

Frank, A. C., Huang, S., Zhou, M., Gdalyahu, A., Kastellakis, G., Silva, T. K., Lu, E., Wen, X., Poirazi, P., Trachtenberg, J. T., & Silva, A. J. (2018). Hotspots of dendritic spine turnover facilitate clustered spine addition and learning and memory. *Nature communications*, *9*(1), 422.

Frey, U., & Morris, R. G. (1997). Synaptic tagging and long-term potentiation. *Nature*, *385*(6616), 533–536.

Frey, U., & Morris, R. G. (1998). Synaptic tagging: implications for late maintenance of hippocampal long-term potentiation. *Trends in neurosciences*, *21*(5), 181–188.

Frey, U., Krug, M., Reymann, K. G., & Matthies, H. (1988). Anisomycin, an inhibitor of protein synthesis, blocks late phases of LTP phenomena in the hippocampal CA1 region in vitro. *Brain research*, *452*(1-2), 57–65.

Fu, M., Yu, X., Lu, J., & Zuo, Y. (2012). Repetitive motor learning induces coordinated formation of clustered dendritic spines *in vivo*. *Nature*, *483*(7387), 92–95.

Fukunaga, K., & Miyamoto, E. (1998). Role of MAP kinase in neurons. *Molecular neurobiology*, *16*(1), 79–95.

Ghandour, K., Ohkawa, N., Fung, C., Asai, H., Saitoh, Y., Takekawa, T., Okubo-Suzuki, R., Soya, S., Nishizono, H., Matsuo, M., Osanai, M., Sato, M., Ohkura, M., Nakai, J., Hayashi, Y., Sakurai, T., Kitamura, T., Fukai, T., & Inokuchi, K. (2019). Orchestrated ensemble activities constitute a hippocampal memory engram. *Nature communications*, *10*(1), 2637.

Giorgi, C., Yeo, G. W., Stone, M. E., Katz, D. B., Burge, C., Turrigiano, G., & Moore, M. J. (2007). The EJC factor eIF4AIII modulates synaptic strength and neuronal protein expression. *Cell*, *130*(1), 179–191.

Gobbo, F., & Cattaneo, A. (2020). Neuronal Activity at Synapse Resolution: Reporters and Effectors for Synaptic Neuroscience. *Frontiers in molecular neuroscience*, *13*, 572312.

Gobbo, F., Marchetti, L., Jacob, A., Pinto, B., Binini, N., Pecoraro Bisogni, F., Alia, C., Luin, S., Caleo, M., Fellin, T., Cancedda, L., & Cattaneo, A. (2017). Activity-dependent expression of Channelrhodopsin at neuronal synapses. *Nature communications*, *8*(1), 1629.

Govindarajan, A., Israely, I., Huang, S. Y., & Tonegawa, S. (2011). The dendritic branch is the preferred integrative unit for protein synthesis-dependent LTP. *Neuron*, *69*(1), 132–146.

Gray, N. W., Weimer, R. M., Bureau, I., & Svoboda, K. (2006). Rapid redistribution of synaptic PSD-95 in the neocortex *in vivo*. *PLoS biology*, *4*(11), e370.

Gunaydin, L. A., Yizhar, O., Berndt, A., Sohal, V. S., Deisseroth, K., & Hegemann, P. (2010). Ultrafast optogenetic control. *Nature neuroscience*, *13*(3), 387–392.

Guzman, S. J., Schlögl, A., Frotscher, M., & Jonas, P. (2016). Synaptic mechanisms of pattern completion in the hippocampal CA3 network. *Science (New York, N.Y.)*, *353*(6304), 1117–1123.

Guzowski, J. F., McNaughton, B. L., Barnes, C. A., & Worley, P. F. (1999). Environment-specific expression of the immediate-early gene Arc in hippocampal neuronal ensembles. *Nature neuroscience*, *2*(12), 1120–1124.

Guzowski, J. F., McNaughton, B. L., Barnes, C. A., & Worley, P. F. (2001). Imaging neural activity with temporal and cellular resolution using FISH. *Current opinion in neurobiology*, *11*(5), 579–584.

Han, J. H., Kushner, S. A., Yiu, A. P., Cole, C. J., Matynia, A., Brown, R. A., Neve, R. L., Guzowski, J. F., Silva, A. J., & Josselyn, S. A. (2007). Neuronal competition and selection during memory formation. *Science (New York, N.Y.)*, *316*(5823), 457–460.

Han, J. H., Kushner, S. A., Yiu, A. P., Hsiang, H. L., Buch, T., Waisman, A., Bontempi, B., Neve, R. L., Frankland, P. W., & Josselyn, S. A. (2009). Selective erasure of a fear memory. *Science (New York, N.Y.)*, *323*(5920), 1492–1496.

Hao, L., Yang, Z., Lei, J. (2018). Underlying Mechanisms of Cooperativity, Input Specificity, and Associativity of Long-Term Potentiation Through a Positive Feedback of Local Protein Synthesis. *Front Comput Neurosci. May 1*;12:25.

Harvey, C. D., Yasuda, R., Zhong, H., & Svoboda, K. (2008). The spread of Ras activity triggered by activation of a single dendritic spine. *Science (New York, N.Y.)*, *321*(5885), 136–140.

Hawkins, J., & Ahmad, S. (2016). Why Neurons Have Thousands of Synapses, a Theory of Sequence Memory in Neocortex. Frontiers in neural circuits, 10, 23.

Hayashi, M. K., Tang, C., Verpelli, C., Narayanan, R., Stearns, M. H., Xu, R. M., Li, H., Sala, C., & Hayashi, Y. (2009). The postsynaptic density proteins Homer and Shank form a polymeric network structure. *Cell*, *137*(1), 159–171.

Hayashi-Takagi, A., Yagishita, S., Nakamura, M., Shirai, F., Wu, Y. I., Loshbaugh, A. L., Kuhlman, B., Hahn, K. M., & Kasai, H. (2015). Labelling and optical erasure of synaptic memory traces in the motor cortex. *Nature*, *525*(7569), 333–338.

Hayashi, Y., & Majewska, A. K. (2005). Dendritic spine geometry: functional implication and regulation. *Neuron*, *46*(4), 529–532.

Hawk, J., Abel, T. (2017). Immediate early genes are activated by latent transcription factors after learning. *Encyclopedia of behavioral neuroscience, 2nd edition*, *Academic Press,* 161-179.

Hebb, D.O. (1949). The Organization of Behavior. *New York: Wiley & Sons.*

Heinrichs, S. C., Leite-Morris, K. A., Guy, M. D., Goldberg, L. R., Young, A. J., & Kaplan, G. B. (2013). Dendritic structural plasticity in the basolateral amygdala after fear conditioning and its extinction in mice. *Behavioural brain research*, *248*, 80–84.

Hirano, T. (2018). Visualization of Exo- and Endocytosis of AMPA Receptors During Hippocampal Synaptic Plasticity Around Postsynaptic-Like Membrane Formed on Glass Surface. *Frontiers in cellular neuroscience*, *12*, 442.

Holtmaat, A., & Svoboda, K. (2009). Experience-dependent structural synaptic plasticity in the mammalian brain. *Nature reviews. Neuroscience*, *10*(9), 647–658.

Holtmaat, A. J., Trachtenberg, J. T., Wilbrecht, L., Shepherd, G. M., Zhang, X., Knott, G. W., & Svoboda, K. (2005). Transient and persistent dendritic spines in the neocortex *in vivo*. *Neuron*, *45*(2), 279–291.

Honkura, N., Matsuzaki, M., Noguchi, J., Ellis-Davies, G. C., & Kasai, H. (2008). The subspine organization of actin fibers regulates the structure and plasticity of dendritic spines. *Neuron*, *57*(5), 719–729.

Hotulainen, P., & Hoogenraad, C. C. (2010). Actin in dendritic spines: connecting dynamics to function. *The Journal of cell biology*, *189*(4), 619–629.

Huff, N. C., & Rudy, J. W. (2004). The amygdala modulates hippocampus-dependent context memory formation and stores cue-shock associations. *Behavioral neuroscience*, *118*(1), 53–62.

Inoue, M., Yagishita-Kyo, N., Nonaka, M., Kawashima, T., Okuno, H., & Bito, H. (2010). Synaptic activity-responsive element (SARE): A unique genomic structure with an unusual sensitivity to neuronal activity. *Communicative & integrative biology*, *3*(5), 443–446.

Izquierdo, I., Furini, C. R., & Myskiw, J. C. (2016). Fear Memory. *Physiological reviews, 96(2)*, 695–750.

Janak, P. H., & Tye, K. M. (2015). From circuits to behaviour in the amygdala. *Nature*, *517*(7534), 284–292.

Jiang, Y., Gong, N. N., Hu, X. S., Ni, M. J., Pasi, R., & Matsunami, H. (2015). Molecular profiling of activated olfactory neurons identifies odorant receptors for odors *in vivo*. *Nature neuroscience*, *18*(10), 1446–1454.

Josselyn, S. A., & Tonegawa, S. (2020). Memory engrams: Recalling the past and imagining the future. *Science (New York, N.Y.)*, *367*(6473), eaaw4325.

Kastellakis, G., & Poirazi, P. (2019). Synaptic Clustering and Memory Formation. *Frontiers in molecular neuroscience*, *12*, 300.

Kawashima, T., Kitamura, K., Suzuki, K., Nonaka, M., Kamijo, S., Takemoto-Kimura, S., Kano, M., Okuno, H., Ohki, K., & Bito, H. (2013). Functional labeling of neurons and their projections using the synthetic activity-dependent promoter E-SARE. *Nature methods*, *10*(9), 889–895.

Keck T., Mrsic-Flogel T. D., Afonso M. V., Eysel U. T., Bonhoeffer T., Hübener M. (2008). Massive restructuring of neuronal circuits during functional reorganization of adult visual cortex. *Nat. Neurosci.* 11, 1162–1167.

Keith, D., & El-Husseini, A. (2008). Excitation Control: Balancing PSD-95 Function at the Synapse. *Frontiers in molecular neuroscience*, *1*, 4.

Kennedy M. B. (2018). The Protein Biochemistry of the Postsynaptic Density in Glutamatergic Synapses Mediates Learning in Neural Networks. *Biochemistry*, *57*(27), 4005–4009.

Kobayashi, H., Yamamoto, S., Maruo, T., & Murakami, F. (2005). Identification of a cis-acting element required for dendritic targeting of activity-regulated cytoskeleton-associated protein mRNA. *The European journal of neuroscience*, *22*(12), 2977–2984.

Kopach, O., & Voitenko, N. (2013). Extrasynaptic AMPA receptors in the dorsal horn: evidence and functional significance. *Brain research bulletin*, *93*, 47–56.

Lai, C.S., Franke, T.F., Gan, W.B.. (2012) Opposite effects of fear conditioning and extinction on dendritic spine remodelling. *Nature, 483*:87–91

Lai, C. S. W., Adler, A. & Gan, W. B. (2018) Fear extinction reverses dendritic spine formation induced by fear conditioning in the mouse auditory cortex. *Proc Natl Acad Sci* USA

Lammel, S., Lim, B. K., Ran, C., Huang, K. W., Betley, M. J., Tye, K. M., Deisseroth, K., & Malenka, R. C. (2012). Input-specific control of reward and aversion in the ventral tegmental area. *Nature*, *491*(7423), 212–217.

Lashley, K. S. (1950). In search of the engram. In Society for Experimental Biology, *Physiological mechanisms in animal behavior. (Society's Symposium IV.)* (pp. 454–482). *Academic Press.*

Lavenex, P., & Amaral, D. G. (2000). Hippocampal-neocortical interaction: a hierarchy of associativity. *Hippocampus*, *10*(4), 420–430.

LeDoux, J. E. (2000). Emotion circuits in the brain. *Annual Review of Neuroscience*, *23*, 155-184.

LeDoux, J. E. (2007). The amygdala. *Current Biology*, *17*(20), R868-R874.

Leutgeb, S., & Leutgeb, J. K. (2007). Pattern separation, pattern completion, and new neuronal codes within a continuous CA3 map. *Learning & memory (Cold Spring Harbor, N.Y.)*, *14*(11), 745–757.

Linnenbrügger, N (2002). imagej.net/ij/ij/plugins/fftj.html

Lisman, J. E., & Grace, A. A. (2005). The hippocampal-VTA loop: controlling the entry of information into long-term memory. *Neuron*, *46*(5), 703–713.

Liu, X., Ramirez, S., Pang, P. T., Puryear, C. B., Govindarajan, A., Deisseroth, K., & Tonegawa, S. (2012). Optogenetic stimulation of a hippocampal engram activates fear memory recall. *Nature*, *484*(7394), 381–385.

Lüscher, C., & Malenka, R. C. (2012). NMDA receptor-dependent long-term potentiation and long-term depression (LTP/LTD). *Cold Spring Harbor perspectives in biology*, *4*(6), a005710.

Ma, S., & Zuo, Y. (2022). Synaptic modifications in learning and memory - A dendritic spine story. *Seminars in cell & developmental biology*, *125*, 84–90.

Mahringer D, Petersen A, Fiser A, Okuno H, Bito H, Perrier JF, Keller G (2019) Expression of c-Fos and Arc in hippocampal region CA1 marks neurons that exhibit learning-related activity changes. *bioRxiv* 644526

Mainardi, M., Gobbo, F., Jacob, A., Faraone, A., Sorokina, O., Zentilin, L., et al. (2019). “Proteomic characterization of the PSD-95 interactome selectively at in vivo potentiated synapses,” in ProMEMO - Proteins and Circuits in Memory. (Copenaghen, Denmark, 5–7 March).

Matsuzaki, M., Ellis-Davies, G. C., Nemoto, T., Miyashita, Y., Iino, M., & Kasai, H. (2001). Dendritic spine geometry is critical for AMPA receptor expression in hippocampal CA1 pyramidal neurons. *Nature neuroscience*, *4*(11), 1086–1092.

Matsuzaki, M., Honkura, N., Ellis-Davies, G. C., & Kasai, H. (2004). Structural basis of long-term potentiation in single dendritic spines. *Nature*, *429*(6993), 761–766.

McHugh, T. J., Jones, M. W., Quinn, J. J., Balthasar, N., Coppari, R., Elmquist, J. K., Lowell, B. B., Fanselow, M. S., Wilson, M. A., & Tonegawa, S. (2007). Dentate gyrus NMDA receptors mediate rapid pattern separation in the hippocampal network. *Science (New York, N.Y.)*, *317*(5834), 94–99.

Major, G., Larkum, M. E., & Schiller, J. (2013). Active properties of neocortical pyramidal neuron dendrites. *Annual review of neuroscience*, *36*, 1–24.

Malenka, R. C., & Bear, M. F. (2004). LTP and LTD: an embarrassment of riches. *Neuron*, *44*(1), 5–21.

Marchetti, L., Bonsignore, F., Gobbo, F., Amodeo, R., Calvello, M., Jacob, A., Signore, G., Schirripa Spagnolo, C., Porciani, D., Mainardi, M., Beltram, F., Luin, S., & Cattaneo, A. (2019). Fast-diffusing p75NTR monomers support apoptosis and growth cone collapse by neurotrophin ligands. *Proceedings of the National Academy of Sciences of the United States of America*, *116*(43), 21563–21572.

Martin, K.C. (2009). Synaptic capture and tagging. *The New Encyclopedia of Neuroscience*, Larry Squire et al.(eds.), Oxford: Academic Press, pp. 719-723

Martin, K. C., Casadio, A., Zhu, H., Yaping, E., Rose, J. C., Chen, M., Bailey, C. H., & Kandel, E. R. (1997). Synapse-specific, long-term facilitation of aplysia sensory to motor synapses: a function for local protein synthesis in memory storage. *Cell*, *91*(7), 927–938.

Messaoudi, E., Kanhema, T., Soulé, J., Tiron, A., Dagyte, G., da Silva, B., & Bramham, C. R. (2007). Sustained Arc/Arg3.1 synthesis controls long-term potentiation consolidation through regulation of local actin polymerization in the dentate gyrus *in vivo*. *The Journal of neuroscience : the official journal of the Society for Neuroscience*, *27*(39), 10445–10455.

Minatohara, K., Akiyoshi, M., & Okuno, H. (2016). Role of Immediate-Early Genes in Synaptic Plasticity and Neuronal Ensembles Underlying the Memory Trace. *Frontiers in molecular neuroscience*, *8*, 78.

Nadel, L., & Moscovitch, M. (1997). Memory consolidation, retrograde amnesia and the hippocampal complex. *Current opinion in neurobiology*, *7*(2), 217–227.

Nader, K., Schafe, G. E., & Le Doux, J. E. (2000). Fear memories require protein synthesis in the amygdala for reconsolidation after retrieval. *Nature, 406(6797)*, 722–726.

Nguyen, P. V., & Woo, N. H. (2003). Regulation of hippocampal synaptic plasticity by cyclic AMP-dependent protein kinases. *Progress in neurobiology*, *71*(6), 401–437.

Nikolaienko, O., Patil, S., Eriksen, M. S., & Bramham, C. R. (2018). Arc protein: a flexible hub for synaptic plasticity and cognition. *Seminars in cell & developmental biology*, *77*, 33–42.

Noguchi, J., Matsuzaki, M., Ellis-Davies, G. C., & Kasai, H. (2005). Spine-neck geometry determines NMDA receptor-dependent Ca2+ signaling in dendrites. *Neuron*, *46*(4), 609–622.

Norman, K.A. (2010) How hippocampus and cortex contribute to recognition memory: revisiting the complementary learning systems model. *Hippocampus 20*:1217–1227.

Okuno, H., Akashi, K., Ishii, Y., Yagishita-Kyo, N., Suzuki, K., Nonaka, M., Kawashima, T., Fujii, H., Takemoto-Kimura, S., Abe, M., Natsume, R., Chowdhury, S., Sakimura, K., Worley, P. F., & Bito, H. (2012). Inverse synaptic tagging of inactive synapses via dynamic interaction of Arc/Arg3.1 with CaMKIIβ. *Cell*, *149*(4), 886–898.

Okuno, H., Minatohara, K., & Bito, H. (2018). Inverse synaptic tagging: An inactive synapse-specific mechanism to capture activity-induced Arc/arg3.1 and to locally regulate spatial distribution of synaptic weights. *Seminars in cell & developmental biology*, *77*, 43–50.

Opazo, P., Labrecque, S., Tigaret, C. M., Frouin, A., Wiseman, P. W., De Koninck, P., & Choquet, D. (2010). CaMKII triggers the diffusional trapping of surface AMPARs through phosphorylation of stargazin. *Neuron*, *67*(2), 239–252.

Pastuzyn, E. D., Day, C. E., Kearns, R. B., Kyrke-Smith, M., Taibi, A. V., McCormick, J., Yoder, N., Belnap, D. M., Erlendsson, S., Morado, D. R., Briggs, J. A. G., Feschotte, C., & Shepherd, J. D. (2018). The Neuronal Gene Arc Encodes a Repurposed Retrotransposon Gag Protein that Mediates Intercellular RNA Transfer. *Cell*, *172*(1-2), 275–288.e18.

Paulin, J. J., Haslehurst, P., Fellows, A. D., Liu, W., Jackson, J. D., Joel, Z., Cummings, D. M., & Edwards, F. A. (2016). Large and Small Dendritic Spines Serve Different Interacting Functions in Hippocampal Synaptic Plasticity and Homeostasis. *Neural plasticity*, *2016*, 6170509.

Pedersen, S. W., Albertsen, L., Moran, G. E., Levesque, B., Pedersen, S. B., Bartels, L., Wapenaar, H., Ye, F., Zhang, M., Bowen, M. E., & Strømgaard, K. (2017). Site-Specific Phosphorylation of PSD-95 PDZ Domains Reveals Fine-Tuned Regulation of Protein-Protein Interactions. *ACS chemical biology*, *12*(9), 2313–2323.

Peirce, J. L., Chesler, E. J., Williams, R. W., & Lu, L. (2003). Genetic architecture of the mouse hippocampus: identification of gene loci with selective regional effects. *Genes, brain, and behavior*, *2*(4), 238–252.

Pelkey, K. A., Chittajallu, R., Craig, M. T., Tricoire, L., Wester, J. C., & McBain, C. J. (2017). Hippocampal GABAergic Inhibitory Interneurons. *Physiological reviews*, *97*(4), 1619–1747.

Petrantonakis, P. C., & Poirazi, P. (2014). A compressed sensing perspective of hippocampal function. *Frontiers in systems neuroscience*, *8*, 141.

Phelps, E. A., & LeDoux, J. E. (2005). Contributions of the amygdala to emotion processing: from animal models to human behavior. *Neuron*, *48*(2), 175–187.

Pinkstaff, J. K., Chappell, S. A., Mauro, V. P., Edelman, G. M., & Krushel, L. A. (2001). Internal initiation of translation of five dendritically localized neuronal mRNAs. *Proceedings of the National Academy of Sciences of the United States of America*, *98*(5), 2770–2775.

Pyronneau, A., He, Q., Hwang, J. Y., Porch, M., Contractor, A., & Zukin, R. S. (2017). Aberrant Rac1-cofilin signaling mediates defects in dendritic spines, synaptic function, and sensory perception in fragile X syndrome. *Science signaling*, *10*(504), eaan0852.

Quirk, G. J., & Mueller, D. (2008). Neural mechanisms of extinction learning and retrieval. *Neuropsychopharmacology: official publication of the American College of Neuropsychopharmacology, 33(1)*, 56–72.

Ramirez, S., Liu, X., Lin, P. A., Suh, J., Pignatelli, M., Redondo, R. L., Ryan, T. J., & Tonegawa, S. (2013). Creating a false memory in the hippocampus. *Science (New York, N.Y.)*, *341*(6144), 387–391.

Raymond, C. R., & Redman, S. J. (2002). Different calcium sources are narrowly tuned to the induction of different forms of LTP. *Journal of neurophysiology*, *88*(1), 249–255.

Redondo, R. L., Kim, J., Arons, A. L., Ramirez, S., Liu, X., & Tonegawa, S. (2014). Bidirectional switch of the valence associated with a hippocampal contextual memory engram. *Nature*, *513*(7518), 426–430.

Restivo, L., Vetere, G., Bontempi, B., Ammassari-Teule, M. (2009). The formation of recent and remote memory is associated with time-dependent formation of dendritic spines in the hippocampus and anterior cingulate cortex. *J Neurosci* 29: 8206–8214

Rogerson, T., Cai, D. J., Frank, A., Sano, Y., Shobe, J., Lopez-Aranda, M. F., & Silva, A. J. (2014). Synaptic tagging during memory allocation. *Nature reviews. Neuroscience*, *15*(3), 157–169.

Roy, D. S., Park, Y. G., Kim, M. E., Zhang, Y., Ogawa, S. K., DiNapoli, N., Gu, X., Cho, J. H., Choi, H., Kamentsky, L., Martin, J., Mosto, O., Aida, T., Chung, K., & Tonegawa, S. (2022). Brain-wide mapping reveals that engrams for a single memory are distributed across multiple brain regions. *Nature communications*, *13*(1), 1799.

Rudy, J.W. (2014). Chapter 9 – Making memories. *The Neurobiology of learning and memory*, 153-173

Runge, K., Cardoso, C., & de Chevigny, A. (2020). Dendritic Spine Plasticity: Function and Mechanisms. *Frontiers in synaptic neuroscience*, *12*, 36.

Sacco, T., Sacchetti, B. (2010) Role of secondary sensory cortices in emotional memory storage and retrieval in rats. *Science* 329, 649–656

Sacktor T. C. (2011). How does PKMζ maintain long-term memory?. *Nature reviews. Neuroscience*, *12*(1), 9–15.

Sala, C., Vicidomini, C., Bigi, I., Mossa, A., & Verpelli, C. (2015). Shank synaptic scaffold proteins: keys to understanding the pathogenesis of autism and other synaptic disorders. *Journal of neurochemistry*, *135*(5), 849–858.

Santoro A. (2013). Reassessing pattern separation in the dentate gyrus. *Frontiers in behavioral neuroscience*, *7*, 96.

Santuy, A., Tomás-Roca, L., Rodríguez, J. R., González-Soriano, J., Zhu, F., Qiu, Z., Grant, S., DeFelipe, J., & Merchan-Perez, A. (2020). Estimation of the number of synapses in the hippocampus and brain-wide by volume electron microscopy and genetic labeling. *Scientific reports*, *10*(1), 14014.

Schafe, G. E., Atkins, C. M., Swank, M. W., Bauer, E. P., Sweatt, J. D., & LeDoux, J. E. (2000). Activation of ERK/MAP kinase in the amygdala is required for memory consolidation of pavlovian fear conditioning. *The Journal of neuroscience: the official journal of the Society for Neuroscience, 20(21)*, 8177–8187.

Schindelin, J., Arganda-Carreras, I., Frise, E., Kaynig, V., Longair, M., Pietzsch, T., Preibisch, S., Rueden, C., Saalfeld, S., Schmid, B., Tinevez, J. Y., White, D. J., Hartenstein, V., Eliceiri, K., Tomancak, P., & Cardona, A. (2012). Fiji: an open-source platform for biological-image analysis. *Nature methods*, *9*(7), 676–682.

Seidenbecher, T., Laxmi, T. R., Stork, O., & Pape, H. C. (2003). Amygdalar and hippocampal theta rhythm synchronization during fear memory retrieval. *Science (New York, N.Y.)*, *301*(5634), 846–850.

Semon, R. (1921) The mneme. *London: Allen, Unwin*

Shatz C. J. (1992). The developing brain. *Scientific American*, *267*(3), 60–67.

Shi, S., Hayashi, Y., Esteban, J. A., & Malinow, R. (2001). Subunit-specific rules governing AMPA receptor trafficking to synapses in hippocampal pyramidal neurons. *Cell*, *105*(3), 331–343.

Siegelbaum, S., Schwartz, J.H., Kandel E.R. (2000) Modulation of synaptic transmission: second messengers. In E Kandel, JH Shwartz, TH Jessell (Eds.) *Principles of neural science, Fourth Edition* (pp.229-239). New York: McGraw-Hill Companies

Squire, L. R. (1987). Memory and brain. *New York: Oxford University Press*
Stephens, G.S., You, J.C., Fu, C.H., Chin, J. (2017) Molecular mechanisms of synaptic plasticity and memory and their dysfunction in Alzheimer's disease. *Learning and Memory: A Comprehensive Reference*, Ed. John H. Byrne et al., Elsevier, London. pp 65-135.

Steward, O., Farris, S., Pirbhoy, P. S., Darnell, J., & Driesche, S. J. (2015). Localization and local translation of Arc/Arg3.1 mRNA at synapses: some observations and paradoxes. *Frontiers in molecular neuroscience*, *7*, 101.

Steward, O., & Schuman, E. M. (2001). Protein synthesis at synaptic sites on dendrites. *Annual review of neuroscience*, *24*, 299–325.

Sun, Y., Chen, X., & Xiao, D. (2007). Tetracycline-inducible expression systems: new strategies and practices in the transgenic mouse modeling. *Acta biochimica et biophysica Sinica*, *39*(4), 235–246.

Sun, X., Lin, Y. (2016). Npas4: Linking Neuronal Activity to Memory. *Trends Neurosci. 39*(4) :264-275.

Szumlinski, K. K., Kalivas, P. W., & Worley, P. F. (2006). Homer proteins: implications for neuropsychiatric disorders. *Current opinion in neurobiology*, *16*(3), 251–257.

Taft, C. E., & Turrigiano, G. G. (2013). PSD-95 promotes the stabilization of young synaptic contacts. *Philosophical transactions of the Royal Society of London. Series B, Biological sciences*, *369*(1633), 20130134.

Tang, S. J., Reis, G., Kang, H., Gingras, A. C., Sonenberg, N., & Schuman, E. M. (2002). A rapamycin-sensitive signaling pathway contributes to long-term synaptic plasticity in the hippocampus. *Proceedings of the National Academy of Sciences of the United States of America*, *99*(1), 467–472.

Teyler, T. J., & DiScenna, P. (1986). The hippocampal memory indexing theory. *Behavioral neuroscience*, *100*(2), 147–154.

Thomas, G. M., & Huganir, R. L. (2004). MAPK cascade signalling and synaptic plasticity. *Nature reviews. Neuroscience*, *5*(3), 173–183.

Tigerholm, J., Migliore, M., & Fransén, E. (2013). Integration of synchronous synaptic input in CA1 pyramidal neuron depends on spatial and temporal distributions of the input. *Hippocampus*, *23*(1), 87–99.

Tonegawa, S., Liu, X., Ramirez, S., & Redondo, R. (2015). Memory Engram Cells Have Come of Age. *Neuron*, *87*(5), 918–931.

Tovote, P., Fadok, J. P., & Lüthi, A. (2015). Neuronal circuits for fear and anxiety. *Nature reviews. Neuroscience*, *16*(6), 317–331.

Tu, J. C., Xiao, B., Yuan, J. P., Lanahan, A. A., Leoffert, K., Li, M., Linden, D. J., & Worley, P. F. (1998). Homer binds a novel proline-rich motif and links group 1 metabotropic glutamate receptors with IP3 receptors. *Neuron*, *21*(4), 717–726.

Tulving, E. (1972). Episodic and semantic memory. In E. Tulving & W. Donaldson, Organization of memory. *Academic Press*.

Ugalde-Triviño, L., & Díaz-Guerra, M. (2021). PSD-95: An Effective Target for Stroke Therapy Using Neuroprotective Peptides. *International journal of molecular sciences*, *22*(22), 12585.

Varga, Z., Jia, H., Sakmann, B., & Konnerth, A. (2011). Dendritic coding of multiple sensory inputs in single cortical neurons *in vivo*. *Proceedings of the National Academy of Sciences of the United States of America*, *108*(37), 15420–15425.

Vetere, G., Tran, L. M., Moberg, S., Steadman, P. E., Restivo, L., Morrison, F. G., Ressler, K. J., Josselyn, S. A., & Frankland, P. W. (2019). Memory formation in the absence of experience. *Nature neuroscience*, *22*(6), 933–940.

White, K.G. (2001) Forgetting functions. *Animal Learning & Behavior 29*, 193–207.

Wortzel, I., & Seger, R. (2011). The ERK Cascade: Distinct Functions within Various Subcellular Organelles. *Genes & cancer*, *2*(3), 195–209.

Wu, Y. I., Frey, D., Lungu, O. I., Jaehrig, A., Schlichting, I., Kuhlman, B., & Hahn, K. M. (2009). A genetically encoded photoactivatable Rac controls the motility of living cells. *Nature*, *461*(7260), 104–108.

Xu, Z., Adler, A., Li, H., Pérez-Cuesta, L. M., Lai, B., Li, W., & Gan, W. B. (2019). Fear conditioning and extinction induce opposing changes in dendritic spine remodeling and somatic activity of layer 5 pyramidal neurons in the mouse motor cortex. *Scientific reports, 9*(1), 4619.

Xu T., Yu X., Perlik A. J., Tobin W. F., Zweig J. A., Tennant K., et al.. (2009). Rapid formation and selective stabilization of synapses for enduring motor memories. *Nature 462*, 915–919.

Yang, G., Lai, C.S., Cichon, J., Ma, L., Li, W., Gan, W.B. (2014) Sleep promotes branch-specific formation of dendritic spines after learning. *Science, 344*:1173–1178.

Yang, Y., Wang, X. B., Frerking, M., & Zhou, Q. (2008). Spine expansion and stabilization associated with long-term potentiation. *The Journal of neuroscience : the official journal of the Society for Neuroscience*, *28*(22), 5740–5751.

Yasumatsu, N., Matsuzaki, M., Miyazaki, T., Noguchi, J., & Kasai, H. (2008). Principles of long-term dynamics of dendritic spines. *The Journal of neuroscience : the official journal of the Society for Neuroscience*, *28*(50), 13592–13608.

Yeckel, M. F., & Berger, T. W. (1990). Feedforward excitation of the hippocampus by afferents from the entorhinal cortex: redefinition of the role of the trisynaptic pathway. *Proceedings of the National Academy of Sciences of the United States of America*, *87*(15), 5832–5836.

Yoshii, A., & Constantine-Paton, M. (2014). Postsynaptic localization of PSD-95 is regulated by all three pathways downstream of TrkB signaling. *Frontiers in synaptic neuroscience*, *6*, 6.

Zhao, X., Li, G., & Liang, S. (2013). Several affinity tags commonly used in chromatographic purification. *Journal of analytical methods in chemistry*, *2013*, 581093.

Zhou, Q., Homma, K. J., & Poo, M. M. (2004). Shrinkage of dendritic spines associated with long-term depression of hippocampal synapses. *Neuron*, *44*(5), 749–757.

Acknowledgments

I would like to thank the following people:

- Prof. Antonino Cattaneo and Prof. Marco Mainardi, for guiding me during this journey;
- Ajesh Jacob, Mariachiara Di Caprio and Francesca Chiara Latini, for helping me and taking part in the SynActive project;
- Vania Liverani and Mariantonietta Calvello, for their essential technical support;
- Francesco Gobbo, Ivan Arisi, Alessandro Ori, Lorena Zentilin, Cinzia Caterino, Alessandro Cellerino, Oksana Sorokina, Maria Cristina Marrone, Silvia Marinelli, J Douglas Armstrong and all those who have collaborated with our group;
- All the people from the Bio@SNS lab and the Neuroscience Institute of the CNR in Pisa;
- My girlfriend, my brother, my parents and my friends, for their unconditional (and salvific) support.